ANGULAR DISTRIBUTIONS AND YIELDS OF THE LIGHT CHARGED PARTICLES IN THE FISSION OF ^{235}U

A Thesis Submitted
in Partial Fulfilment of the Requirements
for the Degree of

DOCTOR OF PHILOSOPHY

By

MADAN MOHAN SHARMA

to the

DEPARTMENT OF PHYSICS

INDIAN INSTITUTE OF TECHNOLOGY KANPUR

NOVEMBER, 1983

14 JUN 1985

87523

TY-1983-D-SHA-ANG

TO

MY PARENTS

It is a fact that the totality of sense experience is so constituted as to permit putting them in order by means of thinking – a fact which can only leave us astonished, but which we shall never comprehend. One can say : the eternally incomprehensible thing about the world is its comprehensibility.

– Albert Einstein

POST GRADUATE OFFICE
Received on 15/12/83

CERTIFICATE

Certified that the work presented in this thesis entitled ''Angular Distributions and Yields of Light Charged Particles in the Fission of ^{235}U'' by Mr. Madan Mohan Sharma, has been done under my supervision and that it has not been submitted elsewhere for a degree.

G.K. Mehta
Professor of Physics
Indian Institute of Technology
Kanpur.

December 13, 1983.

ACKNOWLEDGEMENTS

It is indeed a great honour for me to express my gratitude to my professor Dr. G.K. Mehta who has been a constant source of inspiration and guidance in this odyssey of research into the realm of Nuclear Physics. Being endowed with a unique blend of qualities of patient understanding and incisive judgement of originality in research, he provided me a sustained impetus to brave the challenges encountered in the course of my work. I have derived the benefit of his wise and spontaneous counsel during interactions concerning personal matters. His constant encouragement in all academic endeavours which has been highly instrumental in the quest of knowledge, is greatly appreciated. It has been my great fortune to have been associated with Prof. Mehta who taught me among other things the dignity of work.

When matters of interactive learning are concerned I have benefitted a lot from Dr. S K Sharma. He instilled in me a fervour of enthusiasm which has been very vital in the pursuit of research and sustenance of optimism. He not only gave me a brotherly treatment but counselled on all matters as and when I needed. I am very grateful to him for my association with his group and for innumerable discussions which I had with him.

I acknowledge the unequivocal help and counsel rendered by Professor R.M. Singru in matters related to the broadening of academic dimensions. I am also thankful to him for his suggestions for the revitalization of the activities of Graduate Physics Club which I started to foster the academic interactions. I also acknowledge the encouragement provided by Professor Y.R. Waghmare during the initial phases of the aforesaid venture.

I take this opportunity to express my gratitude to Professor Tulsi Dass who was my teacher during the course work of the Ph.D. program. His able teaching and encouragement infused in me a love for Physics.

I visited Bhabha Atomic Research Centre, Bombay several times for a collaborative program with Fission Physics Section. I would like to thank Dr. S.S. Kapoor, Dr. D.M. Nadkarni, Dr. V.S. Ramamurthy, Dr. C.V.K. Baba, Dr. Ajitanand, Dr. P.N. Rama Rao, Dr. S.K. Kataria and Mrs. Rekha Govil of Nuclear Physics Division, BARC for intensive discussions, their help during the experiments and above all their excellent hospitality which kept my spirits high during my stay at BARC.

I am specially thankful to Dr. Rakesh Popli with whom I had the opportunity of profitable exchanges of ideas and advice on academic and the associated matters.

Dr. Ajit Sinha collaborated with me with sincerity and utmost co-operation. His help during the work is gratefully acknowledged. I would like to express my thanks to Dr. S.C.L. Sharma and Dr. A.K. Nayak for the co-operation and help which I received from them in various ways.

During the experiments many students participated and assisted. In this regard, I acknowledge the help received from Mr. Manoj Kumar Harbola, Miss Anuradha Mishra and Mr. Raghava Verma. I am glad to express my thanks to Mr. Waryam Singh who not only gave active help but also provided the warmth of his friendship while working at computers IBM-1800 and DEC-1090.

Mr. Vishal Saxena deserves more than special thanks. It is difficult to forget the tea-table discussions we used to have together on numerous aspects. His ever-readiness to solve the problems and an analytical approach towards them has greatly benefitted me. Besides, I am highly grateful to him for his friendship and wise and untiring company for the cause of research. The help and company provided by Mr. K. Kiratadas is warmly acknowledged. The help which I obtained from my friend Mr. Dinakar Kanjilal in numerous ways is recorded hereby with pleasure.

I express my thanks to technical crew of Messrs K.M.L. Jha, A.R. Korde, M.M. Gupta, K. Masood, V.K. Sharma, Anil Srivastava and C.B. Srivastava. I extend my gratitude to them not only for the help they generously gave during the running of the accelerator and my experiments but also for providing a period of an unforgettable fraternity. I also acknowledge the unconditional help provided by Mr. Ram Nath and Sri Shiv Prakash.

Mr. L.S. Bajpai is thanked for a commendable job of typing the thesis and Mr. B.K. Jain for tracings. Mr. H.K. Panda and Mr. Lalloo Singh Rathore deserve the credit for neat cyclostyling.

My work would not have been complete without the help of my fiancee Mitra Banerjee. She not only assisted in performing the experiments and the analysis of the data but also provided the moral strength to accomplish the objectives culminating in the present thesis.

I am also thankful to all those who helped me in the present work but their names may be omitted inadvertently. In the end, I acknowledge the support obtained from Department of Atomic Energy, Government of India.

(M. M. SHARMA)

CONTENTS

LIST OF TABLES

LIST OF FIGURES

SYNOPSIS

ANGULAR DISTRIBUTIONS AND YIELDS OF LIGHT CHARGED PARTICLES IN THE FISSION OF ^{235}U

MADAN MOHAN SHARMA
Ph.D.

Department of Physics
Indian Institute of Technology, Kanpur

November 1983

The phenomenon of nuclear fission has acquired an enhanced significance due to some fascinating developments during the past two decades and its overlap with phenomena observed in heavy-ion induced reactions. A variety of revelations have come about on many aspects of fission, and the interplay between collective and the intrinsic degrees of freedom has been examined. Efforts have been made to understand the dynamics of fission process from saddle to scission. But the process of descent from the saddle point is still far from being understood.

A multitude of experiments have been carried out to comprehend various aspects of fission. Light charged particle (LCP) emission serves as one of the means to probe into the configuration of the fissioning nucleus at scission. Various aspects of the LCPs and their correlations with the fission fragments have been

studied leading to a considerable insight into the phenomenon. However, the mechanism of emission of these light charged particles, namely the equatorial and the polar LCPs, is not adequately understood. This is basically due to the rare nature of these phenomena, which makes their experimental studies difficult.

The present work is an effort to explore the behaviour of the yields of the LCPs towards higher excitation energy and the study of their angular distributions. The thesis can be divided into two parts. The first part deals with the comparative yields of the equatorial and the polar LCPs at higher excitation energy and the angular distributions of the long-range alpha particles about the space-fixed axis. The second part relates to the study of the angular distribution of the polar LCPs about the fission fragment direction in thermal neutron induced fission of ^{235}U.

The studies on the equatorial and the polar LCPs have so far been confined mostly to the thermal neutron induced fission. Experiments on the dependence of the LCP emission on excitation energy are expected to divulge important information on this phenomenon. A comparative study of the yields of the equatorial and the polar LCPs has been undertaken in 200 keV and 1 MeV neutron induced fission of ^{235}U. Such a study has been motivated by the fact that there are no data available at higher

excitation energies except an earlier measurement at 600 keV in our laboratory. This is because the cross-section of the polar LCPs in fission is very small. We have devised a detection system with collimators which enables a simultaneous study of equatorial and polar LCPs. The geometry allows the use of a broad area source to provide a reasonable count-rate of the low probability events. The neutron energy region from 100 keV to 1 MeV is important since there is a predominance of p-wave ($\ell = 1$) neutron interaction with the target nucleus (U^{235}, $J^{\pi} = 7/2^{-}$) in this region. It makes the states 2^{+}, 3^{+}, 4^{+} and 5^{+} accessible to the fissioning nucleus at the transition point (saddle state). These positive parity states being low-lying states, the residual excitation energy may be available to other degrees of freedom, namely the LCP emission. This may be reflected in the behaviour of the yields of the LCPs with the excitation energy.

The angular distribution of the binary fission fragments about the projectile direction can be understood in terms of Aage Bohr's theory. However, the behaviour of the angular distribution of ternary fission fragments and the associated equatorial LCPs is unclear and the available data on this aspect are conflicting. The angular distribution of the LCPs about the incident particle direction could provide valuable information

on the emission mechanism of the ternary fission. We have studied the angular anisotropy of the long-range alpha particles (LRAs) emitted in the neutron induced fission of ^{235}U in the energy range 100 keV to 1 MeV. A new technique has been developed for measuring the angular distribution of the LCPs using a simple ΔE-E detector telescope. The results have been discussed in the perspective of the emission mechanism of the LRAs.

The second part of the thesis is aimed at studying the angular distribution of the polar LCPs in thermal neutron induced fission of ^{235}U. The angular distribution of the polar LCPs about the fission axis is important in testing the validity of various hypotheses on the mechanism of the polar emission. But the information on this aspect is not known clearly. We have determined the angular distribution of the polar LCPs by varying the collimator size (1 mm, 2 mm and 3 mm diameter) for exposing the different parts of the polar region. The angular distributions of the polar LCPs were assumed to be Gaussian and Monte Carlo calculations performed for different collimator sizes. The detection efficiencies were calculated as a function of the width of the initial angular distribution. The value of σ for which the detection efficiency ratio (3 mm/2 mm) matched with the observed yield ratio (3 mm/2 mm) gives the variance of the angular distribution. The width of the angular distributions were determined for polar protons, tritons

and alpha particles. The angular distribution of the polar protons has been found to be very narrow compared to those of tritons and alpha particles.

The first chapter refers to the salient features of the fission process. The statistical and dynamical aspects of fission have been discussed. The role of the LRA emission as a probe of the scission stage of the fissioning nucleus has been described.

Chapter II reviews the present experimental status on the equatorial and the polar LCPs with an emphasis on the mechanism of emission of these LCPs. The theories of angular distribution of the fission fragments in the fission of nuclei at energies in excess of the fission barrier have been summarized.

The next chapter gives the details of the experimental set-up used in the present work. The common aspects of the accelerator, the beam transport system and neutron generation have been described. The particle identification technique due to Goulding et al. has been used. The activation technique exploring the contamination in the keV neutrons has been discussed.

Chapter IV concerns the study of the equatorial and polar LCPs emitted in keV neutron induced fission of ^{235}U. The method of detection of the equatorial and the polar LCPs using the collimator configuration has been illustrated. The Monte Carlo simulation has been introduced, which is aimed at estimating the relative

detection efficiencies of the equatorial and the polar LCPs. The results of the measurements have been discussed in the light of the emission mechanism of these LCPs.

The ΔE-E detector telescope, generally used for particle identification, has been employed to derive the information on the angle of the incident particle about the telescope axis. The technique has been used to determine the angular distribution of the long-range alpha particles emitted in the neutron induced fission of ^{235}U in the energy range 100 keV to 1000 keV. This forms the subject matter of Chapter V. This chapter also reviews the prevalent situation on the angular distribution of the ternary fragments and the LCPs about the projectile direction. The distributions of LRAs measured in our work have been found to be peaked perpendicularly to the incident neutron direction at all energies in the above energy region. This has been interpreted to imply that the the LRA emission takes place immediately after the scission.

The details of the angular distribution measurement of the polar LCPs in thermal neutron induced fission have been presented in Chapter VI. The first two sections review the present situation on the angular distribution of the polar LCPs. The details of the collimator configuration used in the measurement of the angular

distribution forms the next part of the chapter. Finally, the results of the measurements have been presented and are discussed with reference to the existing hypotheses on the nature of the polar emission.

The last chapter presents the summary and conclusion of the present work.

CHAPTER I

NUCLEAR FISSION

1.1 Introduction

The history of nuclear fission goes back to 1937 when Hahn and Strassmann[1] observed the splitting of a uranium nucleus into two when bombarded by thermal neutrons. Since then a tremendous stride has been achieved in the arena of Fission Physics. The fission has been observed to take place by exciting a heavy nucleus by energetic charged and uncharged particles, muons and also in nuclei fissioning spontaneously. In all these fission processes, a notable feature is the release of a large amount of energy, which was verified experimentally first by Frisch[2]. The process of fission has evoked an immense interest due to the richness of phenomenon it possesses, and its ability to unveil the interweaving of various degrees of freedom. Far more interesting is the rearrangement of large number of nucleons from a single to a binary system which has stimulated an argument on the prediction of possible existence of elements beyond the ones known at present.

Bohr and Wheeler[3] were the first to give an explanation of the phenomenon. They treated the nucleus in a fashion

analogous to a charged liquid drop with two opposing forces governing the nuclear stability. The concept of charged liquid drop has earned success in describing the general features of nuclear fission and in predicting the binding energies of nuclei. The stability of a nucleus is determined by the interplay between the surface (nuclear) and Coulomb forces acting on the nucleus. The balance between the two forces gives rise to a potential barrier which is surmounted by a nucleus when it receives sufficient excitation energy by bombardment of a particle. However, it has been estimated on the basis of the liquid-drop model that nuclei in the ground state may also quantum-mechanically tunnel through the fission barrier leading to a spontaneous fission. The half-life of spontaneous fission depends upon the height and width of the barrier. It has been predicted[4] in the frame-work of the liquid-drop model that the nuclei with $Z > 120$ would not possess a barrier, thereby having very small half-lives.

The complex state of motion taking place during the fission has been described in terms of collective degrees of freedom, namely vibrations and rotations of the nucleus, coupled to intrinsic degree of freedom (single particle)[5-7]. A compound nucleus is formed when a heavy nucleus captures a neutron. The resulting excitation energy is shared among a large number of degrees of freedom. The fission occurs when a sufficient amount of energy gets concentrated on potential energy of deformation. In the initial phases of deformation the potential energy increases. At a particular nuclear shape where the nucleus is

which exactly balances the decrease in the Coulomb energy. This configuration of the nucleus with maximum potential energy is referred to as the ''saddle point''. The nucleus passes over the saddle point[3,10] and breaks into two fragments at"scission point"where the residual nuclear force acting between the two fragments is extinct. The configuration of the two-fragments touching each other at scission determines various distributions in fission. At the instant of separation the primary fragments, which possess considerable deformation energy in addition to other forms of energy, de-excite through emission of γ-ray, neutrons and sometimes a charged particle. The motion of the nucleus from the saddle to scission involves a coupling between collective and intrinsic degrees of freedom which gives rise to a number of regularities in the fission phenomenon. The dynamics of descent from the saddle to scission is not yet understood despite a large effort invested.

1.2 Salient Features of Fission

The division of a nucleus into two nuclei of comparable mass has been termed as the binary fission. However, sometimes a light charged particle is also accompanied with fission, therefore, the name tripartition or ternary fission is used for this mode of fission. We will discuss the ternary fission in detail in Chapter 2.

After the separation of the fission fragments at scission, they are accelerated by mutual Coulomb repulsion. The fragments reach about 90 % of their final kinetic energies

in approximately 10^{-20} second. These primary fission fragments have a large excess of neutrons over their stable isobars and de-excite through β-emission and neutron evaporation. The time for neutron evaporation is long compared to the time required for acceleration of the fragments implying that the evaporated neutrons are emitted from the fully accelerated fragments. These neutrons form a bulk of all neutron yield during fission. A small fraction (0.2 to 6 %.) of the neutrons, the so-called delayed neutrons continue to come from the uranium after the cessation of the neutron bombardment, and this is explained as neutron emission from highly excited states formed by β-decay of certain fission products where the β-decay energy of the parent nucleus is larger than the neutron binding energy of the daughter nucleus. The remainder of the excitation energy is lost by γ-decay within 10^{-11} second.

The most interesting feature of the fission is asymmetric mass distribution and connected to this aspect are few other properties which reflect allegiance to mass distribution. The average number of neutrons ($\bar{\nu}$) per fission is known for a large number of fissioning nuclei, which is 2.40 for thermal neutron-induced fission of ^{235}U. The value of $\bar{\nu}$ for different nuclei with zero excitation energy (correction being made on the basis of an average value of $d\nu/dE$) has been observed[17] to increase with mass of the fissioning nucleus. This increase in $\bar{\nu}$ indicates the increase in the available energy release in fission, part of which appears as an increase in the kinetic energy of the fragments, and part as an increase in number of

emitted neutrons. Also, the neutron yield has been found to increase with increase in the excitation energy of a nucleus. Since the kinetic energy of the fission fragments has been found to be weakly dependent on the excitation energy, it is obvious that the excess of the excitation energy will be released in the form of enhanced neutron emission. The variation of the number of neutrons $\bar{\nu}$ shows[18] a decline with an increase in total kinetic energy of fragments for a given excitation energy. This can be expected for a fixed energy release from energy balance considerations.

The most interesting aspect of neutron emission is the saw-tooth shaped behaviour with a minimum near A = 132 of the yield of the neutrons with the fragment mass, which was first observed by Fraser and Milton[19]. This variation has been the subject of extensive studies[20-21] due to its relation to the fragment excitation energy. The yield of neutrons is observed to be minimum for fragments near closed shells as the closed-shell nuclides are more stiff against deformation. Maximum neutron yields occur for fragments which are between two shells and are more soft towards deformation. Hence, at the scission configuration the shell structure will determine the deformation energy stored in the fragments. After scission this energy gets converted to excitation energy, therefore producing more neutrons. Thus, the neutron yield is directly correlated with the shell-effects.

The saw-tooth variation of neutron yield with fragment mass ratio in low energy fission is washed out rapidly with

increasing excitation energy[22]. This effect is attributed to a large increase in the neutron yield at A ≃ 130. As the excitation energy is increased, shell-effects disappear, resulting in a more stretched configuration. This implies a lower total kinetic energy release and a higher total excitation energy of the fragments, thus producing more neutrons.

The de-excitation of the fission fragments by γ-decay has been studied as a function of fragment mass[23-26] in the neutron-induced as well as spontaneous fission. The average energy of the γ-rays and the numbers of γ-rays per fission have been found to be a smooth, slow varying function of the fragment mass ratio very similar to the relative yield of neutrons. The high multiplicity of γ-rays from one fragment is related to the low multiplicity in the complementary fragment. This indicates a large difference in the spins of the two fragments and is supported by the shell structure in one fragment.

1.3 Double-Humped Barrier and Associated Properties

The liquid-drop model which could explain some general features of the fission process is inadequate for predicting the properties associated with the shell structure of the nuclei. The existence of spontaneously fissioning isomers, which was discovered by Polikanov et al.[11], could not be explained by liquid drop model. The incorporation of the nucleon shell correction to the liquid drop model by Strutinski[12-14] led to a double-humped fission barrier. The solid line in Figure 1.1 illustrates the structure in the barrier which shows two

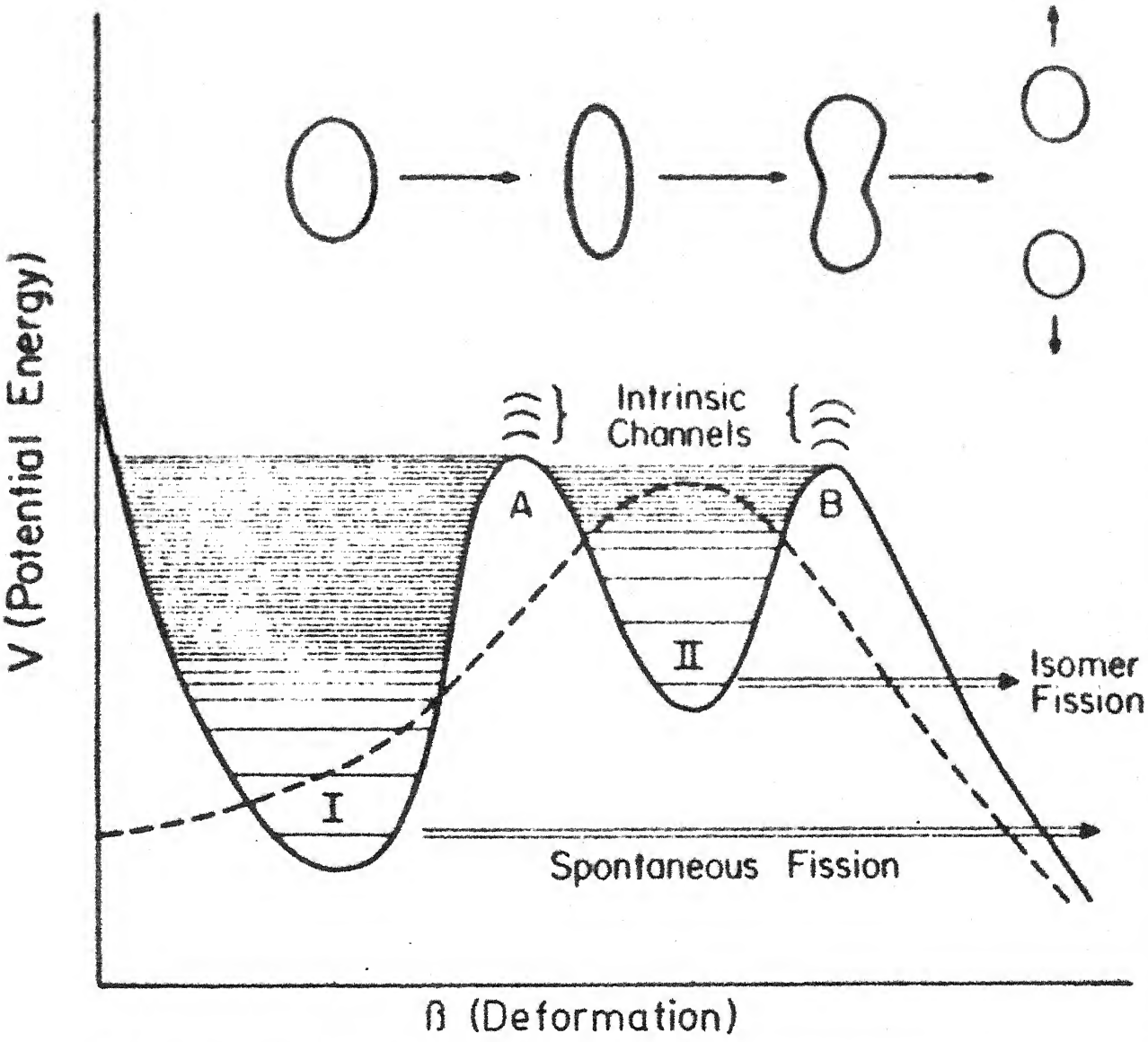

Fig. 1.1. Schematic illustrations of single-humped (---) and double-humped (——) fission barriers. Intrinsic excitations in the first and second wells are designated class I and class II states, respectively. Intrinsic channels at the two barriers are also illustrated. The transition in the shape of the nucleus as a function of deformation is schematically represented in the upper part of the figure. After Vandenbosch and Huizenga, [33]

maxima with a minimum in between. The liquid drop barrier is also shown by dashed curve for comparison. The double-humped character arises due to superposition of a smooth liquid drop (macroscopic) and oscillatory shell-correction (microscopic) part of potential energy. A second minimum occurs in the curve at a deformation close to the liquid drop barrier. This gives rise to vibrational states within this secondary well. The lowest states are meta-stable states decaying very frequently by spontaneous fission. At the high energy end of the spectrum, there exist virtual states that have the property of decaying by neutron evaporation to highly deformed residual nuclei, thus forming spontaneously fissioning isomers. The existence of double-humped barrier was verified experimentally by observing the transitions between the rotational levels of the ^{240}Pu fission isomer. It has been found that the double-humped barrier with its strongly developed secondary well between the barrier peaks is responsible for a range of phenomenon.

The fission of Ac and Ra nuclei[15-16] at relatively high excitation energies exhibits triple-humped mass-yield curve. This feature has been considered as an evidence for symmetric (liquid drop) and asymmetric (shell effects) components. A triple-humped barrier has been hypothized to explain this effect.

The fission process is known to yield a characteristically asymmetric mass distribution in neutron-induced, photon-induced as well as charged particle-induced fission of

actinide nuclei. This observation of mass-asymmetry has been the long-standing puzzle and the liquid drop model could not account for this. The plausible explanation has been advanced in terms of the shell-structure effect on the transition state. This states that the shell-structure effects favour, at an appropriate stage of the fission process, the configurations with deformations deviating from the reflection symmetry[27].

The probability for symmetric fission increases with an increase in the excitation energy. At higher energies, the mass distribution is peaked about a symmetric mass division. Significant progress has been made in calculating the potential energy surface of the fissioning nuclei with the deformation parameters[28-31]. It has been found that the second barrier has an asymmetric shape for actinides. Hence, at low energies an actinide nucleus starts its descent from the saddle point to scission in an asymmetric shape. Mustafa et al.[27] calculated the potential energy surface as a function of the deformation parameters for the fissioning nucleus after the saddle point upto scission configuration. They incorporated shell corrections in the liquid drop model and could explain roughly the mass-asymmetry. The idea of statistical equilibrium which will be discussed in next section, has also been quite successful in predicting[32] the predominance of asymmetric mass-splitting. However, to fully describe the fission process, the dynamical effects of collective inertia and the role of viscosity in the descent from the saddle to scission must be understood.

Bohr and Wheeler[3] introduced the concept of fission exit channels in terms of saddle configurations which are available to the nucleus, to explain the properties associated with fission. The number of such channels accessible to a nucleus is given by $N = 2\pi \langle \Gamma_f \rangle / \langle D \rangle$, where $\langle \Gamma_f \rangle$ and $\langle D \rangle$ are the average fission width and the average spacing between levels in the compound nucleus. For excitation energies slightly above threshold the fissioning nucleus is thermodynamically ''cold'', when it passes over the saddle point since it has invested most of its excitation energy into deformation. Therefore, only a few quantum states called transition states are energetically accessible and are expected to have a spectrum similar to that at ground state deformation. A fission process passing through a single channel would be reflected in the fission properties characteristics of that channel and spin, e.g. angular distribution, mass distribution of the fission fragments, kinetic energy of the fission fragments, average numbers $\bar{\nu}$ of prompt fission neutrons and emission probability of long-range alpha particle. The Bohr theory could be verified if the properties of fission are measured for selective excitation of the nucleus at saddle point. The information on these channels is extracted from the angular distribution of the fission fragments. The theory of the angular distribution, which will be discussed in Appendix, is an interesting consequence of Bohr theory.

The channel spectrum for a fissioning nucleus at saddle point is similar to that of ground state spectrum which are already in an elongated shape. The channels are characterized by quantum number K, the projection of spin about the symmetry axis (refer to Figure A.1 in Appendix). For even-even nuclei, the lowest state has K = 0 corresponding to a paired nucleon configuration. This state is associated with a rotational band given by

$$E_{J,K} = E_K + \frac{\hbar^2}{2\mathcal{J}_{eff}} J(J+1) \qquad (1.3.1)$$

where I is the total angular momentum and $\mathcal{J}_{eff}$ the effective moment of inertia, which depends on the deformation of the nucleus. For nuclei possessing the reflection symmetry, one has, for K = 0, a spectrum with rotational levels having $I = 0^+, 2^+, 4^+, \ldots$. The rotational band also contains the odd I-values having negative parity ($I = 1^-, 3^-, 5^-, \ldots$) but at higher position than positive parity states. Apart from these collective rotational excitations, the nucleus possesses states involving single particle degree of freedom. With each intrinsic excitation which requires the breaking of a nucleon pair, there is associated a rotational band with I = K, K+1, K+2,... and both parities. In odd-A nuclei the lowest K-value is given by the component of angular momentum of the last odd particle in its lowest binding state . With each particle configuration is associated a rotational band with I= K, K+1,K+2.. and both parities.

At small energies of the incident particle, specific effects may occur due to the dominance of a single or a few fission channels. Such effects could be visualized if the experimental studies are carried out, for example, in keV-neutron-induced fission of ^{235}U, where the interaction of $\ell=1$ (p-wave) neutrons leads to 2^+, 3^+, 4^+ and 5^+ states available to the nucleus at saddle point. The angular distribution measurements of the LCPs and fission fragments in this energy region could reflect the properties associated with the saddle state. In this regard the value of K_o^2, which characterizes the deformation of the fissioning nucleus at the saddle point, is an important parameter. This information can be extracted from the angular distribution data.

1.4 Statistical and Dynamical Aspects of Fission

The fission process is regarded as consisting of two stages. First, the ascent of the fissioning nucleus to the saddle point and second, the descent from the saddle point to the scission point where the two fragments begin to separate. The first stage has been understood in terms of the statistical idea of Bohr and Wheeler[3] which asserts that the fissioning nucleus is in thermal equilibrium and the ascent is a slow process. However, the second stage is not well understood and various models have been putforth. The most frequently used models[34] of fission are the adiabatic (dynamical) and the statistical models. The adiabatic model is characterized by the assumption that the single-particle motion follows the collective motion adiabatically. This requires that the collective motion

is fast and the coupling between collective and single particle motion is weak, so that the single particle degrees of freedom can easily readjust to reach new deformation as the distortion proceeds. In the adiabatic approximation the decrease in the potential energy from saddle to scission appears in the collective degrees of freedom at scission, mainly, as kinetic energy associated with the relative motion of the nascent fragments. The liquid-drop-model calculations[35] indicate a time of 10^{-21} to 10^{-20} second for the descent of the compound nucleus from saddle to scission. The statistical model[36] expresses a different view. It postulates a strong mixing of collective and single-particle degrees of freedom. Therefore, the ordered fission motion from the saddle to the scission point is strongly damped. The descent from the saddle point is slow and thermal equilibrium is established instantaneously from the saddle point to the scission point. The energy released in the descent is almost entirely converted into internal excitation energy of two fragments. The damping (viscosity) has been considered in detail[34] and is found to be strong enough to lend support to the statistical model of fission. The statistical approach of Fong has been quite successful in explaining the mass distribution of fission fragments, the excitation energy, the spin distribution and numerous other aspects. It has also been found that the dynamical study based on one-body dissipation mechanism leads to results in excellent agreement with those of the statistical theory and could, therefore, be treated as dynamical interpretation of statistical theory[45].

The motion from saddle to scission is so complicated that it has been difficult to make theoretical estimates in favour of either model. The nuclear configuration at the scission point is a crucial point of consideration in the theory of fission. Various theories give different predictions. The statistical theory predicts[37] that the fission fragments at the scission point have little kinetic energy, of the order of 0.5 MeV. On the other hand, any dynamical theory would lead to a much greater kinetic energy value. Therefore, if the initial energy of the fission fragments at the moment of scission can be checked, the basic question in the fission theory, whether the fission process is slow (statistical) or fast (dynamical) can be resolved on an experimental basis. This objective could be achieved in trajectory calculations of LRA-accompanied fission by calculating the pre-scission kinetic energy of fission fragments and the LRA. Fraenkel[38] obtained a value of 40 MeV for the kinetic energy of the fission fragments at the time of alpha-particle release. This value was close to that predicted by Nix et al.[39] when considering the dynamics of non-viscous liquid drop. These calculations show a support for the adiabatic approximation. However, on the other extreme, Fong found that the experimental results could be reproduced with a value of pre-scission kinetic energy of fission fragments to be less than 1 MeV. The value of this parameter for LRAs was estimated to be about 0.5 MeV by trajectory calculations of Ertel[40]. This provided strong support to the statistical

theory. However, the value of pre-scission kinetic energy of fission fragments obtained by Gavron[42] was between 7 to 14 MeV, which is in agreement with value of 8 MeV by Guet et al.[43]. These results are neither consistent with dynamical model nor the statistical model. The present experimental evidence, therefore, does not allow to single out a mechanism from both of these models. It may be likely that the fission process is somewhere in between the two extreme assumptions. This requires the weakening of the assumptions in both models, i.e. in dynamic model it is necessary to take into account viscosity and in statistical model to incorporate an incomplete statistical equilibrium.

As an intermediate approach Nörenberg[44] proposed that there is a statistical equilibrium between the collective degrees of freedom at the scission point and the coupling between the collective degrees of freedom is strong. The coupling of single-particle degrees of freedom to collective degrees is weak which results in a number of quasi-particle excitations at the saddle point. Various features of fission can be described in terms of number of quasi-particle excitation at the saddle point and the collective temperature which characterizes the statistical equilibrium of the collective degrees of freedom at the scission point.

The model tries to predict the symmetric to asymmetric mass-yield ratio as a function of excitation energy. Since the model examines various aspects as a function of compound-nuclear excitation energy, the available data is not sufficient

to test the theory. Therefore, it is desirable to study various properties of fission with the excitation energy of the fissioning nucleus. Besides, the model needs to be explored further.

It is clear that the dynamical evolution of the system from the region of the saddle point to that of scission is not adequately understood. The complete theory for the descent from the saddle point to scission point, which could explain all the observed features in fission, is yet to be developed. Such a theory requires to incorporate the friction (viscosity), the non-equilibrium statistical idea and the quantal features.

1.5 LCP Emission : A Probe

The light charged particles (LCPs) have been observed to be emitted with small probability both in spontaneous and induced fission. Of the LCPs generally believed to be emitted between nascent fragments, α-particle emission occurs with largest probability $(2\text{-}3)\times10^{-3}$ per fission. This is also referred to as long-range alpha (LRA) accompanied fission. The LCPs are focussed perpendicular to fission axis due to the Coulomb field of fission fragments. This provides a signature for the identity of this rare process where the LCPs are thought to be emitted very near the scission. Therefore, the experimental features of these LCPs would be reflection of the properties at scission, that is, the process is capable of disclosing the configuration of the fissioning system at scission. The LCP-emission is expected to probe the dynamics of the fissioning nucleus at scission, the viscosity and the

division of energy among various degrees of freedom. This requires the study of energy-angular correlations between the LCP and the fragments and above all their unambiguity is needed to be established.

Recently, alpha particles have been found to be produced in a direction perpendicular to the fission fragments in heavy-ion induced fusion-fission reaction[46]. The authors suggest that these α-particles come from the neck region between the fragments in the same way as in neutron-induced fission of actinide nuclei. Owing to many similarities in neutron-induced fission and heavy-ion reactions, the studies on alpha emission in heavy-ion induced reactions are also expected to help in probing the scission stage of the fissioning nucleus.

REFERENCES

1. O. Hahn and F. Strassmann, Naturwissenschaften 27 (1939) 11.
2. O.R. Frisch, Nature 143 (1939) 276.
3. N. Bohr and J.A. Wheeler, Phys. Rev. 56 (1939) 426.
4. A.E.S. Green, Phys. Rev. 95 (1954) 1006.
5. N. Bohr, Nature 137 (1936) 344.
6. N. Bohr and F. Kalckar, Dan. Mat. Fys. Medd. 14 (1977) No.10.
7. A. Bohr, Dan. Mat. Fys. Medd. 26 (1952) No. 14.
8. A. Bohr and B.R. Mottleson, Dan. Mat. Fys. Medd. 27 (1953) No. 16.
9. D.L. Hill and J.A. Wheeler, Phys. Rev. 89 (1953) 1102.
10. L. Meitner and O.R. Frisch, Nature 143 (1939) 239.
11. S.M. Polikanov, V.A. Druin, V.A. Karnaukhov, V.L. Mikheev, A.A. Pleve, N.K. Skobelev, V.G. Subbotin, G.M. Ter-Akopyan and V.A. Fomichev, Sov. Phys. JETP 15 (1962) 1016.
12. V.M. Strutinski, Sov. J. Nucl. Phys. 3 (1966) 449.
13. V.M. Strutinski, Nucl. Phys. A95 (1967) 420.
14. V.M. Strutinski, Nucl. Phys. A122 (1968) 1.
15. E. Konecny, H.J. Specht and J. Weber, Proc. Symp. on Phys. and Chem. of Fission, Rochester (1973) Vol. 2, p. 3.
16. J. Weber, H.C. Britt, A. Gavron, E. Konecny and J.B. Wilhemy, Phys. Rev. C13 (1976) 2413.
17. J.R. Huizenga and R. Vandenbosch, In ''Nuclear Reactions'' (Eds. P.M. Endt and P.B. Smith), Vol. II (1962) North-Holland Publ., Amesterdam.
18. H.R. Bowman, J.C.D. Milton and S.G. Thompson, Phys. Rev. 129 (1963) 2133.

9. J.S. Fraser and J.C.D. Milton, Phys. Rev. 93 (1954) 818.

0. J. Terrell, Phys. Rev. 127 (1962) 880.

1. J. Terrell, Proc. of Symp. on Phys. and Chem. of Fission (Salzburg, 1965), IAEA, Vienna (1965) p. 3.

2. C.J. Bishop, R. Vandenbosch, R. Aley, R.W. Shaw and I. Halpern, Nucl. Phys. A150 (1970) 129.

3. S.A.E. Johansson, Nucl. Phys. 60 (1964) 378.

4. J.C.D. Milton and J.S. Fraser, Phys. Rev. 111 (1958) 877.

5. G.V. Valskii, G.A. Petrov and Y.S. Pleva, Sov. J. Nucl. Phys. 8 (1969) 171.

6. F. Pleasonton, R.L. Ferguson and H.W. Schmitt, Phys. Rev. C6 (1972) 1023.

7. M.G. Mustafa, U. Mosel and H.W. Schmitt, Phys. Rev. C4 (1971) 2185.

8. P. Möller and S.G. Nilsson, Phys. Lett. B31 (1970) 283.

9. M. Bolsterli, E.O. Fiset, J.R. Nix and J.L. Norton, Phys. Rev. C5 (1972) 1050.

0. H.C. Pauli, T. Lederberger, M. Brack, Phys. Lett. B34 (1971) 264.

1. M. Brack, Jens Damgaard, A.S. Jensen, H.C. Pauli, V.M. Strutinsky and C.Y. Wong, Rev. Mod. Phys. 44 (1972)320.

2. A.V. Ignatyuk, Sov. J. Nucl. Phys. 9 (1969) 208.

3. R. Vandenbosch and J.R. Huizenga, ''Nuclear Fission'' Academic Press, New York (1973).

34. L. Wilets, ''Theories of Nuclear Fission'', Clarendon - Press, Oxford (1964).

35. R.W. Hasse, Nucl. Phys. A128 (1969) 609.

36. P. Fong, Phys. Rev. 135 (1964) B1339.

37. P. Fong, Phys. Rev. 102 (1956) 434.

38. Z. Fraenkel, Phys. Rev. 156 (1967) 1283.

39. J.F. Nix, Nucl. Phys. A130 (1969) 241.

40. P. Fong, Phys. Rev. C2 (1970) 735.

41. J.P. Ertel, in ''Statistical Theory of Nuclear Fission'', Gordon and Breach, New York (1965) p. 191.

42. A. Gavron, Phys. Rev. C11 (1975) 580.

43. C. Guet, H.A. Nifenecker, C. Signarbieux and M. Ashgar, Proc. of Symp. on Phys. and Chem. of Fission, (Jülich, 1979), IAEA, Vol. 2 (1980) p. 247.

44. W. Nönenberg, Proc. of Symp. on Phys. and Chem. of Fission, (Vienna, 1969), IAEA (1969) p. 51.

45. P. Fong, Proc. of Symp. on Phys. and Chem. of Fission, (Jülich, 1979), IAEA, Vol. 2 (1980) p. 373.

46. W.W. Wilcke, J.P. Kosky, J.R. Birkelund, M.A. Butler, A.D. Dougan, J.R. Huizenga, W.U. Schröder, H.J. Wollensheim and D. Hilscher, Phys. Rev. Lett. 51 (1983) 99.

CHAPTER II

LIGHT CHARGED PARTICLE EMISSION IN FISSION

2.1 Introduction

Light charged particle accompanied fission is a rare mode of fission (<1 % of normal binary fission) in which a light charged particle is emitted along with two fission fragments. The study of the LCP emission assumes significance due to its connection with the physical description of the scission configuration. The angular distribution of these particles about the fission fragments is particularly striking. It is sharply peaked perpendicular to the fission fragment direction. This has been found to have an important implication that the LCP is emitted from the vanishing neck region between the two nascent fission fragments while the fragments are still close together[1]. Its subsequent motion can be understood in terms of the effect of the Coulomb field of the two fragments. The final angle and the energy of the LCPs point towards a belief that they must be produced close to or at

scission i.e. either during the course of the actual tearing apart of the fragments or very soon after. Due to emergence of these particles at right angles to the direction of the fragments, the name ''equatorial emission'', has been synonymously used with ''ternary fission'', or LRA emission (due to predominance of alpha particles). Apart from alpha particles other charged particles are also observed to be emitted during fission. A large body of work regarding the study of the third particle emitted during fission has been carried out by many authors as quoted in References 2, 3 and 4, the details of which will be given in Section 2.2.

Although most of the charged particles believed to be emitted close to scission are steered perpendicularly to the fission axis by the Coulomb field of the fragments, a small fraction (≤ 2 %) of the LCPs are found to be emitted[5] at small angles to the fission axis. These so called ''polar particles'' have been studied in thermal neutron-induced fission of ^{235}U, ^{233}U and the spontaneous fission of ^{252}Cf. The mechanism of this phenomenon is far from clear and many hypotheses have been advanced, none of which is able to account for the existing data. The main impediment in understanding the polar emission arises due to extremely low probability of emission occurring only once per 10^5 fissions. This warrants the use of ingenius methods to study various

aspects of this process. In Section 2.3, we discuss various endeavours which have been undertaken to gather experimental information and to test the compatibility of various models concerned.

2.2 Equatorial Emission

The emission of equatorial LCPs from the neck between two fragments near scission is confirmed by an extensive body of data on the angular distribution about the fragment axis. The relative intensities of the LCPs and various correlations with the associated fragments have been used as input in three-body trajectories in order to derive information on the scission configuration. However, the multiplicity of the initial variables does not provide a definite answer. In the following, we discuss various experimental aspects which have contributed to our understanding of the phenomenon. The models aimed at explaining the experimental observations have also been discussed.

a) Experimental status

The alpha particles constitute the major fraction (>90 %) of the LCPs. The tritons are the next most abundant particle, about 6 %. of the alphas. The intensity of the protons have been found to vary between 1% and 2 %. by various authors[6,7,9,15]. Other charged

particles namely the isotopes of He, Li, Be, B, C, N and O are also seen to be emitted during fission[6-14]. The relative intensities of the species above ^{6}He have been found to be less than 0.1 %. of the alpha particles. The absolute yields of higher species are not well known. However, the results on the yields of protons, tritons and deuterons relative to alpha particles due to various works[6,7,9,15] are consistent.

The attempts to study the LCPs have mostly been directed to the fission of nuclei ^{234}U, ^{236}U and ^{252}Cf. It has been determined empirically[16] that the probability of emission of alpha particles from different nuclei is a linear function of the parameter $\xi = 4Z-A$. Nobles[17] investigated a correlation of the yield with the fissility parameter Z^2/A. A significant increase in the yield with Z^2/A has been observed. This implies that the yield is dependent on the amount of deformation at scission as the liquid drop model calculations[49] predict an increase in deformation at scission with Z^2/A.

The excitation energy dependence of the LCP emission is not adequately understood. The measurements have been made in thermal neutron-induced fission, spontaneous fission or fission induced by very energetic particles.

The yield of light particles has been found to decrease by 25 %. in case of thermal neutron fission of ^{235}U ($E^{*} \simeq 7$ MeV) than spontaneous fission of ^{252}Cf ($E^{*} = 0$).

Adamov et al.[24] compared the relative yields of protons, tritons and alpha particles in the fission of ^{235}U induced by 14 MeV neutrons with that in thermal neutrons. The relative yields were almost similar at these two energies within the experimental errors. But, there is an indication of an increase in the yield[7] at excitation energies beyond 15 MeV. However, at higher energies second and higher chance fissions contribute to the yield, which gives rise to several different species fissioning at different excitation energies. Nadkarni et al.[18] measured the probability of emission of alpha particles in neutron-induced fission of ^{235}U at thermal, 2, 3 and 4 MeV energies of neutrons. The results showed near constancy of the yield within the statistical error of 10 %. . Coleman et al.[19] measured the production rate of long-range alpha particles in fission of ^{232}Th and ^{238}U induced by 10.5 MeV protons and 29.5 and 42.0 MeV beam of alpha particles. The observed yield in charged particle-induced fission is similar to the result obtained in earlier measurements of spontaneous and neutron-induced fissions. The observation that the probability of light charged particle emission is rather insensitive to the excitation energy indicates that the emission of the particles can not possibly be attributed to the simple evaporation process.

The relative yields of different LCPs emitted during fission has been the subject of study in many works. The alpha particles constitute the majority (90 %.) of them as mentioned above. Tritons form the next major section of the LCPs, as evidenced from the works in References 6, 7, 9, 10, 11, 15, 20. The intensity of tritons in these measurements is observed to vary between 6 to 8 %. of the alpha yield in the fission of ^{236}U. Vorobiev et al.[10] have performed comprehensive studies on the relative yields of various light ions. The intensity of isotopes beyond ^{6}He is found to go down by approximately four orders of magnitude compared to the alpha particles. Therefore, the light particles with reasonable probability of emission are protons, deuterons, tritons and alpha particles. The Table 2.1 summarises the yields and the angular distributions of LCPs obtained by various authors. A rough correlation between the particle yield and the removal energy E_R required to release the particle into the space between the fragments has been estimated[3]. This removal energy is estimated to be 20 MeV or more for all light particles and is comparable to the total deformation energy at scission for binary fission. Thus, the light particles are expected to be emitted with configurations having unusually large energy of deformation, that is, only in a few rare events. As we will discuss below,

Halpern[3] proposed that LCP emission is caused by the sudden collapse of the neck of the elongated nucleus and the LCP is left behind in the process of rupture. Halpern obtained estimates of probability of various LCPs which were correct within an order of magnitude.

The angular distributions of all light charged particles have, invariably, been found to be peaked perpendicular to the fission fragments both in the spontaneous fission as well as in particle-induced fission. The most probable angle is weakly dependent upon the charged particle emitted. The angular distribution measurements have been performed by various authors[9,20,29]. Table 2.1 summarizes the parameters obtained in various measurements. Fluss et al.[21] used an experimental arrangement with an angular dispersion of about 5° which was significantly better than that of 12° in the experiment of Tsuji et al.[22] and 13° obtained by Cumpstey and Vass[20]. Most of these experiments agree on the value of most probable angle for alpha particles with respect to the light fragment at $84.5^{\circ} \pm 0.5^{\circ}$ and FWHM of the angular distribution to be about $17.0^{\circ} \pm 1.0^{\circ}$. Guet et al.[23] also obtained a comparable value of $18.7 \pm 0.8^{\circ}$ for the width in the thermal neutron-induced fission of ^{235}U for alpha particles above 1.25 MeV. For ^{3}H particles, the most probable angle of emission[20] is $86.5^{\circ} \pm 1.0^{\circ}$ with a width $17^{\circ} \pm 1^{\circ}$. The angular

Table 2.1

Relative intensities of emission and the mean and full width at half maximum (FWHM) of the energy and angular distributions of equatorial LCPs emitted in fission.

LCP	Fissioning Nucleus	Yield (per 100 α-particles)	Energy Distribution		Angular distribution about light fragment	
			Mean (MeV)	FWHM (MeV)	Mean (deg)	FWHM (deg)
Proton	$^{236}U^{*}$	1.02 ± 0.01[a]	8.9 ± 0.2[a]	5.9 ± 0.4[a]	-	-
	^{252}Cf	1.6 ± 0.2[c]	9 ± 2[c]	6 ± 2[c]	91[e]	90[e]
Deuteron	$^{236}U^{*}$	0.6 ± 0.02[a]	7.5 ± 2[c]	6.6 ± 0.6[a]	-	-
	^{252}Cf	0.63 ± 0.03[c]	7 ± 2[c]	7 ± 1[c]	91[e]	66[e]
Triton	$^{236}U^{*}$	6.67 ± 0.04[a]	8.4 ± 0.1[a]	6.7 ± 0.2[a]	-	-
	^{252}Cf	5.9 ± 0.2[c]	8.3 ± 0.5[d]	7.0 ± 1.2[d]	86.5[d]	17 ± 1[d]
^{4}He	$^{236}U^{*}$	100	16.0 ± 0.1[a]	9.6 ± 0.2[a]	81.3 ± 0.4[b]	18.5 ± 0.8[b]
	^{252}Cf	100	15.6 ± 0.5[d]	11.2 ± 1.4[d]	84.5 ± 0.5[d]	17 ± 1[d]
^{6}He	$^{236}U^{*}$	1.81 ± 0.02[a]	12.2 ± 0.3[a]	9.2 ± 0.6[a]	-	-
	^{252}Cf	2.4 ± 0.5[c]	12.5 ± 0.7[d]	9.0 ± 1.0[d]	86.0 ± 1[d]	13 ± 3[d]

(i) $^{236}U^{*}$ is the cpmpound nucleus formed by capture of thermal neutron by ^{235}U.

(ii) The yields are calculated for alpha particle yield as 100.

(iii) Proton and deuteron angular distributions were obtained without distinction between the light and heavy fragments.

(iv) a - [62], b - [29], c - [7], d -[20], e - [9].

distribution of tritons was found to be wider by about 4^{o} or 5^{o} than for alpha particles, according to Raisbeck and Thomas[9]. However, they did not distinguish between the light and heavy fragments. Similar results were predicted by Adamov et al.[24]. After applying recoil correction to these results, it was discovered[20] that the tritons have angular distribution very similar to the alpha particles. The correlation of the most probable angle and the widths of the angular distributions with energy of the particle have been studied by Fluss et al.[21] and Cumpstey and Vass[20]. The angular distributions of tritons and alpha particles are observed to broaden as kinetic energy of the particle increases. As the alpha-particle energy increases above 23 MeV, the emission becomes isotropic and then peaks along the polar angles. A similar trend is observed for ^{3}H emission. This variation has been explained by the trajectory calculations due to Boneh, Fraenkel and Nebenzahl[26] suggesting that the particles with high initial kinetic energy escape faster from the ''storm-region'' and are thus less focussed by the fission fragments. The mild variation of the average angle with particle energy also arises due to the same reason.

The situation in the case of protons is somewhat anomalous compared to tritons and alphas. The proton angular distribution has been noted[9] to be much broader

($\sigma = 38^{o}$) compared to other particles. Raisbeck and Thomas[9] performed trajectory calculations on the basis of Halpern's model which will be discussed in the following subsection. They assumed that the two fragments are formed at some time zero and start moving under their mutual Coulomb repulsion. The third particle appears at some time ($\simeq 0.5 \times 10^{-21}$ sec) later at a point between the two fragments. Using the same set of parameters which reproduce the alpha particle spectra, they calculated the angular and energy distribution of protons and other particles. The agreement with the measured energy spectra were found to be good for tritons and alpha particles. However a discrepancy for less abundant particles such as Be, C and Li was found. For protons, a striking disagreement was observed with measured spectra, both in the angular and energy distributions.

The broad angular distribution of protons has been ascribed by Halpern[26] to the relatively less strong absorption of nucleons in nuclear matter than more complex particles. Thus they are expected to be released over much larger volume, thereby broadening the distribution of final angle. This could also be explained by other approach such as uncertainty principle. Thus, there may be several ways to account for the differences in characteristics between proton and other light particles. However, the inconsistency in the angular and energy

distributions of protons with the characteristics of other particles and the model calculations gives grounds to believe that there are some real differences in the release conditions of protons than other particles. Also, it is interesting to note that the proton angular distribution in polar emission, as will be described in Chapter 6, is also quite different compared to polar alpha particles and tritons. In the light of these facts, a different emission mechanism for the protons, could, therefore, be speculated.

The energy distributions of the LCPs are found to be Gaussian with the most probable value being strongly dependent upon the charge of the emitted particles. In Table 2.1, we summarize the mean energies and the widths (FWHM) of the distributions obtained in various measurements. The most probable energy increases with the charge of the particles. However, for helium isotopes. the most probable energy decreases with increasing mass.

The most probable energy has been found to be minimum for the most probable angle ($\bar{\theta}_{LCP}$)[20,21,22] and increases in going to the either side of $\bar{\theta}_{LCP}$. Piasecki et al.[27] observed that the most probable energy has a minimum value 15.5 MeV near 83° for ^{4}He, rising on either side to values of 24 MeV and 23 MeV at 0° and 180° respectively for the fission of ^{236}U. These results are in conformity with other works in References 20,21 and 22.

However, variation of the standard deviation of energy distribution with angle is not very striking in the equatorial region but for the reportedly narrow distribution in the vicinity of polar angles. Tritons also have similar variations as mentioned above for alpha particles except that the maximum probable energy is about half (ratio fluctuates near 1.8) that of alpha particles at maximum probable angle. A similar situation prevails in the polar region which will be discussed in Section 2.3. The factor of 2 can be accounted for by the charge ratio between alpha particle and triton. This arouses speculations that the configurations at the time of release of triton and alpha particle are more or less identical for equatorial emission.

Now we discuss some characteristics of the ternary fragments and the correlations associated with them. The average total fission-fragment kinetic energy displays a decrease[28-29] with increase in the alpha-particle energy, with an anti-correlation of - 0.45. The angular spread of the alpha particles is found to decrease with the total fission fragment kinetic energy[29]. The most probable angle $\bar{\theta}_{\alpha L}$ decreases with increasing mass ratio which has been confirmed by the studies of Guet et al.[29], Gazit et al.[30] and partly by Choudhury et al.[31] for the fission of ^{235}U. However, this dependence has been found[32] to be relatively weak

in case of ^{252}Cf. This aspect of fission is unclear as yet and deserves to be studied further experimentally with an objective to provide important information on the relative deformation of the two fragments at scission. There are numerous other correlations which are sought to be used in three-body trajectory calculations to arrive at the best set of initial variables describing scission configuration.

The characteristics such as mass distribution and total kinetic energy distributions of the fission fragments associated with the LCP emission have been investigated[33-35]. The studies on the mass and kinetic energy distributions in α-accompanied fission demonstrated that the binary and ternary mass distributions are qualitatively similar and the kinetic energy distribution can be quantitatively accounted for. But, from the mass distribution it can not be predicted that which fragment produced the LCP. Nevertheless, the neutron yield measurements as a function of mass ratio R reveal that α-particles are emitted from those fragments which have the largest deformation energy at scission.

b) Models

Several hypotheses have been advanced for the emission mechanism of the LCPs. However, none of them is successful in explaining all the observed features. In

the following, we discuss the basic ingredients of these models.

(i) Carjan's pre-scission model

According to this model due to Carjan et al.[36-37], the emission of the charged particles takes place before scission. The calculations of the α-clustering probability along all points of nuclear surface indicate that there is a conspicuously high probability of formation of α-particles in the neck shortly before the scission. The authors produce argument that for all nuclei, the α-emission occurs between the saddle and scission at the same distance from the saddle i.e. at the same pre-scission kinetic energy. In support of this inference are the experimental correlations such as $\langle dE_\alpha/dE_k \rangle$ and $\langle dE_k/dE_\alpha \rangle$ to be similar for the fission of ^{236}U and ^{252}Cf. On the basis of this, one tends to assume that the initial configurations at scission do not differ much from ^{236}U to ^{252}Cf, which is compatible with the fact that the fragments possess the same kinetic energies at the instant of alpha-emission in these nuclei. However, the model requires further elaboration so as to compare its predictions with the hitherto well-established experimental features.

the following, we discuss the basic ingredients of these models.

(i) Carjan's pre-scission model

According to this model due to Carjan et al.[36-37], the emission of the charged particles takes place before scission. The calculations of the α-clustering probability along all points of nuclear surface indicate that there is a conspicuously high probability of formation of α-particles in the neck shortly before the scission. The authors produce argument that for all nuclei, the α-emission occurs between the saddle and scission at the same distance from the saddle i.e. at the same pre-scission kinetic energy. In support of this inference are the experimental correlations such as $\langle dE_\alpha/dE_k \rangle$ and $\langle dE_k/dE_\alpha \rangle$ to be similar for the fission of ^{236}U and ^{252}Cf. On the basis of this, one tends to assume that the initial configurations at scission do not differ much from ^{236}U to ^{252}Cf, which is compatible with the fact that the fragments possess the same kinetic energies at the instant of alpha-emission in these nuclei. However, the model requires further elaboration so as to compare its predictions with the hitherto well-established experimental features.

(ii) Pre-scission evaporation model

This is the model which has been advanced by Ramanna et al.[38] based upon the experimental observations in 14 MeV neutron-induced fission of ^{238}U. The underlying assumption is that the alpha particle emission is the consequence of evaporation from the excited nucleus at the instant between the saddle and scission points. The model comtemplates that the alpha particle anisotropy about the space-fixed axis should exhibit the fore and aft peaking in fast neutron fission of ^{235}U as a manifestation of evaporation from the compound nucleus. The model found support from the measurements of Nadkarni[39-40] in 3 MeV neutron-induced fission of ^{235}U. However, it is not consistent with our data which will be discussed in Chapter 5, and that of Atneosen et al.[41]. The observed weak dependence of the LCP-yield with excitation energy also goes against this hypothesis. Moreover, the model has not been subjected to the test for LCPs other than alpha particles.

(iii) Sudden-snap model

This model states that the release of the LCP takes place through the sudden snap of the neck. On the basis of the energy and angular distributions of the particles, Halpern[3] argued that the LCPs are emitted from the space between the fragments at times close to

that of the snapping of the neck (i.e., near scission). The relative probability of emission of various particles has been proposed in terms of the energy required to release particles into the region between the fragments. The removal energy of alpha particle is given by

$$E_R = B_\alpha + \frac{3}{2} V_\alpha$$

where B_α is the average binding energy of an alpha particle to one of the fragments and V_α represents the Coulomb potential of the alpha particle placed midway between the fragments. Accordingly, E_R has been estimated[25] to be roughly 24 MeV for alpha particle. The minimum amount of kinetic energy with which the α-particle is born, has been calculated to be about 4 MeV on the basis of the uncertainty principle. Thus, α-emission costs around 28 MeV which is a significant fraction of the total energy. The fact that the total kinetic energy release in ternary fission is roughly equal to that in binary fission and that the fragment kinetic energy reduces in case of ternary fission implies that the mean fragment separation at the time of division is larger in the LRA accompanied fission. Therefore the LRA-emission occurs only in those configuration in which enough energy has been stored through the abnormally long neck between the fragments at the instant of scission. The model has been developed qualitatively and agrees with a variety of

observations. However, the relative yields of the LCPs predicted by the model and the sudden approximation have not been understood quantitatively.

(iv) The statistical model

The salient features of the statistical model have already been discussed vis-a-vis dynamic model in Chapter 1. The statistical model[52], it may be recalled, is based upon a simple assumption that the descent from the saddle point to scission is so slow a process that statistical equilibrium is established instantaneously throughout the descent. The instantaneous equilibrium at the moment just before the two fragments separate, determines the relative probabilities of different nuclear configurations corresponding to different modes of fission. The condition of statistical equilibrium at the scission point enables to calculate theoretically the mass distribution, charge distribution, kinetic energy distribution and prompt neutron distribution etc. These calculations involve the information about the excitation energy of the fragments and the level-density parameters. The scission point represents the moment at which the two fragments and the α-particle separate from one another. This point, therefore, is the final condition of the descent from the saddle to scission. The statistical theory of fission predicts a complete specification of the final condition

of the fission process. This condition can be used as the initial condition of the three-body trajectories to predict many properties of fission. Many features of fission have been found to be qualitatively consistent with this approach when shell-effects are also incorporated.

Underlying the statistical assumption[51], the fission fragments at the scission point show a little kinetic energy of the order of 0.5 MeV in contrast to a much greater kinetic energy predicted by any dynamical theory. The statistical theory also leads to the conclusion that the α-particle is expected to have a most probable kinetic energy at the scission point of about 0.5 MeV. Ertel[53] first used the statistical theory determined initial conditions to simulate the three-body trajectories. The calculated angular correlation of α-particle was consistent with the experimental one. The calculated α-particle kinetic energy as a function of mass ratio was also in good agreement with the experiments. Employing this approach Fong[43] was able to obtain the ratio of 1:461 for LRA fission to binary fission. The result agrees well with the experimental ratio of 1 to 449 ± 30. These results provided a support to the scission configuration predicted by statistical theory. Besides, recent studies on spin distribution[54], excitation energy[55] and variance of kinetic energy distribution[56] lend further support to validity of the statistical approach.

2.3 Polar Emission

Most of the LCPs, as discussed in the preceding section, are emitted perpendicular to the fission fragments. It is believed on the basis of their angular distributions that they are born somewhere in the vicinity of scission from the neck of the stretched configuration. The calculations[44] have demonstrated that the strong Coulomb deflection off the fission-axis cannot register these LCPs in a cone of half-apex angle 45° (to be referred to as shadow cone) about the fission-axis. However, a small fraction of alpha particles, to be called as polar particles, were found to be emitted at small angles with respect to the fission axis[4]. The experimental information on the polar LCPs is scanty. Unlike the equatorial LCPs, their characteristics do not give any unambiguous picture of the origin of their emission. Various models pertaining to the nature of this phenomenon are prevalent: pre-scission emission from the fragment polar tips[36-37], snapping of the nuclear surface[3], bending of the trajectories by nuclear force[45], diffraction and transmission through fission fragments[46] and the evaporation from fission fragments[27,47,48]. This section reviews the present experimental status of polar emission and the salient features of above models.

a) Experimental status

The polar emission has mostly been studied in thermal neutron-induced fission of ^{233}U, ^{235}U and in the spontaneous fission of ^{252}Cf only. Therefore, a definite relationship of the attributes (namely intensities and the energy spectra) to the nucleus undergoing fission is not known. However, a comparison[50] of these aspects of polar emission in thermal neutron-induced fission of ^{233}U and ^{235}U indicates a weak dependence on the fissioning nuclei.

The relative intensity of the polar and equatorial α-particles has been measured[27] to be 5×10^{-3} in the case of ^{235}U fission. The ratio of polar to equatorial emission (P/E) depends upon the borderline defined between the polar and equatorial regions. Piasecki et al.[61] have used the convention of setting 25° and 155° as demarcation lines between the polar and equatorial regions. The model-dependent approaches to the decomposition of the angular distribution lead to many times higher value of P/E ratio than experiments indicate. Therefore, the angular distributions predicted by the models could provide a check on their validity, which we will discuss in detail in Chapter 6. The absolute intensities of the polar LCPs along the light fragments (L-emission) and heavy fragments (H-emission) as measured by Piasecki et al.[60] in the fission of ^{236}U and Nowicki et al.[48] for spontaneous

fission of ^{252}Cf are produced in Table 2.2. It may be noticed that the yield of polar LCPs along the light fragment is about 3 times than that along the heavy fragment. This makes an important point of check for any model on the nature of polar emission. The intensity ratio L/H of polar emission agrees well with the prediction of evaporation model (we will refer to it in this section below) for alpha particles.

The measurements on the energy distributions of the polar LCPs have been performed by various authors[5,27,50,60,63]. Table 2.3 gives the mean values and the second moments of the energy distributions of the polar LCPs for L-emissions and H-emissions. The energy of the polar LCPs is higher than the corresponding equatorial LCPs and the width of the energy distributions of polar LCPs has been found to be about half the width of the equatorial LCPs. A comparison of the spectra values for $^{236}U^{*}$ and ^{252}Cf indicates that the mean values and dispersions of polar-particle energies are close in both the cases. However, the energy spectra of polar α-particles are slightly wider in ^{252}Cf than in ^{236}U while the opposite trend is noticed for polar protons. The mean kinetic energy of the polar LCPs has been observed[48] to be weakly dependent on the fragment mass as in case of equatorial emission[64].

The mean values of energy distribution of polar tritons and alpha particles are different by a factor of

Table 2.2

Experimental intensities of polar light charged particles. [After Piasecki et al.[61]].

LCP	^{236}U				^{252}Cf		
	Polar emission Piasecki et al. [60]			P/E Ratio	Polar emission Nowicki et al. [48]		
	L-emission	H-emission	L/H Ratio		L-emission	H-emission	L/H Ratio
p	30.5±2 (±0.6)	44.5±4 (±1)	2.0±0.2	0.17±0.33	35.0± 2 (±1)	(33.0±3)±1	3.9±0.3
d	2.8±0.5(±0.6)	3.4±0.9(±0.7)	2.4±0.9	$(3\pm1)\times10^{-2}$	7.2±0.6(±1.5)	5.7±1.1(±1.2)	4.8±1.0
t	9.2±1.2(±0.9)	8.0±1.5(±0.8)	3.3±0.6	$(7.2\pm1.3)\times10^{-3}$	13±1(±2)	18±2(±3)	2.7±0.3
^4He	100	100	2.9±0.2	5×10^{-3}	100	100	3.8±0.2
^6He	0.06	0.2	-	-	0.05	0.2	-

i) L-emission and H-emission refer to the emission of LCP along the light and heavy fragment trajectories respectively.

ii) The errors given in the table are of statistical origin. The errors given in parenthesis correspond to maximum system errors involved in the particle identification.

iii) The P/E values given are based on the value 5×10^{-3} for alphas.

Table 2.3

The first two moments of the energy distributions of the polar light charged particles. [After Piasecki et al.[61]]

LCP	Fissioning Nucleus	Mean Value		Discription		Reference
		L-emission	H-emission	L-emission	H-emission	
Alpha particle	$^{234}U^{*}$	22.8±0.1	22.2±0.3	3.0±0.2	2.8±0.4	Andreev et al.[50]
	$^{236}U^{*}$	22.8±0.2	22.5±0.4	3.0±0.2	2.8±0.5	Andreev et al.[50]
	$^{236}U^{*}$	24.5±0.1	23.5±0.1	2.9±0.1	2.5±0.1	Piasecki et al.[60]
	^{252}Cf	25.5±0.1	24.8±0.1	3.4±0.1	2.7±0.1	Nowicki et al.[48]
Triton	$^{236}U^{*}$	15.3±0.2	13.6±0.3	2.7±0.2	2.0±0.2	Piasecki et al.[60]
	^{252}Cf	15.3±0.2	14.0±0.3	2.6±0.2	2.6±0.3	Nowicki et al.[48]
Deuteron	$^{236}U^{*}$	13.1±0.3	11.6±0.3			Piasecki et al.[60]
	^{252}Cf	13.6±0.2	12.8±0.5			Nowicki et al.[48]
Proton	$^{236}U^{*}$	11.2±0.1	11.2±0.2	2.5±0.2	2.8±0.3	Piasecki et al.[60]
	^{252}Cf	11.4±0.2	11.3±0.1	2.2±0.1	2.0±0.1	Nowicki et al.[48]

The errors in this table are statistical only.

about 2 as in the case of equatorial tritons and alpha particles. This fact can be explained by the difference between the charges of tritons and alpha particles. It implies that the polar LCPs are subjected to Coulomb force of the fragments in the same way as the equatorial ones. This may point towards a similarity in the emission mechanisms of the equatorial and polar LCPs with different scission configurations.

The kinetic energy of the fission fragments moving in the same direction as polar particle is lower than that in binary fission, the difference being maximum for α-particles (Figure 2.1). The difference has partly been explained by a recoil effect (linear momentum conservation) due to particle emission. However, a similar decrease of the energy of the fragment moving opposite to the particle has also been noticed. This can not be reconciled by recoil effect. But, this may imply that polar emission occurs when the fissioning nucleus is unusually stretched at scission, which affects both the fission fragments. The observed difference in kinetic energies has been found to be independent of fragment mass ratio for thermal neutron fission of ^{233}U and ^{235}U by Andreev et al.[50]. This provides a speculation that there are some differences in the scission configuration of binary fission and polar LCP accompanied fission.

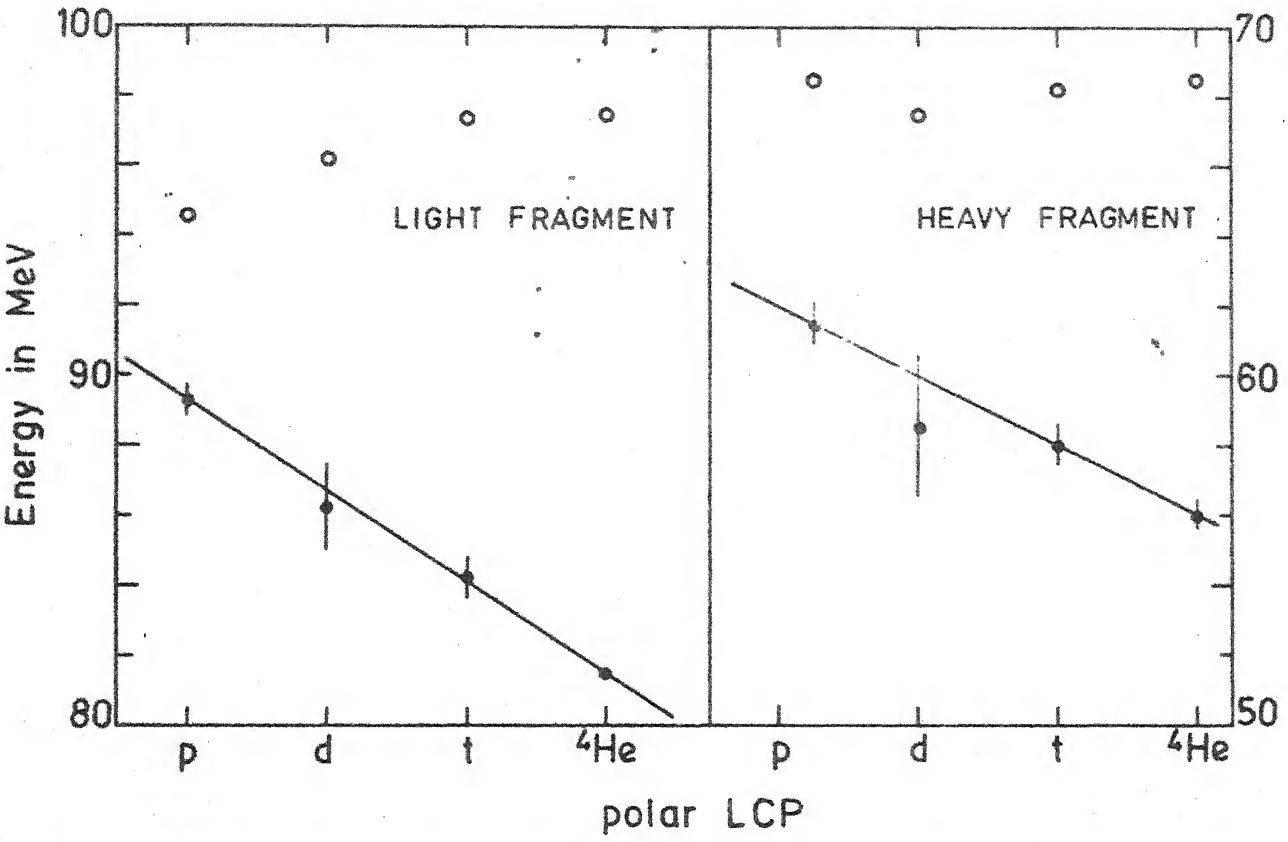

Fig. 2.1. Measured mean energies of light and heavy fragments moving along and opposite to the polar light charged particle (LCP) emitted in thermal neutron induced fission of ^{235}U. '•'- Corresponds to the fragments along the polar LCP while 'o'-corresponds to those moving in opposite direction. Lines are only visual fits. (Data taken from Piasecki et al. [61])

The mass distributions of the fission fragments moving along the polar particles have been studied by Piasecki et al.[60] for $^{236}U^{*}$ and Nowicki et al.[48] for ^{252}Cf. There is an striking asymmetry observed in these distributions compared with the mass distributions in binary fission. This asymmetry stems from the difference between the intensities of the polar LCPs moving along the light fragment and the heavy fragment. A comparison of the mass distribution in polar emission with that in binary fission also reveals that the mass of the light fragment moving along the alpha particle is, on the average, smaller by 2.5 amu than in binary fission. A similar trend has been observed in equatorial emission accompanied by alpha particle[28,34]. However, in case of H-emission, no visible differences in mass of the fragment are observed. This fact is in conflict, if one assumes that the polar emission is due to evaporation from a fragment. Nowicki et al.[48] observed in the case of polar proton emission in ^{252}Cf fission that the final mass of the light fragment is even higher than in bipartition. This result was earlier obtained by Nardi et al.[12] for equatorial emission of proton in the spontaneous fission of ^{252}Cf. A small shift of this kind has also been confirmed in the case of polar proton emission in the neutron-induced fission of ^{235}U. These observations of the increase in fragment mass in polar emission make the proton case as anomalous and this factor is difficult to be accommodated by any model at present.

The excitation energy dependence of the emission probability of charged particle has been studied by Nowicki et al.[48] for the spontaneous fission of ^{252}Cf . They determined the total excitation energy of both the fission fragments using the Q-values for a given fragment mass ratio and the data on kinetic energies. The emission probability of the polar alpha particles has been found to increase with the excitation energy. For a fission fragment of fixed mass the excitation energy is quite widely distributed with a FWHM $\lesssim$ 20 MeV. The strong increase of the emission probability with the fission fragment excitation energy should result in some preference for the fragments belonging to high-energy tail of the excitation energy distribution. Therefore, the excitation energy of those fragments which emit charged particles should be higher than in the average bipartition. These observations have been found to be in good agreement with the evaporation hypothesis.

Although a quite good idea of the polar emission has already been acquired, a clear picture has not yet emerged and there are many correlations which remain to be established beyond ambiguity. The knowledge of the angular distributions of polar LCPs and the dependence of polar emission on excitation energy of compound nucleus could help to give a clue to a mechanism for this phenomenon. A comparative study of the equatorial and polar LCPs could provide a link between the processes associated with the equatorial and polar emission. The present work is an effort in this direction.

b) Models

The mechanism of the polar emission is still far from clear and a variety of models have been proposed, as aforesaid, to explain this rare aspect. The models can be divided into two categories. The first type of models explain the cause of the polar LCP-emission similar to the equatorial emission i.e. particles produced in the neck region and taking a course along the polar region due to different conditions. The second type of models describe the polar emission like a post-scission effect. Some of these models partly explain some of the experimental features, however, none of these models has claimed the success in explaining all the existing data on polar emission. We give below the outline of these hypotheses.

(i) Pre-scission emission model

This model which was advanced to explain the equatorial emission was extended to cover the polar emission as well. Carjan et al.[36-37] who calculated the clustering probability of α-particles just before the scission on the surface of the deformed nucleus, observed a small portion of alpha particles formed on the fragment polar tips besides a sizeable probability in the neck (corresponding to equatorial emission). This explains the emission of the polar LCPs as taking place from

polar tips. Another variant of argument suggested by these authors says that an alpha particle clustered in the neck is transferred to the polar tips in the process of deformation towards scission. This takes place through one-body mechanism rendering the alpha particle emitted in this region of lowered Coulomb barrier. Such a mechanism, however, requires a very long mean free path in the interior of the nucleus.

Since the model needs to be developed further to predict the angular distribution, intensity and energy spectra, it is difficult to assess the validity of this hypothesis at present. But if the hypothesis is true, one could ask, what mechanism transfers the energy from the necking-in region to the polar tips making the cluster emission possible just before the scission. The model does not provide answer to this question as yet. The authors of this model argue that if the deficit of four mass-units is corrected, the mass distribution in alpha-accompanied fission coincides in all respects with that in binary fission. They contend that only the emission before the moment of scission could preserve the mass distribution. However, in the proton-accompanied polar emission in ^{252}Cf, the light fragment occurs to be heavier on the average by a few mass units than in binary fission. This fact can not be reconciled with the above argument of the authors. Thus, due to these drawbacks

the model needs to be examined further.

(ii) Snapping of the nuclear surface

This model also, which was originally proposed to explain ternary fission (equatorial emission) by Halpern[3], has tried to explain the phenomenon of polar emission. According to this hypothesis, polar emission takes place due to the same cause as equatorial emission. The remnants of the neck after the snapping back of nuclear surface are transferred to the outer poles due to fragment vibration. The relative probability of emission from the light fragment compared to the heavy fragment is explicable on the basis of the fact that probability of emission is larger for the fragments with longer navel. Therefore, if it is assumed that the emission along light fragment trajectory really takes place from the light fragment and that along heavy fragment from heavy fragment, the light fragment navel being longer than that of heavy fragment predicts the mass deficit from light fragment during polar emission. The model seems to be able to explain the observed mass distribution except that the case of proton emission in the fission of ^{252}Cf, where the light fragment mass is even more than in binary fission, can not be accommodated.

(iii) Nuclear orbiting

The hypothesis of a glory-like nature of the polar emission in fission was studied by Dakowski et al.[45]. The light particle trajectories most of which land up into the equatorial region due to strong deflection off the fission-axis, are bent into the polar region under the action of Coulomb and nuclear potentials of the deformed fission fragments. This requires a particular range of impact parameters and velocities. The classical calculations[45] of the three-body trajectories governed by Coulomb, nuclear and friction forces were performed. The fragment deformation was taken into account by incorporating the quadrupole deformation parameter in Woods-Saxon potential used for nuclear force. It was possible to find the initial conditions which are conducive to the bending of alpha-particle in polar region. However, the model could not explain the experimental data unless very dubious assumptions are made concerning the localization of the charged particle starting points and the diffuseness of the fission fragment surface. The model, however, still deserves to be investigated further.

(iv) Scattering by fragments (wave phenomenon)

The models of polar emission which employ classical nature of trajectories leave some room for quantum effects. This is due to the fact that at very

87523

low starting energy ($\simeq$ 1 MeV) of the alpha particle, the ratio of the fragment radius to the reduced de Broglie-wavelength λ is about 2-5. Therefore, efforts[46,50] have been made to investigate the quantum-mechanical scattering of the LCPs by the optical potential of two fission fragments. Andreev et al.[50] solved the time-independent Schrödinger equation by numerical integration. They obtained the polar to equatorial ratio for alpha-particles which was in agreement with the experimental value. Kordyasz[46] performed the quantum-mechanical calculations for the scattering of protons born from the neck by the fission fragments in the neutron-induced fission of ^{235}U. Due to complicated nature of the problem, the Schrödinger equation was solved by approximating the fission fragments to be stationary (time-independent), equal and spherical. The particles were assumed to be emitted from a spherical isotropic source positioned midway between the fragments. The calculations[46,47] could fit the experimental value of the polar to equatorial ratio for alphas particles, tritons and protons. For protons the ratio $N(0^{o})/N(90^{o})$ which is very high, could be explained by assuming the fragments to be sufficiently close to each other at the moment of emission. The model is still in the preliminary stage and can be explored further to include the mass assymetry, deformations of the fission fragments and the time dependence of their motion.

(v) Evaporation model

The model[27,45,48] proposes that the emission of the polar LCPs is a manifestation of evaporation from the fully accelerated fission fragments. As is well known, the deformation energy of the fragments is converted some time after the scission into the excitation energy. The de-excitation of such fragments occurs mainly via neutron and γ-ray emission. Therefore, it is possible that other channels of de-excitation, for example, the charged particle evaporation, may also exist. The model tries to explain the experimentally observed fragment masses, energy angular distributions and the intensities of the polar LCPs in terms of above hypothesis. This model is apparently the most studied one in detail. Piasecki and Blocki[45] were able to reproduce the experimental values of mean fragment masses in case of polar emission along light fragment using the statistical model of de-excitation. The statistical model used was the angular momentum dependent evaporation model employing Fermi-gas level-density formula. The calculated relative intensities of emission of various particles agree well with the experimental values for ^{236}U as well as ^{252}Cf. The L/H ratio predicted by this model for alpha particles emitted in the fission of ^{236}U agrees with experimental value within error. It should be stressed that due to poor knowledge of the polar-

emission angular distributions, the experimental intensities are known within a factor of 1.5-2

The calculated dependence of emission probability of alpha particle on the fragment mass has been found to resemble the experimental results, but the agreement is not satisfactory in the cases of both ^{236}U and ^{252}Cf. Other experimental observations which the evaporation model has reproduced are the mean value of the total excitation energy of the fragments observed in coincidence with alpha particles and the dependence of emission probability on the total fragment excitation energy. Although, the model has met success in explaining some experimental facts, it is not in agreement with observed results on few accounts. The angular distribution of polar protons which is observed to be very narrow experimentally (which we will explore in Chapter 6) can not be explained by this hypothesis. Moreover, the mean energies of the polar alpha particles and tritons are predicted to be substantially higher than the observed values. The disagreement, it seems, could be due to either incorrect knowledge of the inputs to the evaporation model or the uncertainties in the experimental results, e.g., the angular distributions. Nevertheless, this model is most detailed and could be used with better inputs to explain the phenomenon of the polar emission.

Apart from these models, there are few other models, namely the effect of scission neutrons, delayed tripartition and a rotating navel which try to explain the polar emission. However, these hypotheses which are too preliminary have been discarded from the basic arguments alone.

A comparative view of all the models discussed in this section reveals that the evaporation model and the nuclear orbiting hypothesis are the ones which can be investigated quantitatively in a semi-classical manner to predict various experimental features.

REFERENCES

1. Tsien San-Tsiang, Journal de Physique et le Radium 9 (1948) 6.
2. N. Feather, Proc. of Symp. on Phys. and Chem. of Fission, IAEA Vienna, 1969, p. 83.
3. I. Halpern, Ann. Rev. Nucl. Sci. 21 (1971) 245.
4. R. Vandenbosch and J.R. Huizenga, "Nuclear Fission", Academic Press, New York (1973).
5. E. Piasecki, M. Dakowski, T. Krogulski, J. Tys and J. Chwaszczewska, Phys. Lett. 33B (1970) 568.
6. S.W. Cosper, J. Cerny and R.C. Gatti, Phys. Rev. 154 (1967) 1193.
7. S.L. Whetstone, Jr., and T.D. Thomas, Phys. Rev. 154 (1967) 1174.
8. J. Blocki, J. Chwaszczewska, M. Dakowski, T. Krogulski, E. Piasecki, M. Sowinski, A. Stagnes and J. Tys, Nucl. Phys. A127 (1969) 495.
9. G.M. Raisbeck and T.D. Thomas, Phys. Rev. 172 (1968) 1272.
10. A.A. Vorobiev, V.T. Grachev, A.P. Komar, I.A. Kondurov, A.M. Nikitin, A.I. Yegorov and Yu. K. Zalite, Phys. Lett. B30 (1969) 332.
11. V.N. Andreev, V.G. Nedopekin and V.I. Rogov, Sov. J. Nucl. Phys. 8 (1969) 22.
12. E. Nardi, Y. Gazit and S. Katcoff, Phys. Rev. C1 (1970) 2101.

13. D.L. Horrocks and E.B. White, Nucl. Phys. A151 (1970) 151.

14. J.B. Natowitz, A. Khodai-Joopari, J.M. Alexander and T.D. Thomas, Phys. Rev. 169 (1968) 993.

15. M. Dakowski, J. Chwaszczewska, T. Krogulski, E. Piasecki and M. Sowinski, Phys. Lett. 25B (1967) 213.

16. N. Feather, Proc. of Symp. on Phys. and Chem. of Fission, Vol. 2 (Vienna, 1969) 83.

17. R.A. Nobles, Phys. Rev. 126 (1962) 1508.

18. D.M. Nadkarni and S.S. Kapoor, Nucl. Phys. and Solid State Phys. 13B (1970) 73.

19. J.A. Coleman, A.W. Fairhall and I. Halpern, Phys. Rev. 133 (1964) B724.

20. D.E. Cumpstey and D.G. Vass, Proc. of Symp. on Phys. and Chem. of Fission, (Jülich 1979) IAEA (Vienna) Vol. II (1980) 223.

21. M.J. Fluss, S.B. Kaufmann, E.P. Steinberg and B.D. Wilkins, Phys. Rev. C7 (1973) 353.

22. K. Tsuji, A. Katase, Y. Yashida, T. Katayama, F. Toyofuku and H. Hamamoto, Proc. Symp. on Phys. and Chem. of Fission, (Rochester, 1973), IAEA, Vienna (1974) Vol. 2, p. 405.

23. C. Guet, C. Siguarbieux, P. Perrin, H. Nifenecker, B. Leroux and M. Ashgar, J. Phys. Lett. 39 (1978) L213.

24. V.M. Adamov, L.V. Drapchinsky, S.S. Kovalensko, K.A. Petrazhak and I.I. Tyutyugin, Sov. J. Nucl. Phys. 13 (1971) 540.

25. I. Halpern, Proc. of Symp. on Phys. and Chem. of Fission (Salzburg, 1965) Vol. 2 IAEA, Vienna (1965) p. 369.

26. Y. Boneh, Z. Fraenkel and I. Nebenzahl, Phys. Rev. 156 (1967) 1305.

27. E. Piasecki and J. Blocki, Nucl. Phys. A208 (1973) 381.

28. M. Ashgar, C. Carles, R. Chastel, T.P. Doan, M. Ribrag and C. Signarbieux, Nucl. Phys. A145 (1970) 657.

29. C. Guet, C. Signarbieux, P. Perrin, H. Nifenecker, M. Ashgar, F. Caitucoli and B. Leroux, Nucl. Phys. A314 (1979) 1.

30. Y. Gazit, A. Katase, G. Ben-David and R. Morch, Phys. Rev. C4 (1971) 223.

31. R.K. Choudhury and V.S. Ramamurthy, Phys. Rev. C18 (1978) 2213.

32. Z. Fraenkel, Phys. Rev. 156 (1967) 1283.

33. G.K. Mehta, J. Poitou, M. Ribrag and C. Signarbieux, Phys. Rev. C7 (1973) 373.

34. H.W. Schmitt, J.H. Neiler, F.J. Walter and A. Chetham-strode, Phys. Rev. Lett. 9 (1969) 427.

35. E. Nardi, Y. Gazit and S. Katcoff, Phys. Rev. 182 (1969) 1244.

36. N. Carjan, A. Sandulescu, V.V. Pashkerich, Phys. Rev. C11 (1975) 782.

37. N. Carjan, J. Phys. 37 (1976) 1279.

38. R. Ramanna, K.G. Nair and S.S. Kapoor, Phys. Rev. 129 (1963) 1350.

39. D.M. Nadkarni, BARC Report-318 (1967), India.

40. D.M. Nadkarni, Nucl. Phys. A112 (1968) 241.

41. R.A. Atneosen, T.D. Thomas and B.G. Garvey, Phys. Rev. 139 (1965) B307.

42. P. Fong, Phys. Rev. C2 (1970) 735.

43. P. Fong, Phys. Rev. C3 (1971) 2025.

44. R. Piasecki, M. Dakowski, J. Blocki and L. Nowicki, INR Report 1720/IA/PL/A (1977).

45. M. Dakowski, E. Piasecki and L. Nowicki, Acta. Phys. Pol. B9 (1978) 933.

46. A.J. Kordyasz, J. Phys. G : Nucl. Phys. 6 (1980) L123.

47. E. Piasecki and J. Blocki, Acta. Phys. Pol. B5 (1974) 247.

48. L. Nowicki, E. Piasecki, A. Kordyasz, M. Kisielinski, J. Sobolewski, W. Czarnacki, H. Karwowski, P. Koczon and C. Signarbieux, Nucl. Phys. A375 (1982) 187.

49. J.R. Nix, Nucl. Phys. A130 (1969) 241.

50. V.N. Andreev, V.G. Nedopekin, V.I. Rogov, Yad. Fiz. 25 (1977) 732.

51. P. Fong, Phys. Rev. 102 (1956) 434.

52. P. Fong, ''Statistical Theory of Nuclear Fission'', Gordon and Breach, New York City (1969).

53. J.P. Ertel, M.S. Thesis, Emory University (1968) published in Reference 52 above.

54. D.C. Aumann, W. Gückel, E. Nirschl and H. Zeising, Phys. Rev. C16 (1977) 254.

55. M. Ashgar, C. Guet and P. Perrin, Nucl. Phys. A298 (1978) 13.

56. Yu. A. Lazarev, Atomic Energy Review 15 (1977) 75.

57. A. Kordyasz, Report INR 1860/IA/PL/A (1980).

58. T.D. Thomas, Nucl. Phys. 53 (1964) 552.

59. D.G. Sarantites and B.D. Pate, Nucl. Phys. A93 (1967) 545, 567.

60. E. Piasecki, M. Sowinski, L. Nowicki, A. Kordyasz, E. Cieslak and W. Czarnacki, Nucl. Phys. A255 (1975) 387.

61. E. Piasecki and L. Nowicki, Proc. Symp. on Phys. and Chem. of Fission (Jülich, 1979) IAEA, Vienna (1979) p.193.

62. P.D. Hondt, C. Wagemans, A. Dec Lercq, G. Barrequ and A. Deruytter, Nucl. Phys. A346 (1980) 461.

63. V.M. Adamov, L.V. Drapchinsky, S.S. Kovalenko, K.A. Petrzhak, L.A. Pleskachevsky and I.I. Tyutyugin, Phys. Lett. 48B (1973) 311.

64. G.K. Mehta, J. Poitou, M. Ribrag and C. Signarbieux, Phys. Rev. C7 (1973) 373.

CHAPTER III

EXPERIMENTAL DETAILS

This chapter describes some common aspects of the experimental set-up for the present work. Section 3.1 highlights the salient features of the accelerator and the beam transport system. Section 3.2 deals with the neutron generation using various targets and the calculation of the thickness of tritium targets. The particle identification technique has been discussed in Section 3.3. The three-parameter data acquisition system and its accessories are described in Section 3.4. The last section 3.5 describes the details of the activation technique, which has been used to examine the level of thermal neutron background in the fast neutron flux.

3.1 Accelerator

The experimental facility utilized was 2 MV Van de Graaff Accelerator at Indian Institute of Technology, Kanpur. The machine is manufactured by High Voltage

Engineering Corporation, Massachusetts, USA, and can provide positive ion beams upto 100 μA beam current. A proton beam obtained from the accelerator was used to generate neutrons from $^{7}Li(p,n)$ and $^{3}H(p,n)$ reactions. The energy stability of the beam was $\simeq \pm 4$ keV. However, the slit stabilization system fabricated in our laboratory[1] enhanced the energy stability further upto $\pm$ 0.5 keV. The energy of the machine was calibrated by measuring the proton energy threshold of 1.880 MeV in case of $^{7}Li(p,n)$ reaction and 1.019 MeV for $^{3}H(p,n)$ reaction, with an accuracy of $\pm$ 4 keV. The $^{27}Al(p,\gamma)$ reaction was exploited to calibrate the machine with an accuracy of $\pm$ 1 keV by monitoring a sharp resonance at 992 keV.

Figure 3.1 shows the beam transport system. The focussing of the beam at the target was achieved using quadrupole lenses, which provided a beam spot of diameter 5 mm. The aluminium grill arrangement as shown in Fig. 3.1 diminished the possibility of the scattered neutrons from being directed at the fissile source. Yet, there was some contamination due to scattered neutrons from various sources(as discussed in Section 3.5) influencing the fast neutron flux. But, it was found to have a negligible effect on the experiment.

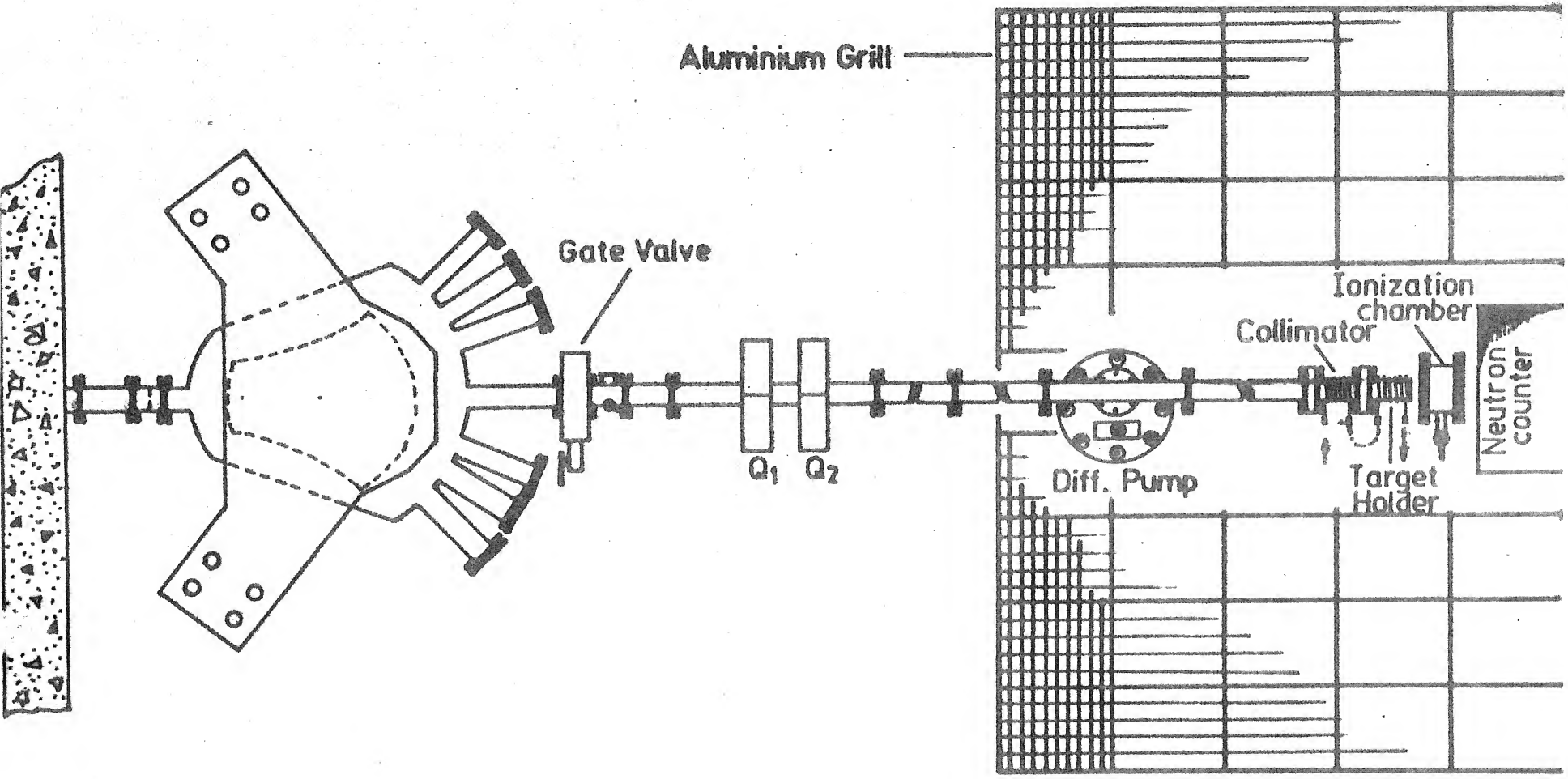

Fig. 3.1 Schematic diagram of beam transport system.

3.2 Neutron Generation

(a) Neutron targets

The neutrons were generated from $^{7}Li(p,n)$ and $^{3}H(p,n)$ reaction. Thin lithium targets were prepared by evaporating lithium metal on copper backing in vacuum. Nitrogen gas was inlet in the evaporation chamber after lithium deposition, which reduced the oxidation of lithium. The targets were stored in an evacuated desiccator. These targets were used to produce neutrons of energy upto 220 keV.

Thermal neutrons were obtained from thick lithium foil by thermalizing the neutron flux obtained from $^{7}Li(p,n)^{7}Be$ reaction. Slowing down of neutrons was accomplished by juxtaposing a slab of paraffin wax to the target holder.

$^{3}H(p,n)$ reaction provided neutrons of energy from 250 keV to 1 MeV. Tritium targets were procured from the Isotope Division, Bhabha Atomic Research Centre, Bombay. The target consists of tritium gas absorbed in the titanium layer deposited on copper disk over an area of diameter 2 cm. The number of tritium atoms equal the number of atoms of titanium in the target. The use of a 12 Ci target causes a neutron energy spread of $\pm$ 270 keV, which was calculated from the thickness of the target as following :

As the unit curie of activity is defined as that quantity of radioactive material which gives 3.7×10^{10} disintegrations per second, the number of tritium atoms present in a 12 Ci target would be given by

$$N = 3.7 \times 10^{10} \times 12$$

which gives the number of tritium atoms in the target

$$N = 2.493 \times 10^{20}$$

Therefore the number of titanium atoms (the ratio of titanium to tritium is 1:1)

$$= 2.493 \times 10^{20}$$

This corresponds to a titanium layer of thickness

$$x = \frac{NA}{N_{av}S} = 6.32 \text{ mg/cm}^2$$

where A, S and N_{av} stand for mass number of titanium, the area of the target and the Avogadro number respectively.

The stopping power of protons in the titanium being considerably larger than in tritium, the incident proton beam loses energy substantially in titanium. Therefore proton energy loss in the target can be calculated from dE/dx value of proton in titanium alone using range-Energy tables[2]. The loss of proton energy of 2 MeV in a 12 Ci tritium target gives rise to a spread

of ± 240 keV in the proton beam energy. The corresponding neutron energy was determined from the kinematical equations of the reaction.

(b) Neutron target holder

The targets were mounted in a neutron target holder which is shown in Fig. 3.2. The target holder consists of a cylindrical copper assembly fitted with circular tubes around it to allow the cooling of the target and the collimator with chilled water in circulation. It prevented the target heating and 50 μA beam of proton at 2 MeV at the target could be used conveniently without damage to the latter. Separate target holders for tritium, thin lithium and thick lithium targets connected to water chilling system were used.

(c) Neutron detector

A standard long counter consisting of a BF_3 proportional counter covered by a thick coaxial cylinder of paraffin was employed to monitor the neutron flux. The counter has an efficiency of detection practically constant for neutron energies above 1 MeV. The response of counter for thermal neutrons goes down to 70 % of the maximum value. The counter was not used for any normalization of experimental results but served as an indicator for deterioration of the neutron target after its prolonged use.

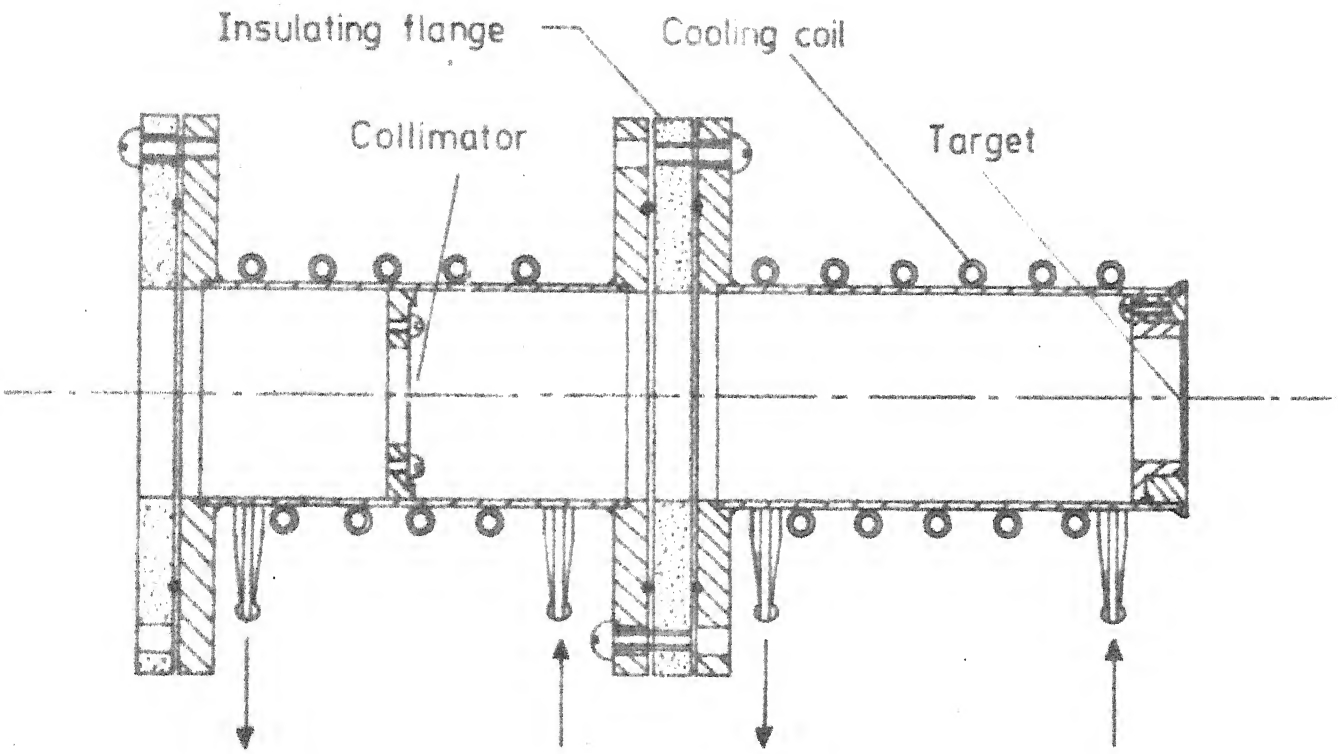

Fig. 3.2 The neutron target holder and collimator.

3.3 Particle Identification

Experiments involving the emission of light charged particles, which seek to study the detailed picture (nature) of various LCPs, invariably resort to a particle identifier. Recognition of the type of light charged particles emitted from the target and measurement of their energy constitutes the essential function of a particle identifier. Various methods are used to identify the particle species. However, a solid-state detector ''telescope'' using a thin ΔE transmission type detector in conjunction with a thick E-detector makes an identifier capable of separating the light ions. Separation of light ions such as proton, deutron, triton and helium isotopes is obtained due to a substantial change in energy loss between two neighbouring isotopes. The incident ions pass through the ΔE-detector sampling the ionization along the track where the energy loss is proportional to dE/dx value of the ion and thickness Δx of the detector. The E-detector stops the ion receiving the remainder of energy E. The summed $(\Delta E+E)$ signal gives a measure of the total particle energy and the pattern of ΔE and E signals provides identification. Various algorithms are used to generate a parameter whose value is characteristic of a specific type of ion, by suitable manipulations of E and ΔE signals. The algorithms are based on Bethe-Bloch equation

$$-\frac{dE}{dx} = B(Z_e^2 M/E) \ln(b \frac{E}{M}) \qquad (3.3.1)$$

where B is a constant independent of ion parameters; E, M and Z_e represent the total energy, mass and the effective charge of ion respectively (at high velocities for light ions, $Z_e \cong Z$). For $\Delta E \ll E$, and a limited energy range, if it is assumed that the ions are fully stripped and the logarithmic term varies slowly with E, Equation (3.3.1) can be written as

$$(E + \frac{1}{2} \Delta E) \Delta E \simeq K M Z^2 \qquad (3.3.2)$$

The term $E + \frac{1}{2}\Delta E$ in Equation (3.3.2) is the average ion energy while passing through the ΔE detector. Thus, if particles of different energy, mass and charge are detected by ΔE and E detectors, different isotopes will be represented by different hyperbolae in the $(E + \frac{1}{2}\Delta E, E)$ plane, each corresponding to a MZ^2 value. It is worth noting that MZ^2 provides a unique value for each light ion. However, due to variation of ΔE with angle of incidence, ignoring the variation of logarithmic term and the assumption of $\Delta E \ll E$, identification by this ''multiplier'' algorithm becomes less distinctive.

The other method due to Goulding et al.[3] utilizes the well known fact that the range of a particle of charge Z and mass M varies as a fixed power of energy in a large energy region, i.e.

$$R = K E^{\alpha} \qquad (3.3.3)$$

where K is a particle-dependent parameter and α lies in the vicinity of 1.7 for light ions namely protons, tritons and alpha particles. Since $K \alpha (1/MZ^2)$, Equation (3.3.3) can be rewritten as

$$R = \frac{K'}{MZ^2} E^{\alpha} \qquad (3.3.4)$$

where K' is a constant. If Δx be the thickness of ΔE detector, then

$$x = R(E + \Delta E) - R(E)$$

$$= \frac{K'}{MZ^2} [(E + \Delta E)^{\alpha} - E^{\alpha}] \qquad (3.3.5)$$

or $$(E + \Delta E)^{\alpha} - E^{\alpha} = \frac{\Delta x}{K'} . MZ^2 \qquad (3.3.6)$$

The particle identification function is defined as

$$PI = (E + \Delta E)^{\alpha} - E^{\alpha} \qquad (3.3.7)$$

Therefore

$$PI \alpha MZ^2 \qquad (3.3.8)$$

This particle identification function (PI) is a unique characteristic of a particular isotope and is independent of total energy E of the particle. Since this algorithm is based on range-energy relationship, it has been found very convenient over the broad range of E and ΔE values.

We have used a particle telescope consisting of a totally depleted 50 μm thick silicon surface-barrier

ΔE-detector and a 500 μm thick silicon surface-barrier E-detector. As is apparent from Equation (3.3.6) that PI value for a particle is proportional to thickness Δx of the detector, 50 μm thick ΔE-detector was chosen to ensure a distinct difference in energy loss ΔE between two successive isotopes. The E and ΔE signals derived from the detectors were used to generate a particle-identification spectrum using Goulding's ''range'' algorithm. The value of the index α was chosen to be 1.76. A clear separation of peaks in PI spectrum for protons, tritons and alpha particles was achieved. A plot between ΔE and E channel numbers was also prepared, which is given in Chapter IV. This displays the grouping of different LCP types around different rectangular hyperbolae. The spread in the points arises due to resolution of E and E-detectors and the uncertainty in the ΔE-detector thickness with varying angle of incidence.

3.4 Three-Parameter Data Acquisition System

Multiparameter Data Acquisition Systems play an important role in experiments, where correlation among various parameters is studied. Such systems acquire the data in the form of digitized information (e.g. the channel number) transduced through analog-to-digital converters (ADC's). The systems can be categorized as off-line and on-line. In the off-line system, the

information so stored is analyzed later on a general-purpose computer for obtaining various parameteric correlations and results of the experiment. However, an on-line facility employs the data acquisition system coupled to a special purpose dedicated computer. This computer consists of a processor which can analyze data in real time through a set of precoded instructions. This processor is capable of executing a wide range of arithmetic and logical operations.

We have used an off-line three-parameter data acquisition system. In the following, we describe various constituents of the system.

(a) Data acquisition system

The three-parameter data acquisition system (3PS) consists of three identical data acquisition systems, each made up of an analog-to-digital converter (ADC) and a set of decade scalers. The ADC's receive the analog pulse as input and digitize the information inherent in the amplitude of the pulse. Each acceptable input pulse must conform to certain conditions in amplitude and timing. This process, referred to as ''analog-to-digital conversion'', effectively assigns a channel number proportional to the pulse height of each accepted pulse. This number developed in the scaler is called the channel address corresponding to the input pulse

and may lie between 0 and 999. The conditions for the acceptibility of the pulse are set by front panel adjustments on 3PS. A 'sensitivity' discriminator is set to discriminate against the noise. An 'upper level' discriminator control determines the maximum limit of the acceptable pulse amplitude, which if exceeded, inhibits the completion of conversion. The 'conversion gain' control governs the dispersion of pulse height spectrum i.e., channel per unit energy. Also, there is a zero-shift control on each ADC, which is implemented using a 'threshold' potentiometer. This positions the zero-setting of channel address corresponding to higher or lower values of pulse height without changing the dispersion. The input pulse amplitude must exceed this bias in order to generate valid output from the ADC. An appropriate circuitry in the host system permits the use of each of the three converters in either independent mode or in coincidence with an external signal. The prompt-coincidence gates of all operating converters are closed, except when an externally generated -10 V pulse is given to a prompt-coincidence connection on the front panel.

The final digitized information of each ADC is presented in Binary-Coded Decimal (BCD) word format in a serial order. The serial information is further appended with a special character to uniquely identify

the segment of information from each ADC. The composite array of information is called one 'word' which consists of 12 bits (or characters) made up of three bits from each parameter corresponding to a channel number (000 to 999) and three special characters. The system has no memory to hold the information. An interface, therefore, transfers this information in a special format onto a magnetic tape operating in incremental mode. After the information is thus recorded, the scalers associated with the ADC's are cleared and the ADC's are enabled to to process the new event.

(b) Interface

The interface links the 3PS and the magnetic tape recorder (MTR). It provides control or command signals and transfers the data from the 3PS after making them compatible with the MTR. It also presents on its front panel a 12-digit numeric display for each word recorded, a 4-digit display for a 'Record Counter' and a 2-digit display for 'Parity Error Counter'. Record length selector on the interface panel allows to select one of four different record lengths, i.e. 32, 64, 128 and 256 events per record. The interface provides switches for a manual insertion of identifier-labels like Beginning of Tape (BOT), End of Record (EOR) and End of File (EOF). Also, the interface permits a recording in manual mode

of some data or information on magnetic tape.

(c) Magnetic tape

The magnetic tape recorder (MTR) records the digital data on a magnetic tape. Present system has a seven track, IBM compatible digital recorder which accepts the data in binary or binary-coded decimal (BCD) format. There exist three packing density options : 200, 556 or 800 bits per inch (bpi). The data on magnetic tape is recorded as an event-by-event word in incremental mode. During the transfer of data vertical parity is generated and checked. Longitudinal parity is also checked at the end of each record.

(d) Software

The data were recorded at 200 BPI, each record containing 64 words, which was selected by a switch on the front panel of interface. The structure of the words has been discribed in Section 3.4(b) and can be schematically represented as

X X X O X X X O X X Y =

Ist Parameter 2nd Parameter 3rd Parameter

The three set of three digits (formed by X's) correspond to ADC output separated by special character (represented by O's). The twelfth character = (equal to sign) denotes

the end of the word. The '0' and '=' have a BCD code of 82 and 821 respectively. The magnetic tape was read on the computer IBM-1800.

A software program was developed to identify the special characters and ADC parameters. The program, which separates the information from the three parameters was written in FORTRAN and assembly language. It checks the number of '=' characters between two End of Records (EOR's) and gives a print out of all events in a record in the form as displayed above. The program also looks for wrongly placed equal to (=) signs and skips that event. All the records between two End of Files (i.e. one file) are read. The data were read on IBM-1800 and events from each such file were obtained in the form of punched cards. The information thus retrieved was transported to DEC-10 disk through card-reader. The data were analyzed on DEC-1090 Computer at I.I.T. Kanpur.

3.5 Neutron Flux Contamination

The fission cross-section for ^{235}U at thermal neutron energy is very large ($\simeq$ 580 barns) compared to the value ($\simeq$ 1.2 - 1.5 barns) for keV neutrons. This large factor in the ratio of $(\sigma_f)_{th}$ to $(\sigma_f)_{fast}$ would imply that even 1 % thermal neutron background present in the

experiment would cause an effective background of 500 %. In other words, it is important to make sure that thermal neutron background is such, that the phenomenon being investigated has the contributions from thermal neutrons within the error limits of the experiment. A check of the magnitude of thermal neutrons contaminating the fast neutron flux, therefore, becomes mandatory before performing an experiment with the latter.

The laboratory has been designed to minimize the thermal neutron background. The neutron producing target and the detection system of the experiment lie in the centre of the beam room. The beam room is an almost hemispherical room of considerably large size. A neutron-pit consisting of an aluminium grill and a basement beneath the aluminium grill minimizes the scattering of neutrons with hydrogeneous material. The neutron target holder is surrounded by copper tubes which circulate the chilled water to cool the target. The elastic scattering of neutrons by circulating water and nearby electronic units and reflections from distant walls of the beam room contribute to the thermal neutron background at the fissile source. However, efforts were made to minimize the presence of scattering material near the experimental site. The amount of thermal neutrons admixing the keV neutron flux was determined by the activation technique.

(a) Activation technique

The technique consists of irradiation of ^{115}In by neutrons forming ^{116}In, which subsequently decays to ^{116}Sn through β^- emission. The ground state of ^{116}Sn decays with a half life of 13 seconds and the isomeric first excited state decays with a half-life of 54 minutes producing cascade γ-rays from the excited state of ^{116}Sn. The short-lived state activity decays very fast leaving only 54 minutes activity to be observed. The activation cross-section for the 54 minutes activity is 150 barns for thermal neutrons compared to 200 millibarns at 200 keV neutron energy. This fact makes the indium foil a good detector for thermal neutrons.

The investigation of the thermal neutron contamination is accomplished by measuring the cadmium ratio by this method. The cadmium ratio is defined as the ratio between the observed neutron intensity as revealed by a particular detector (e.g. ^{115}In in this case) to the intensity observed by the same detector surrounded by a layer of cadmium. Figure 3.3 shows the total absorption cross-section[4] of cadmium as a function of the neutron energy. The curve indicates that cadmium is practically opaque to the thermal neutrons, but transparent to the neutrons of energy above 0.4 eV. To determine the cadmium ratio, two indium foils, one encapsulated in cadmium and a bare one were exposed to 200 keV neutron flux obtained

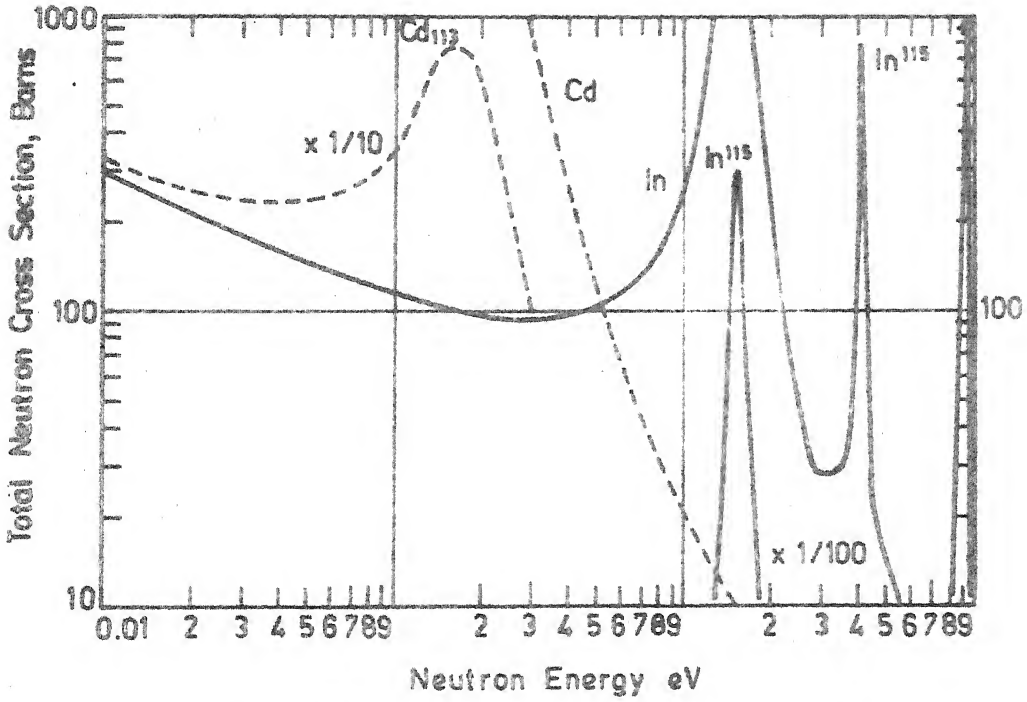

Fig. 3.3 Total neutron cross section as a function of neutron energy for cadmium and indium.

from $^{7}Li(p,n)$ reaction for about one half-life (50 minutes). Both the foils were placed in an identical configurations so as to receive equal flux of neutrons. The foils were left for about 5 minutes to allow ^{116}In ground state ($T_{1/2}$ = 13 second) to decay, after irradiation. The gamma-rays emanating from both the foils were counted one after the other with a NaI(Tl) scintillator detector. The logarithm of the activity as measured by detector was plotted against time t at which measurement of activity was done (with the end-point of irradiation as origin). The Figure 3.4 shows the two least squares fitted straight lines for the respective foils. The straight lines are represented by

$$\ell n\, A(t) = \ell n A(o) - \lambda t \qquad (3.5.1)$$

The slope and intercept of the straight lines give half-life and initial activity. The measured half-life is in good agreement with the known half-life ($\simeq$ 54 minutes).

(b) Results

The cadmium ratio is given by

$$R = \frac{A_o\ (Bare)}{A_o(Cd)} \qquad (3.5.2)$$

where A_o denotes the initial activity (t = 0). This can be written as

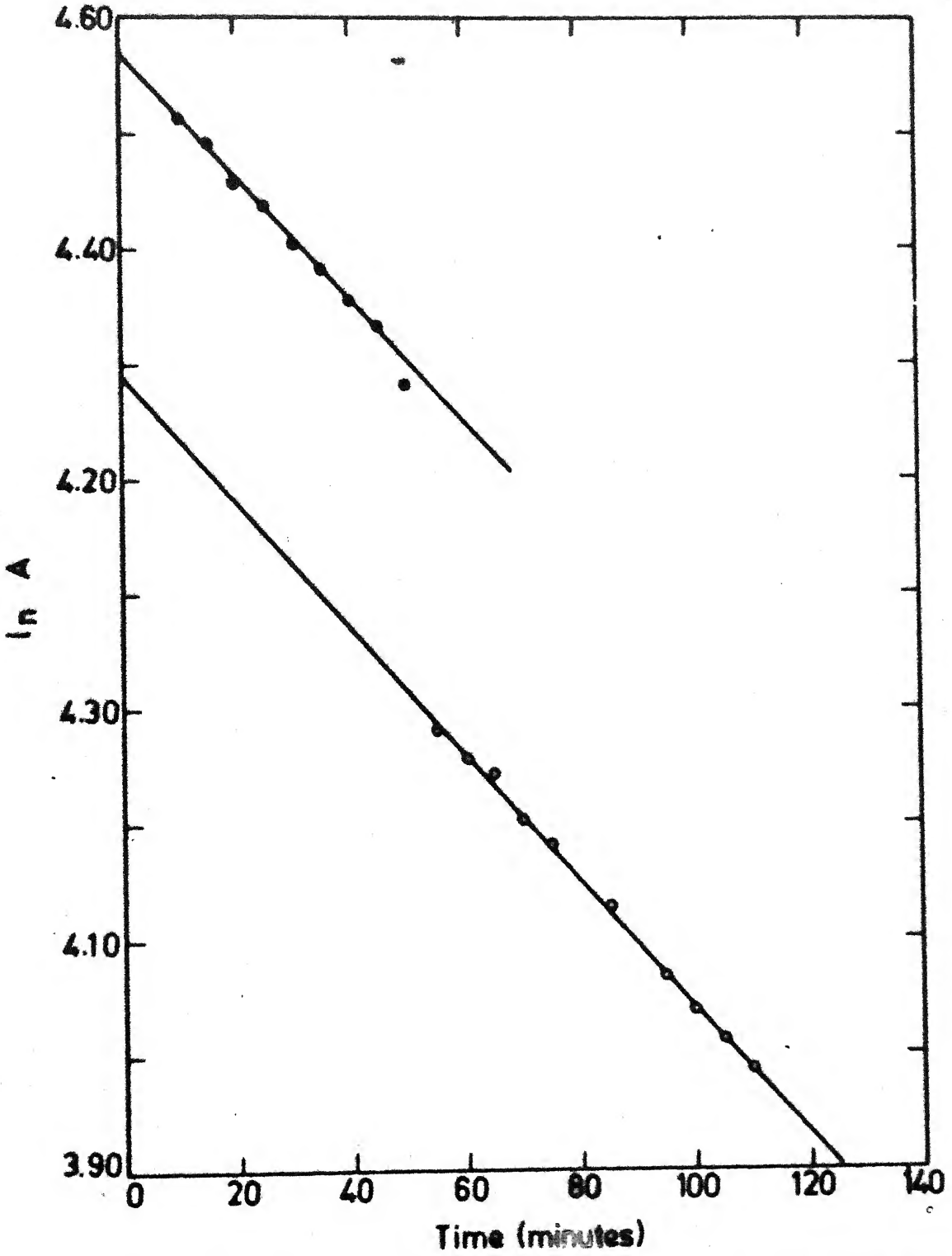

Fig. 3.4 Logarithm of the activity as a function of time for cadmium covered [•] and uncovered [○] foils.

$$\frac{A_o\ (\text{Bare})}{A_o(\text{Cd})} = \frac{N_1\ (\phi_{th}\ \sigma_{th} + \phi_k\ \sigma_k)}{N_2\ \phi_k\ \sigma_k} \qquad (3.5.3)$$

subscripts th and k refer to the thermal and keV neutrons respectively. N_1 and N_2 are the number of ^{115}In atoms in the bare and cadmium wrapped foils as determined by weighing the two. Thus the ratio between fast and thermal neutron fluxes becomes

$$\frac{\phi_k}{\phi_{th}} = \frac{A_o(\text{Cd})\ N_2\ \sigma_{th}}{N_1\ \sigma_k} \left[\frac{1}{A_o(\text{Bare}) - \frac{N_2}{N_1} A_o(\text{Cd})}\right] \qquad .... \quad (3.5.4)$$

From the experimental values of A_o's and known values of σ_{th} and σ_k for indium, the ratio ϕ_{th}/ϕ_k was determined. The fraction of thermal neutrons present in 200 keV neutron flux was estimated to be $\leq$ 0.006 %. Consequently, it amounts to the contamination of about 2.5 % in fast fission cross-section. This effect is well within the error limits of the experiment. The thermal neutron contamination is expected to be even smaller than this at neutron energies higher than 200 keV.

REFERENCES

1. Switching and Stabilization System for 2 MeV Van de Graaff Laboratory, Technical Report VDG/13/76, I.I.T. Kanpur.

2. L.C. Northcliffe and R.F. Schilling, Nucl. Data Tables, A7 (1970) 233.

3. F.S. Goulding and B.G. Harvey, Ann. Rev. Nucl. Sci. 25 (1975) 167.

4. W.D. Bygrave, P.A. Treado and J.M. Lambert, in Accelerator Nuclear Physics (High Voltage Engineering Corporation, Massachusetts), (1970) 138.

CHAPTER IV

EQUATORIAL AND POLAR EMISSION IN FAST NEUTRON INDUCED FISSION OF ^{235}U

4.1 Introduction

The study of the emission of the equatorial and the polar LCPs in fast neutron induced fission is described in this chapter. Most of the earlier works[1] pertaining to the polar and equatorial emission have been confined to the thermal neutron induced fission. The experimental arrangements used to study these aspects were such that either the equatorial or the polar nature of the LCPs could be studied at a time. The low value of fission cross-section in fast neutron fission and the rare mode of emission of polar LCPs makes the comparative study of two aspects difficult. We have devised[2] a detection system which enables a simultaneous study of the equatorial and the polar emissions. The geometry allows the use of a broad area source to provide a reasonable count-rate of the low probability events. The natural advantage of the present geometry is that the uncertainties of normalization

between the polar and the equatorial LCPs could be evaded. The following section describes the detection geometry of the experiment in detail.

4.2 The Detection System

The schematic diagram of the detection system is shown in Figure 4.1. The LCPs are seen by a particle telescope as described in Section 3.3 and the fission fragments are detected by a combination of two ionization chambers. A single ionization chamber has been divided into two by a multi-hole collimator made of aluminium. The collimator which is grounded, serves as a common electrode (cathode) of both the ionization chambers. The ^{235}U source mounted on a circular plate acts as the collector of one of the ionization chambers, which we will refer to as the Lower Ionization Chamber (LIC). The LIC is operated with +100 V on the collector (^{235}U source). An aluminium foil mounted above the collimator serves as the collector of other ionization chamber, to be referred to as the Upper Ionization Chamber (UIC). The thickness of the aluminium foil was so chosen as to prevent the natural alpha particles and fission fragments from ^{235}U from reaching the particle telescope. A positive potential of +200 V was applied to the aluminium foil (collector of UIC). The ionization chamber were filled with a mixture of 95 % Argon and 5 % Methane gas at 85 cm pressure of mercury. The direction

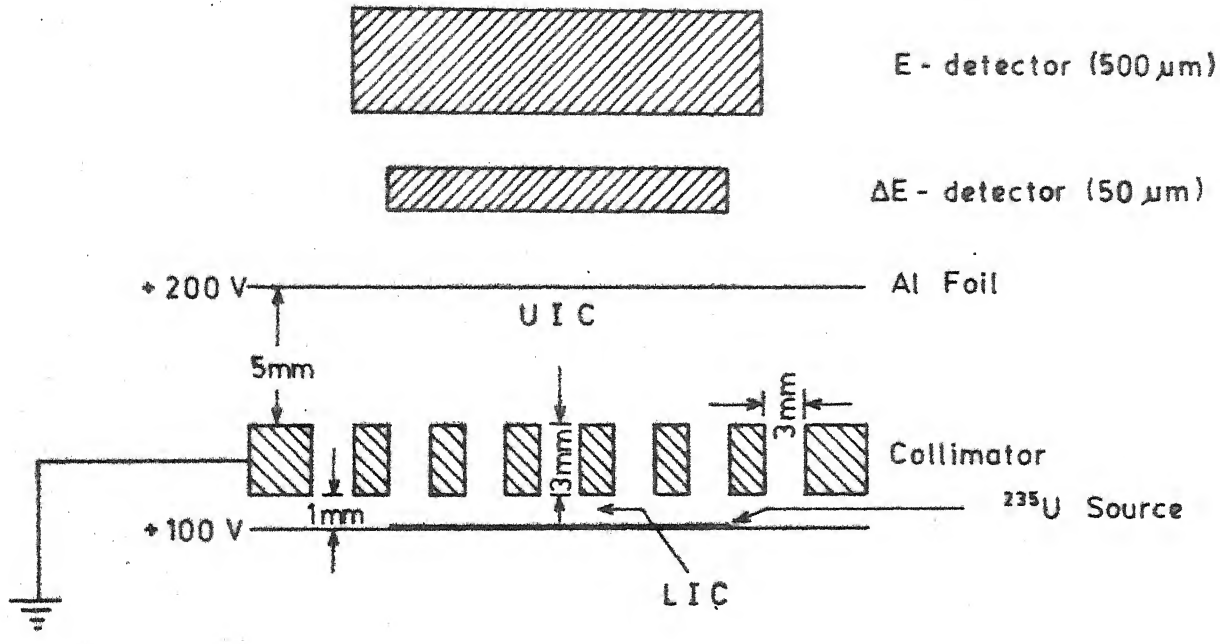

Fig. 4.1 Schematic diagram of the detection system.

of incidence of neutrons was parallel to the electric field direction. The fissile source was 93.7 % enriched ^{235}U of thickness 5 mg/cm^2 spread uniformly over an area of 4 cm^2 on a circular nickel backing.

Most of the fission fragments emanating from ^{235}U source are stopped in LIC except a few which pass through the collimator. The fission fragments which cross the collimator holes will leave a trail of ionization in the LIC and stop in the UIC, thereby giving signal from both the LIC and the UIC. The light charged particles (LCPs) are detected by a telescope consisting of ΔE and E-detectors. The method of the identification of the equatorial and the polar LCPs is illustrated in Figure 4.2, where the detection geometry with a representative collimator hole is given. As shown in Figure 4.2a, if an LCP is detected in coincidence with a fission fragment stopped in the LIC, the event is identified as an equatorial one. Thus, an equatorial event is characterized by a three-fold coincidence in the LIC, ΔE- and E-detectors. On the other hand, a polar event is recognized (Figure 4.2b) if an LCP is found to be in coincidence with a fission fragment detected in the LIC and the UIC i.e., when a four-fold coincidence in the LIC, UIC, ΔE- and E-detectors is observed.

The collimator configuration i.e., the thickness of the collimator plate, the collimator hole diameter and

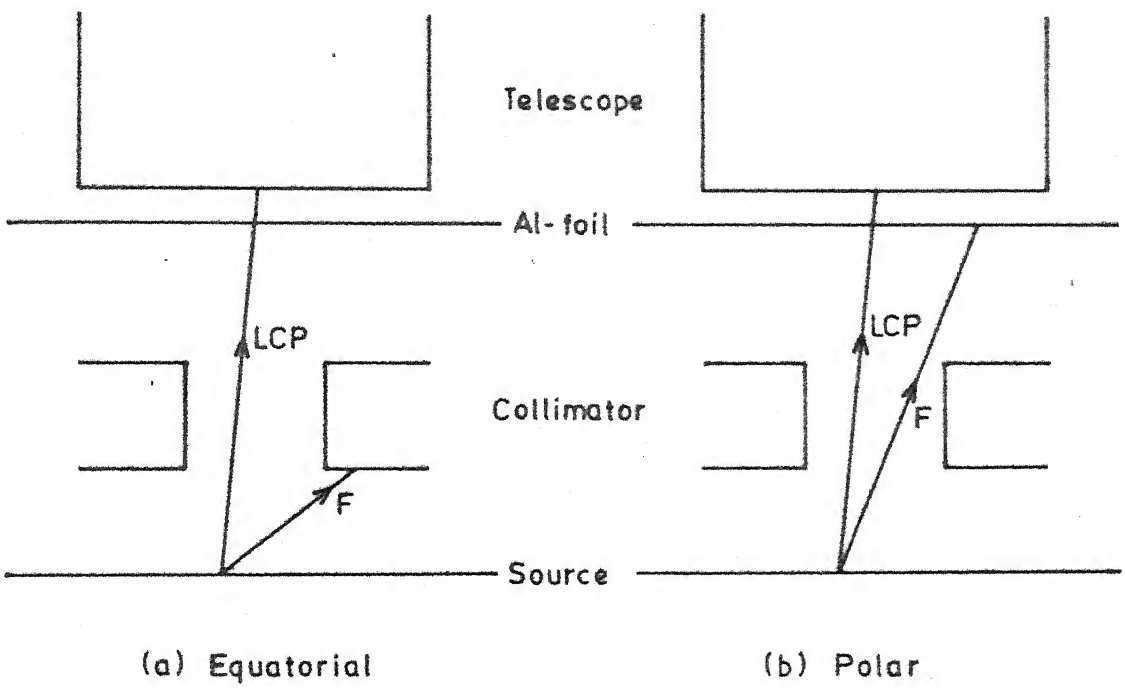

Fig. 4.2 Schematic illustration of detection of equatorial and polar events in a representative configuration.

the distance between two nearest neighbouring holes was chosen such that it fulfills two requirements.. First, the fission fragment or the LCP emitted from any point of the ^{235}U source is allowed to traverse through one and only one collimator hole. In other words, the trajectories originating from some point of the source enter the UIC region only from one hole. Secondly, the angular correlation conditions of the equatorial and the polar LCPs with respect to the fission fragments should be fulfilled. These conditions are met by choosing particular values of collimator parameters. The holes in the collimator plate were made in a hexagonal closed packing structure so that any two nearest neighbours are always equidistant. The distance of the collimator plate and the ^{235}U source (i.e., the thickness of LIC) was kept as 1 mm. The diameter of the collimator holes which was selected to be 3 mm ensured that in the event of occurrence of a polar emission, the angle substended by the LCP with fission fragment direction lies within $\pm 20^{o}$. Similarly the equatorial event also satisfies the fragment LCP angular correlation for its equatorial nature. In the present system, every collimator hole with an area of the broad source below it, gives a semblance of an independent detection system. Thus, the use of a broad area source with a multi-hole collimator satisfying aforesaid conditions, is possible in this system. The thick backing of the source allows only one

fragment to be monitored by the LIC. The LIC and the UIC signals are used to derive only the coincidence information. Any other information about the fragments was not procured.

4.3 Electronic Circuitry

The schematic diagram of the electronic set-up used in the present experiment is shown in Figure 4.3. The circuitry employs electronic modules which furnish coincidence amongst various combinations of detector signals namely the LIC, the UIC, ΔE- and E-detectors. Each detector was connected to a preamplifier and a linear amplifier. The E- and ΔE-detectors use low noise pre-amplifiers. The pulses from preamplifiers were shaped by amplifiers with a time constant of 0.5 μsec. The timing single channel analyzers (TSCA) were used to generate timing pulses from the LIC and the UIC. The timing pulses formed the inputs to a low coincidence unit which looked for a coincidence between the UIC and the LIC (which exists only for a polar event). The coincidence resolving time of this unit was determined by an overlap between its inputs. The coincidence output was algebraically added to the TSCA output from the LIC, using a Sum and Invert unit of ORTEC. The resultant would have two different levels (pulse heights) based upon the fact whether the UIC signal was present or not, as the LIC signal always exists for the equatorial as well as the polar event. This two-level logic pulse as denoted by 'F', decides the

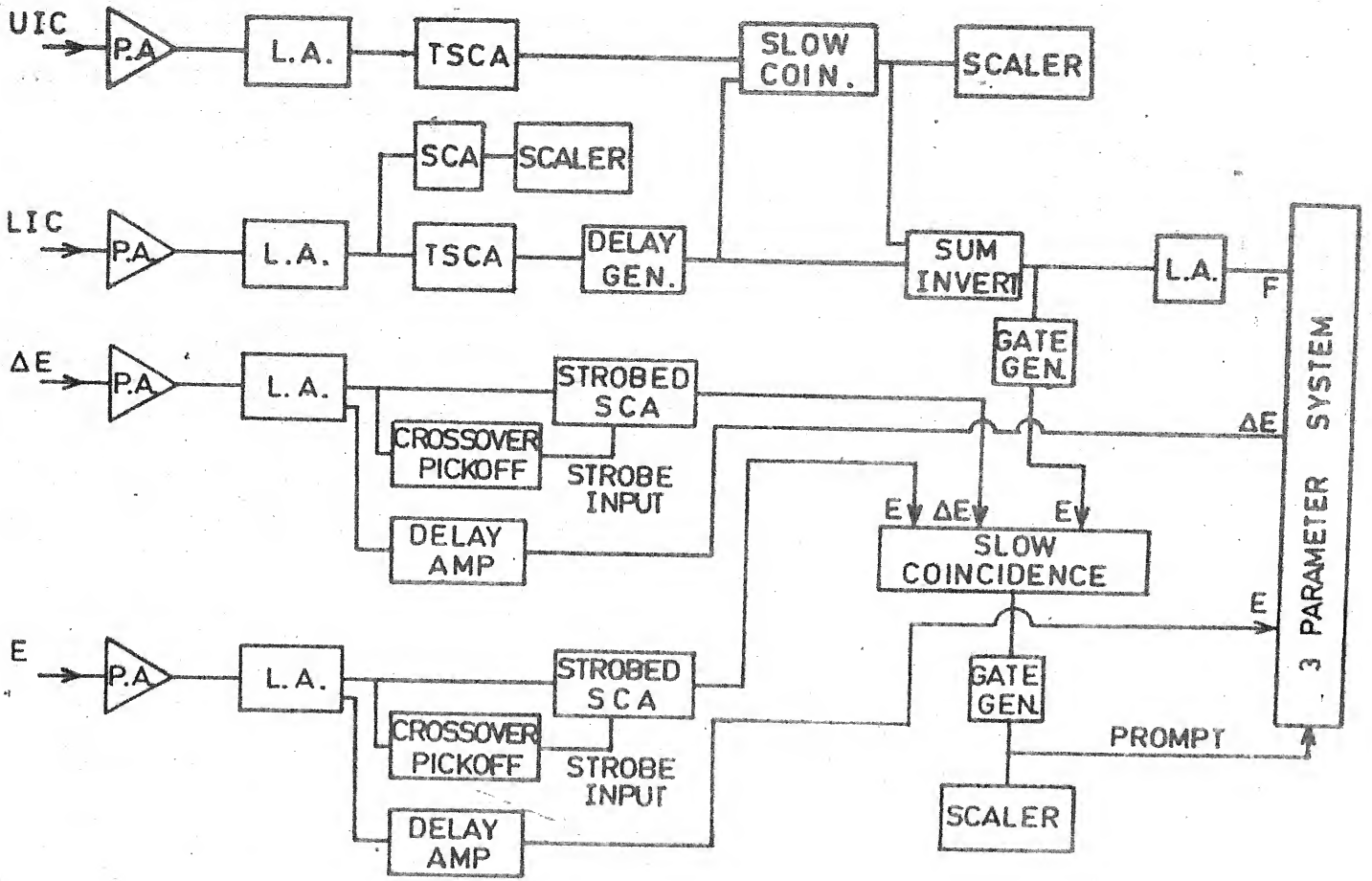

Fig. 4.3 Schematic diagram of the electronic circuit and data recording system.

equatorial or the polar character of the event, the high level corresponding to a polar event and the low level representing an equatorial event. The bipolar outputs from the Linear Amplifier of the E- and ΔE-channels were fed to a set of Crossover Pickoff and Strobed SCA, thus generating standard pulses for the E and ΔE signals. The Crossover Pickoff's produce a fast timing pulse at the instant when the bipolar pulse Crosses the time axis. The timing pulse goes to Strobed SCA as strobe input, which subsequently generates a stable timing output. The energy cut-off values in the E- and ΔE-detectors were set by lower level discriminators in the Strobed SCA. The ΔE cut-off was fixed at 0.75 MeV and that in E-detector at 1.5 MeV. The coincidence in E, ΔE signals and logic signal 'F' is achieved by a Slow Coincidence unit, the output of which generates a gate pulse of width 2 μsec. with an amplitude of -10 V. This pulse acts as the ''Prompt'' signal for the three-parameter system (3PS). The ΔE, E and F pulses coming from linear amplifier are suitably delayed with the help of Delay Amplifier modules to look for their coincidence with ''Prompt'' pulse. The information about the ΔE, E and the two-level logic pulse F (indicating the equatorial or the polar nature) is recorded by 3 ADC's event-by-event on the magnetic tape as described in Section 3.4.

4.4 Energy Calibration

The E- and ΔE-detectors were calibrated independently using a thin alpha source of ^{241}Am. The pulse height of the ORTEC pulse generator was normalized to 5.477 MeV α-particle for calibrating the 10-turn potentiometer of the pulse generator in terms of energy of the particle in MeV. Separate normalizations for both the detectors were obtained. The calibrated pulse generator was utilized for calibration of the ADCs in 3PS for the E and ΔE channels. The conversion gains of the ADCs and the gains of Linear Amplifier were so set as to get a dynamic range of 30 MeV and 10 MeV for the E- and ΔE-channels respectively. The calibration data were recorded event-by-event on the magnetic tape and were analyzed to obtain the final energy calibration. The linearity of the calibration was checked through the dynamic range of the E- and ΔE-detectors.

4.5 Experimental Procedure

The energy resolution of the E- and ΔE-detectors was measured by monitoring the ^{227}Ac spectrum. The calibration of the detectors was performed as discussed in the previous section. The energy cut-offs in the ΔE and E detectors were set electronically at 0.75 and 1.50 MeV respectively. The LIC and the UIC cut-offs were so set as to disallow the pulses due to natural alpha

particles. The LIC counts practically represented the total number of fission fragments detected in the chamber except a few below cut-off level.

The experiment was performed at 200 keV and 1 MeV neutron energies. Thermal neutron runs were interposed between all consecutive fast runs as a measure to check the consistency of the whole set-up. The calibration was performed before and after every run. A constant vigil was kept at the leakage current of detectors and an appropriate compensation was made for the increase in the leakage current. The counting rates of the following were kept track of every half an hour : neutron count-rate, fission count-rate and UIC $\wedge$ LIC ($\wedge$ sign denotes the Boolean 'AND'). The number of the equatorial events (LIC $\wedge$ E $\wedge$ E) and the polar events (UIC $\wedge$ LIC $\wedge$ E $\wedge$ E) and total number of fissions and neutrons were monitored. The constancy of the ratio of number of neutrons to number of fissions at a particular neutron energy ensured the consistency of the fission counting system and the fission bias-level in the LIC. Thermal neutron runs were taken with a thick lithium target. The fission count-rate at a proton beam current of 35 μA was about $4\text{-}5\times10^5$/min. The typical count-rates observed for the equatorial and polar LCPs were about 150/hr. and 10/hr. respectively. However, for the fast runs, the fission count-rate for the same beam current went down to a value of ~~6×10^4~~ $3\text{-}4\times10^4$/min.

and correspondingly the count-rates for the equatorial and the polar events were 8-10/hr. and 0.5/hr. respectively. Such a low counting rate of LCPs necessitated long runs for fast neutrons.

The data were recorded event-by-event on a 7-track magnetic tape in incremental mode. The three parameters recorded were the E-pulse, the ΔE-pulse and a two level flag identifying the polar or the equatorial character of the event. The data were analyzed at IBM-1800 and DEC-1090 computer at I.I.T. Kanpur.

4.6 The Monte Carlo Calculation of Detection Efficiency

The efficiency of the detection system was determined using the Monte Carlo technique. The technique uses random sampling to simulate a physical problem. A stochastic model is set up and by sampling from appropriate probability distributions, the required numerical answer to the problem is estimated.

Let p(x) be a probability density function for a variable x in the interval $a \leq x \leq b$, then

$$\xi = P(x) = \int_a^x p(x)\, dx \qquad (4.6.1)$$

Equation 4.6.1 determines x uniquely as a function of ξ, where ξ is a uniformly distributed random variable in the interval (0,1) and P(x) represents the cumulative probability distribution function. The selection of the

value of a random variable distributed according to a given probability distribution plays a central role in the Monte Carlo calculations. Incorporating the probability law which governs the behaviour of the system components and subjecting the random variables thus generated to physical constraints, the Monte Carlo method simulates on computer the processes occuring in the real experiment. The samples drawn under various contraints constitute the inferences concerning the system.

a) Method

The present computation pertains to the estimation of the relative detection efficiencies of the equatorial and the polar light charged particles by the detection system described in Section 4.2. The fission fragment and the light charged particle events are generated stochastically by employing pseudo-random numbers and the three-fold and four-fold coincidences are sought depending upon the admissibility of the events according to the geometric constraints. Figure 4.4 shows schematically the parameters involved in the detection efficiency calculations. The area of radius R_s represents the ''useful'' source area beneath the collimator hole contributing to the detection efficiency, where we have considered a single collimator hole as a

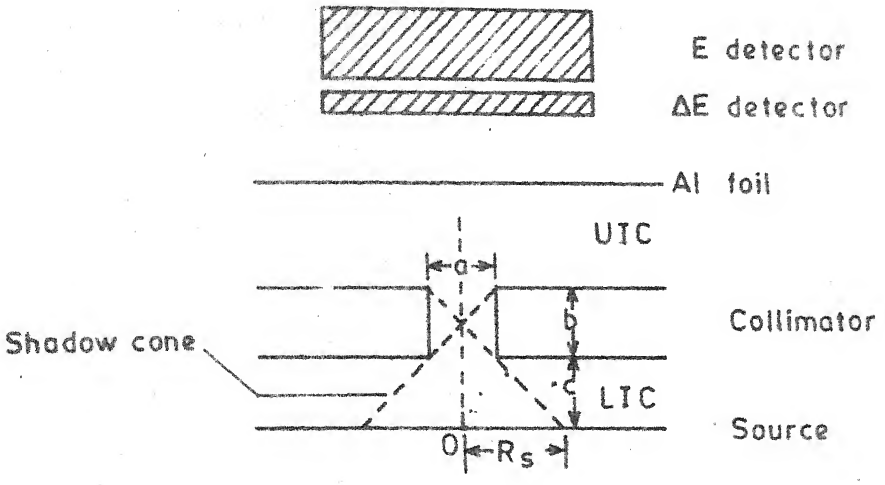

Fig. 4.4 Schematic diagram giving parameters used in detection efficiency calculation.

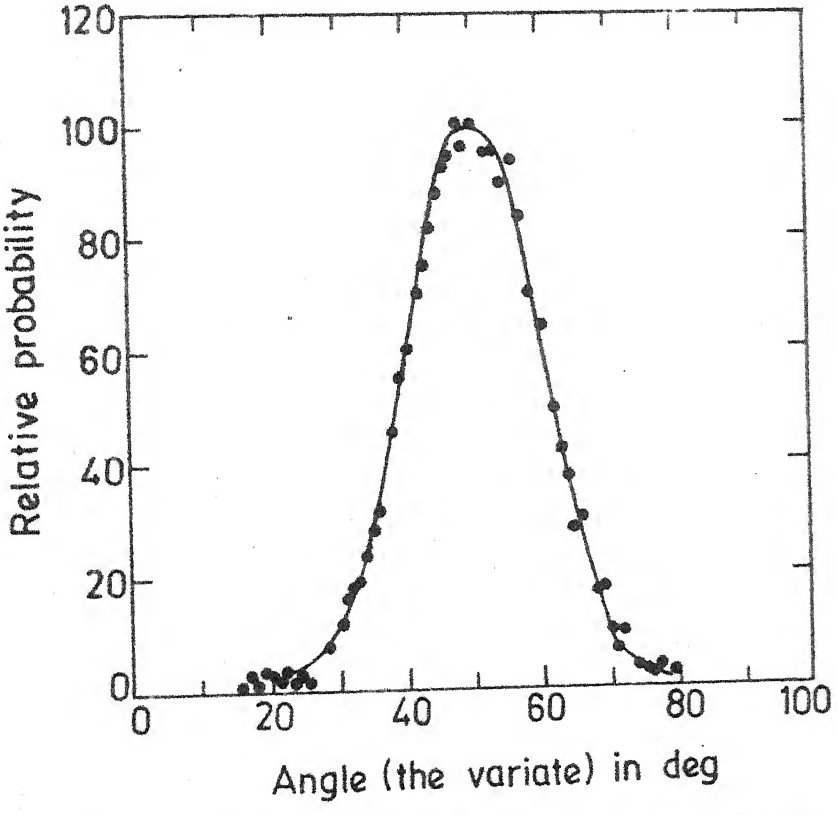

Fig. 4.5 Gaussian curve with standard deviation 10° and centered around 50° as generated by random numbers.

representative collimator hole. The flow of the sequence of the calculations is illustrated below.

The point of origin of a fission fragment on the source (circle of radius R_s below a collimator hole) is chosen by generating random coordinates (x,y) as

$$x = (2\xi_1 - 1) R_s \qquad (4.6.2)$$

$$y = (2\xi_2 - 1) R_s \qquad (4.6.3)$$

where ξ_1 and ξ_2 denote uniformly distributed pseudo-random numbers generated concomitantly and R_s represents the radius of the source. The radial distance $\sqrt{x^2+y^2}$ of the point thus generated determines whether the point is contained within the source area, otherwise it is rejected and a new set of values is tried again.

The directions θ and ϕ of the fission fragment originating from this point are selected by using another set of random variables ξ_3 and ξ_4 with an apriori assumption that the fission fragments are emitted isotropically at all solid angles in the thermal neutron induced fission. The point of emission is taken as the origin of the coordinate frame attached to the fission fragment while the normal to the source is taken as Z-axis. Since the neutron direction coincides with the Z-axis, there is an azimuthal symmetry of emission probability about this axis. Therefore ϕ_F is chosen randomly within 0 and 2π and assigned uniform probability

given by

$$\phi_F = 2\pi\xi_3 \qquad (4.6.4)$$

The angle θ_F is chosen by subjecting Equation 4.6.1 to isotropicity of emission in all solid angle elements with an assumption that only one out of the two fragments will be detected (2π-solid angle). Thus,

$$\text{Cos } \theta_F = \xi_4 \qquad (4.6.5)$$

The direction of the LCP emission is highly correlated with the fragment direction. The equatorial LCPs are emitted with an angular distribution peaking at 90° about the fission axis, if one does not distinguish between the light and heavy fragments. The angular distribution of the equatorial LCPs is known to be Gaussian with FWHM (Full Width at Half Maximum) varying from 20° to 90°. The polar LCP angular distributions are found to be peaking along the fragment direction with FWHM of 20° to 40°.

The direction of the LCP emission is defined by angles θ_α and ϕ_α in a coordinate frame with its Z-axis along the fragment direction and the origin coinciding with the point of emission. Due to symmetry about the fission fragment direction, the angle ϕ_α is generated randomly within 0 and 2π with uniform probability using the random variable ξ_5. The angle θ_α is generated from

a normal random variable t in a distribution N(0, 1) with zero mean and unit variance by taking

$$\theta_\alpha = a + \sigma.t$$

where a and σ represent the mean and variance of the distribution to be generated. The normal random variable t can be drawn from uniformly distributed pseudo-random number ξ_6 as given by[3]

$$\frac{1}{\sqrt{2\pi}} \int_{-\infty}^{t} e^{-\frac{x^2}{2}} dx = \xi_6 \qquad (4.6.6)$$

A typical LCP spectrum generated in this way is shown in Figure 4.5.

The transformation of the spherical angles from the fragment-fixed system to the space-fixed system is accomplished by using the Euler rotation matrix[4]. On six random variables chosen concurrently as above, the geometrical constraints are applied. For the fragment as well as the LCP, it is determined whether they hit the lower surface of the collimators or pass through it. This furnishes the information if the event is liable to give three or four-fold coincidence (equatorial or polar event). The distances of the points of passage through the collimator hole are calculated from the axis of the telescope. This determines whether the LCP is detected or not. This procedure is carried out for a very large number of mathematical events to simulate

the experiment. The number of such events producing the three-fold (four-fold) coincidence constitutes the relative detection efficiency of the equatorial particles (polar particles). Due to the use of a broad area source and the finite-size of the particle telescope, the collimator holes at different distances from the space-fixed axis (the axis of telescope and the fissile source) contribute differently to the detection efficiency. An average efficiency is found by assigning appropriate weight factors to different collimator holes. The simulation has been performed as described above using the known angular distributions of various LCPs as input.

The detection system does not distinguish between the light and heavy fragments. This fact has been taken into account in the efficiency calculations. The recoil of the fragments due to the LCP emission has also been taken care of. The fragments originating from the interior of the fission source suffer an energy loss particularly for grazing emissions. Therefore, a loss of some fragments is incurred due to the lower level cut-off in electronics for the ionization chamber. This effect is incorporated in the calculation of the detection efficiencies by putting a cut-off in the angle (θ_c) for the emitted fragments. The value of θ_c was chosen so as to reproduce the accepted value of the yield of the equatorial alpha particles from the calculated detection

efficiency of the alpha particles produced in the equatorial emission.

(b) The relative detection efficiencies

The relative detection efficiencies of the equatorial and the polar LCPs depend on their angular distributions which subsequently has a bearing on the relative yields of various LCPs. The Monte Carlo calculations as discussed above were performed to evaluate the relative detection efficiencies. Figure 4.6 shows the calculated detection efficiency for the equatorial and the polar LCPs as a function of the variance (second moment) of the angular distributions. The efficiencies for the equatorial and the polar LCPs are normalized with respect to the fragments detected in the lower and upper ionization chambers respectively. The detection efficiencies were determined by using the previous data of other authors. While the measurements by Raisbeck and Thomas[5] on the equatorial protons and tritons were used, the data on the equatorial alpha particles obtained by Fluss et al.[6] with significantly better angular dispersion ($\simeq 5^{\circ}$) were made use of. However, due to unavailability of any measurement in case of fast neutron induced fission, we resorted to the naive assumption that the angular correlations of the LCP with the fragments does not undergo significant

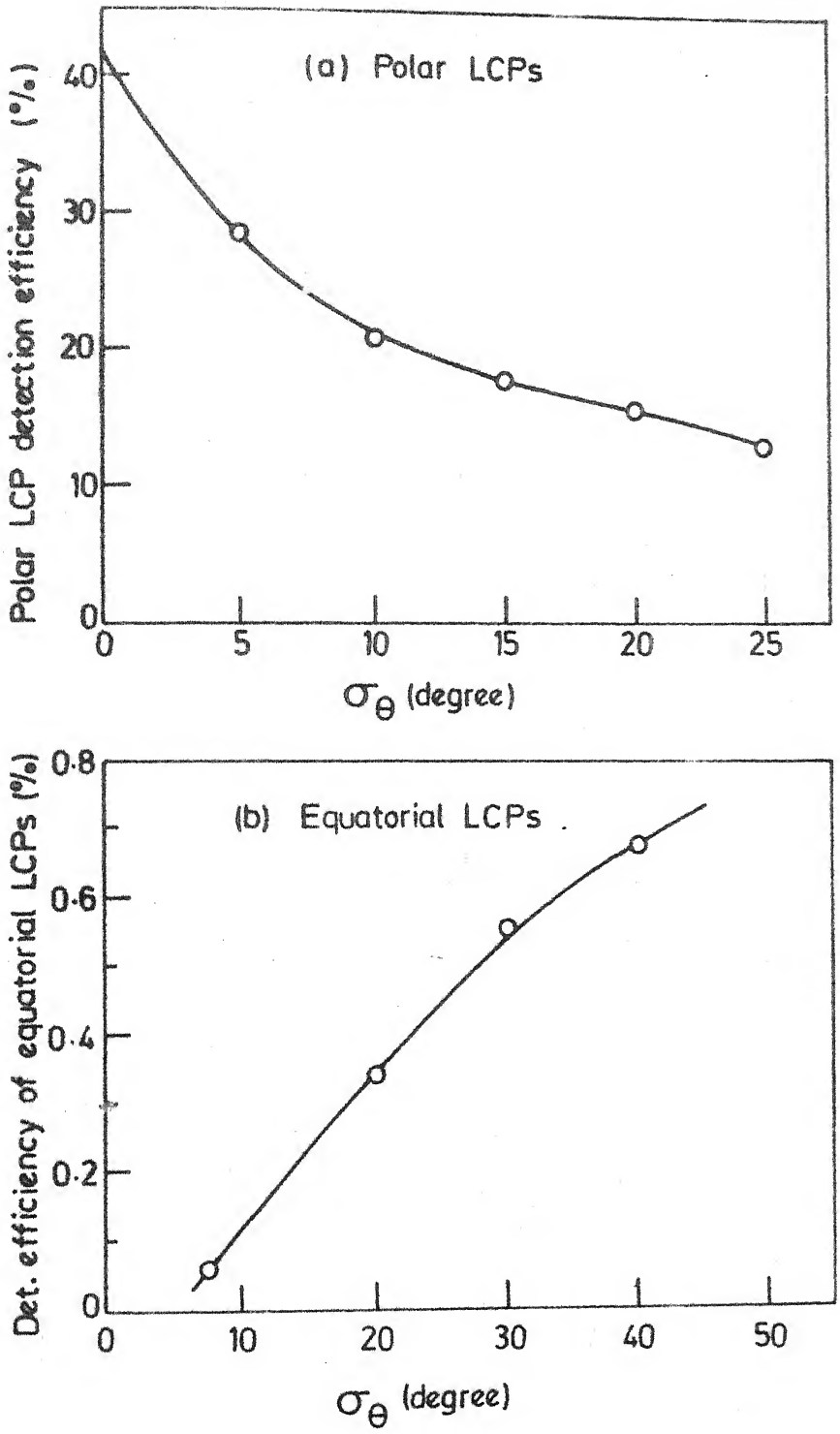

Fig. 4·6 Detection efficiencies of the equatorial and polar LCPs

change compared to thermal fission. Therefore, the detection efficiency calculations for the equatorial LCPs in fast neutron fission were made by using the same angular distributions as in thermal neutron fission. In regard to the polar emission, the angular distributions are known only very approximately. The measurements by Adamov et al.[7] and Piasecki et al.[8] were referred to while calculating the detection efficiencies of the polar LCPs.

Due to statistical nature of the calculations, the inherent error in the efficiencies are of the order 10 %.

4.7 Random Coincidence Contributions

In view of the very low count-rate of the LCPs, particularly of polar particles, it is necessary to keep a check whether there are events of the non-fission origin. The spurious contribution may arise from secondary reactions due to the prompt neutrons in fission and the neutron beam with the detector material and the aluminium foil used in the experiment. The keV neutrons used in the experiment are not expected to contribute to this due to the fact that the charged particle channels are not open at this energy.

The average energy of the prompt neutrons produced in thermal neutron fission of ^{235}U is about 2 MeV beyond

which the probability of emission falls exponentially. The cross-section of (n,p) reaction in aluminium is about few millibarns (mb) in the vicinity of this energy in comparison with a cross-section of about 100 mb for equatorial protons and about 20 mb for polar protons. Thus the expected errors due to contaminations do not seem to be negligible particularly for polar particles. However, the constraints imposed by the three-fold and four-fold coincidences for the equatorial and the polar events respectively more or less preclude the observation of such fortuitous events. The estimates on the basis of the count-rates indicate that the contribution due to chance coincidence in the equatorial and the polar LCPs is less than 1 %. In addition, the background runs with proton beam below the threshold of the neutron production were taken to see the effect of background gamma rays. The background due to such sources was found to be almost nil. The low energy pulses due to gamma background in the E- and ΔE-detectors were biased off by setting electronic cut-offs at 1.5 and 0.5 MeV respectively.

4.8 Results

The particle identification (PI) spectra of the LCPs obtained in thermal, 200 keV and 1 MeV neutron induced fission are displayed in Figure 4.7. A clear

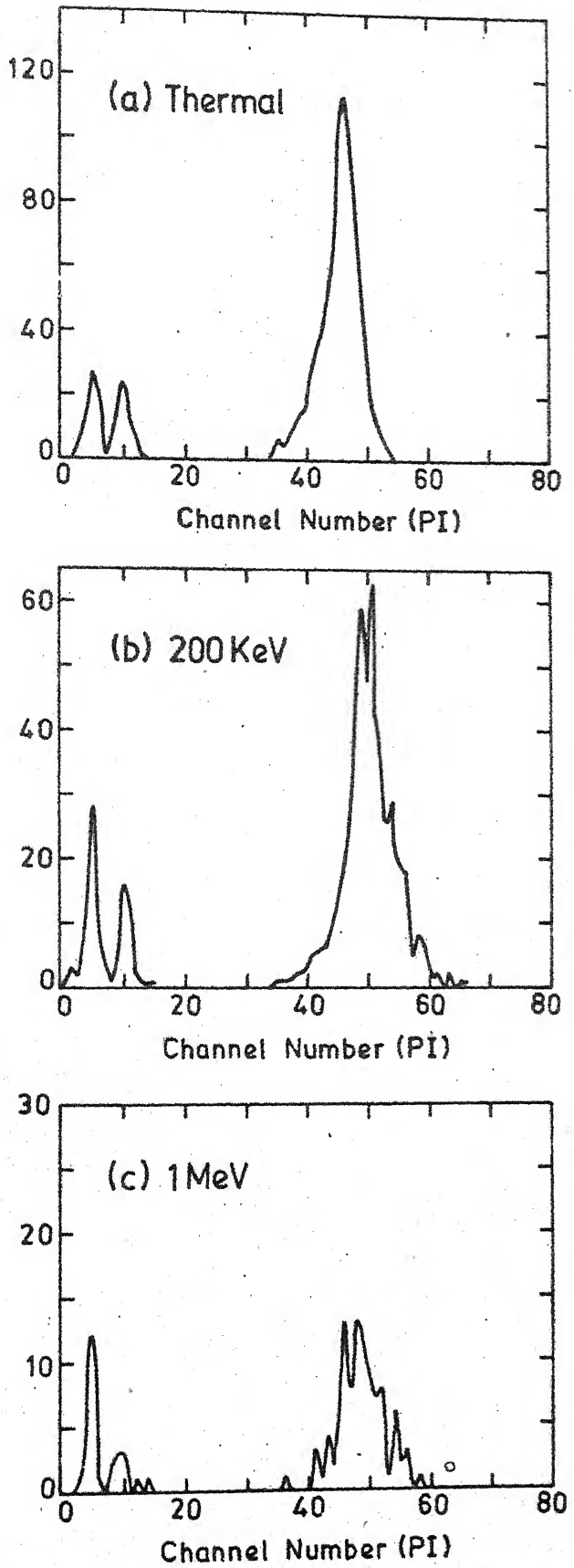

Fig. 4.7 Typical PI spectra obtained in thermal, 200 keV and 1MeV neutron induced fission.

identification of the protons, tritons and alpha particles was achieved in the PI spectra as can be seen from figure.

a) Energy distribution of the LCPs

The energy spectra of the equatorial LCPs emitted during fission at above energies are shown in Figure 4.8. The energy distributions of the alpha particles and tritons for thermal neutron fission are within one standard deviation of the known energy spectra (refer to the Table 2.1). The observed mean energies for α-particles and tritons are 14.8 ± 1.9 MeV and 8.1 ± 0.5 MeV respectively. A comparison of the energy spectra at various excitation energies indicates that there is no perceptible change in the mean values and variances of energies in going from thermal to the fast neutron runs.

The proton energy spectrum should not be taken too seriously because of insufficient depletion depth of the E-detector used in our experiment. The telescope stops completely the protons only upto energy about 10 MeV and the ones with energy above 10 MeV suffer only a partial absorption of the energy.

The polar LCP measurements have so far been confined to the thermal neutron induced fission. The energy spectra of the polar LCPs have been studied[1] and the energy distributions in case of these LCPs have been found to be higher than the equatorial LCPs as discussed

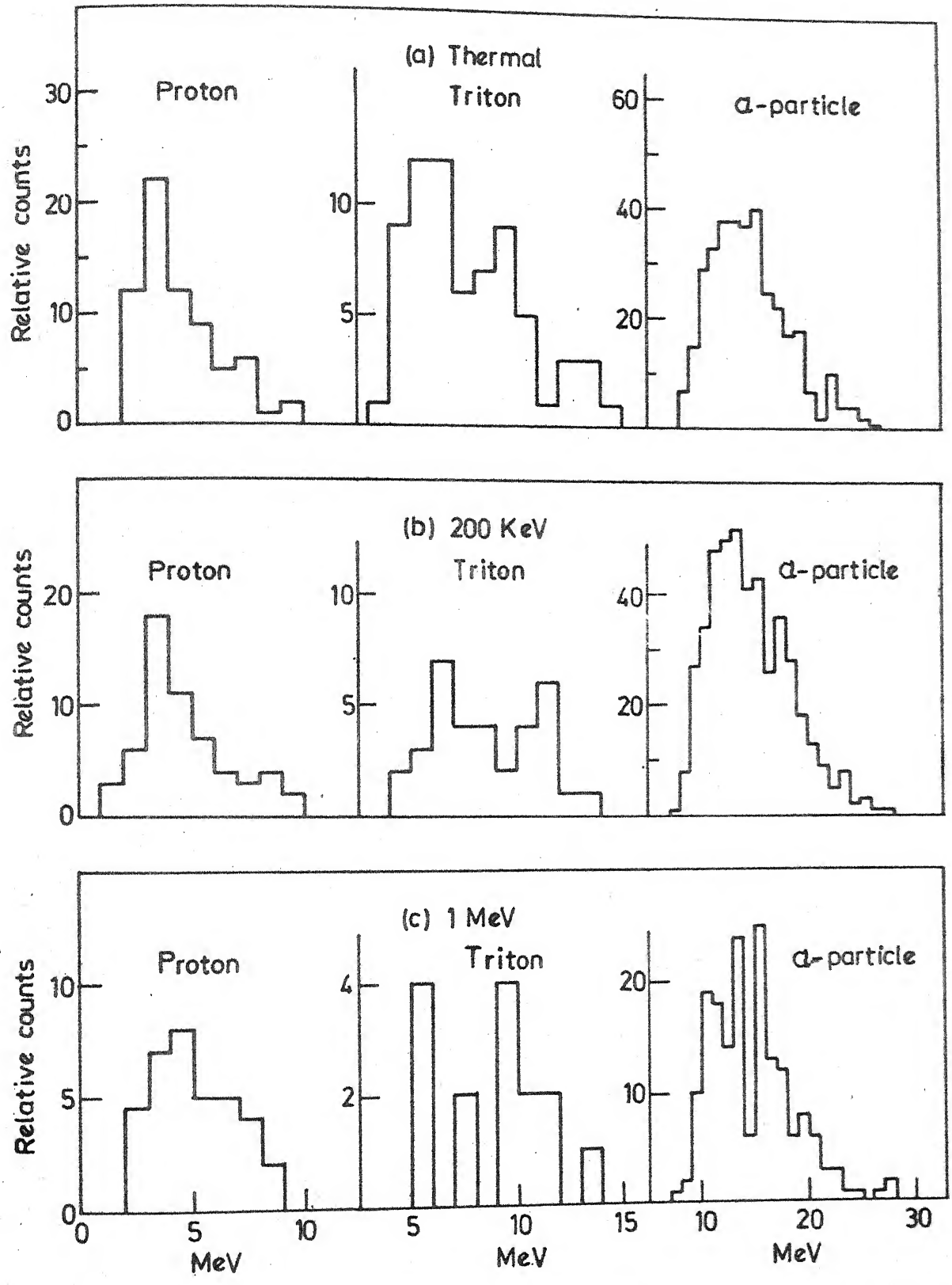

Fig. 4-8 The energy spectra of equatorial LCPs at various neutron energies.

in Section 2.3. The mean energy of the polar alpha particles in our experiment for thermal neutron induced fission are consistent with the previous measurements[1]. We have not presented the spectra due to low statistics. However, for the sake of comparison between the equatorial and the polar alpha particles in thermal neutron fission we produce the observed energy distributions in Figure 4.9. A distinct difference is visible between the two spectra which demonstrates that our technique is unambiguous in identifying the equatorial and polar LCPs in a single experiment. The previous measurements[13-15] have found that the energy distribution of the polar LCPs are twice as narrow as the equatorial ones (Refer to Table 2.2). The energy distribution of the polar alpha particles is broader in our experiment. This can be ascribed to the energy angular correlations[12] for the LCPs in the polar region as the energy spectrum is contributed by the alpha particles in the polar region from 0^{o} to 35^{o} about the fission axis in the present experiment, whereas in the previous measurements[13-15] the acceptance angle was within a narrow cone about the fission axis.

b) <u>The relative intensities of the LCPs</u>

The relative yields of the equatorial and the polar LCPs were determined using the relative detection efficiencies as calculated in the preceding section.

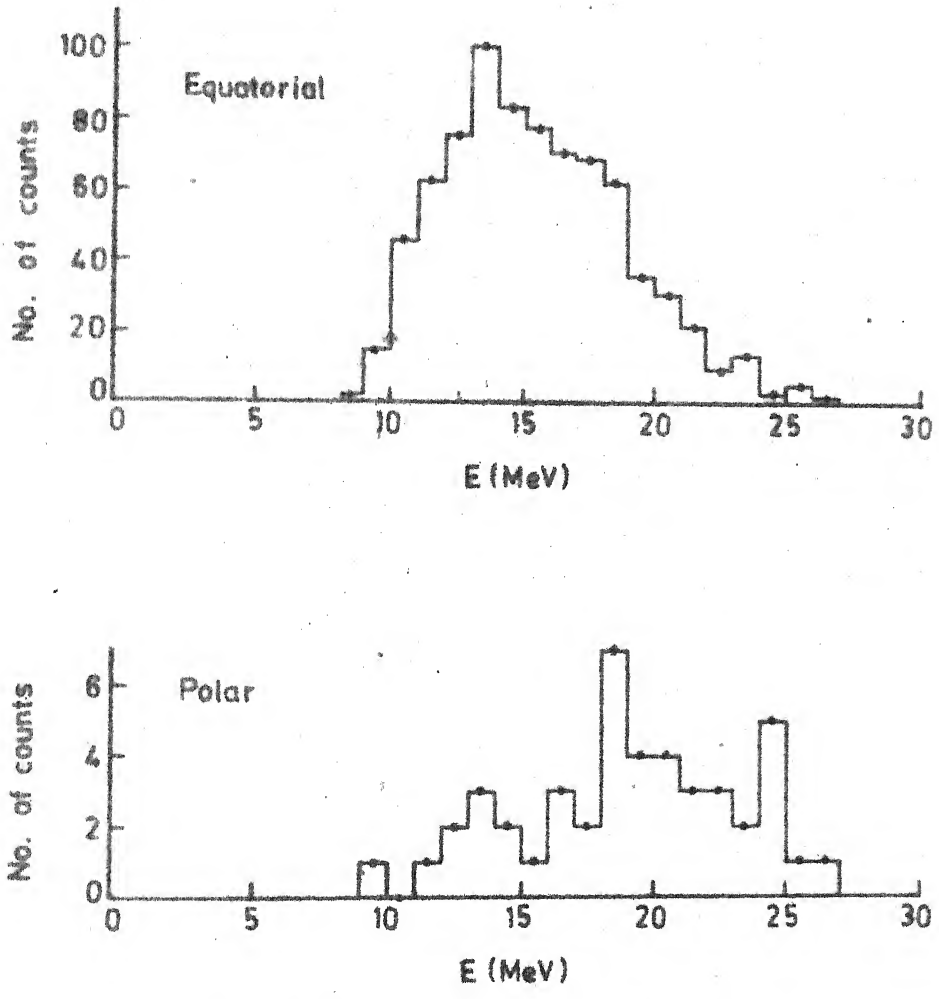

Fig. 4.9 Energy spectra of equatorial and polar α-particles

Table 4.1 summarizes the relative yields of the equatorial LCPs at thermal, 200 keV and 1 MeV neutron energies and correspondingly the relative yields of the polar LCPs are presented in Table 4.2. The yields have been normalized relative to an alpha particle intensity of 100 for thermal run, the normalization being done independently for both the equatorial and the polar LCPs. It can be seen from Table 4.1 that the triton yield relative to the alpha particles agrees with the known value for thermal neutron fission (Refer to Table 2.1) within the errors. The yield of equatorial protons relative to alpha particles in our measurement is 2.8 ± 0.3 in comparison to 1.5 to 2 % observed earlier[17].

Table 4.1 : The relative intensities of the equatorial LCPs at various neutron energies.

Particle	Thermal neutron fission	200 keV neutron fission	1 MeV neutron fission
^{1}H	2.8 ± 0.3	4.0 ± 0.7	6.5 ± 0.9
^{3}H	8.7 ± 0.9	8.0 ± 1.4	11.9 ± 2.3
^{4}He	100 ± 3.1	101 ± 4.9	101 ± 6.4

Table 4.2 : The relative intensities of the polar LCPs at various neutron energies.

Particle	Thermal neutron fission	200 keV neutron fission	1 MeV neutron fission
^{1}H	21.9 ± 4.4	22.8 ± 5.3	47.1 ± 13.3
^{3}H	14.5 ± 2.8	16.7 ± 8.3	43.5 ± 17.4
^{4}He	100 ± 12.2	80 ± 17.5	126 ± 29.2

The yield ratios of various LCPs in 200 keV and 1 MeV runs with the thermal run are presented in Table 4.3.

Table 4.3 : Comparative study of the equatorial and the polar LCPs.

LCP	200 keV/thermal		1 MeV/thermal	
	Equatorial	Polar	Equatorial	Polar
^{1}H	1.45 ± 0.25	1.05 ± 0.39	2.31 ± 0.41	2.14 ± 0.74
^{3}H	0.93 ± 0.19	1.15 ± 0.67	1.40 ± 0.30	3.04 ± 1.55
^{4}He	1.01 ± 0.05	0.80 ± 0.20	1.01 ± 0.07	1.26 ± 0.32

The errors indicated in Tables 4.1, 4.2 and 4.3 are entirely of the statistical origin. The uncertainty in detection efficiencies due to errors in the angular distributions have not been included in Tables 4.1 and 4.2. However, it must be mentioned that the yield ratios at 200 keV and 1 MeV compared to the thermal fission (Table 4.3) are free of uncertainties in the detection efficiencies. This is, of course, with the assumption that a little change in the excitation energy at 200 keV and 1 MeV compared to the thermal neutrons will not alter significantly the angular correlation between the LCP and the fragments. As will be discussed in Chapter 5, higher excitation energy may result in a small change in the width of the LCP angular distribution about fission axis, but the effect of this on the yields will be within the statistical errors in our experiment. The results will have to be appropriately modified if a significant change in the LCP-fragment correlations are observed for the equatorial and the polar LCPs.

The information on the angular anisotropy of the ternary fragments and the LCPs about the neutron direction is, at present, conflicting as we will discuss in Chapter 5. Therefore, the effect due to this in our calculations was not incorporated. We will investigate this aspect experimentally in the following chapter. However, the estimates show that upto a maximum of 7 % decrease

in the equatorial efficiency will occur if the fragment anisotropy increases by 17 %. in forward directions as observed in the case of binary fission.

An examination of Table 4.3 reveals that at 200 keV neutron energy, the yields of the equatorial and the polar alpha particles and tritons do not show appreciable change as compared to the thermal fission[9]. The equatorial proton yield shows a small increase at 200 keV. At 1 MeV neutron energy both the equatorial and the polar protons exhibit an increase, but in case of tritons the errors are large. The alpha particles, however, do not seem to show much variation in the yields at higher excitation energies.

4.9 Discussion

A comparison of the results at 200 keV and 1 MeV neutron energies brings out the observation that there is a similarity in the variation of the equatorial and the polar LCPs in going from thermal to higher energies upto 1 MeV. Also, there is definitely an increase in the equatorial and the polar yields of protons at 1 MeV in contrast to the near constancy (within errors) of the alpha particle and triton yields both in the polar and the equatorial modes of emission. The alpha particles seem to retain the same trend at 200 keV as in 1 MeV neutron fission. However, Sharma et al.[10] reported an

increase of about 20 %. in the yields of the equatorial alpha particles at 200 keV neutron energy compared to thermal neutron fission. They used a 2π-geometry where the detection of the fragments was uninhibited in all directions. Besides, the neutron energy spread in their measurements was small. Our measurement, on the other hand, do not indicate any increase but the present results can not be directly compared with the results of Reference 10 due to basically different detection geometries. The masking of the 20 %. increase in the alpha particle yield could be attributed to the anisotropy of the ternary fragments and the LCPs about the space-fixed axis notwithstanding the preferential detection of the ternary fragments off the neutron direction. The large anisotropy ($\simeq$90 %.) of the LRAs around 200 keV perpendicular to the neutron direction as will be reported in the next chapter, would imply a similarly large anisotropy of the associated fragments peaking along the neutron direction. This factor could be responsible for the constancy of the alpha particle yield at 200 keV in our measurements in contrast to a 20 %. increase observed by Sharma et al.[10] compared to the thermal neutron fission.

In the earlier measurements[2,11] in our laboratory on the polar and the equatorial LCPs in 600 keV neutron induced fission of ^{235}U, the protons both the equatorial

and the polar type, were found to indicate a large increase compared to the thermal neutron fission. The alpha particles did not show any significant variations. The results demonstrated the identical behaviour of the alpha particles as in the present work. Therefore, a fact emerges that the alpha particle yield is not very sensitive to the excitation energy. The tritons also seems to behave in the same way as the alpha particles, although they show an increase at 1 MeV compared to thermal fission but the errors for tritons yields are large in our measurement. The tritons and alpha particles, thus, can be treated as exhibiting the similar behaviour at higher excitation energies. This behaviour is apparent both in the equatorial and the polar emissions. As will be discussed in Chapter 6, our results on the angular distributions of the polar tritons and alpha particles also show a similarity.

A comparison of the yields of the equatorial and polar LCPs at 200 keV and 1 MeV as compared to the thermal neutron fission enunciates a similarity in the variations in the yields with neutron energy. The present results further strengthen our earlier conclusion[11] as to the similarity in the variations of the equatorial and the polar LCPs with excitation energy.

REFERENCES

1. E. Piasecki and L. Nowicki, Proc. Symp. on Phys. and Chem. of Fission (Jülich, 1979), Vol. 2, (1980) 193.
2. A.K. Sinha, M.M. Sharma, S.C.L. Sharma, G.K. Mehta and D.M. Nadkarni, Nucl. Phys. and Solid State Phys. Symp. (India) 23B (1980).
3. I.M. Sobol, ''The Monte Carlo Method'', Mir Publishers, Moscow (1975).
4. H. Goldstein, ''Classical Mechanics'', Addison - Welsley (1980) p. 109.
5. G.M. Raisbeck and T.D. Thomas, Phys. Rev. 172 (1968) 1272.
6. M.J. Fluss, S.B. Kauffmann, E.P. Steinberg and B.D. Wilkins, Phys. Rev. C7 (1973) 353.
7. V.M. Adamov, L.V. Drapchinsky, S.S. Kovalenko, K.A. Petrzhak, L.A. Pleskacheosky and I.I. Tyutyugin, Phys. Lett. 48B (1973) 311.
8. E. Piasecki and J. Blocki, Nucl. Phys. A208 (1973) 381.
9. M.M. Sharma, A.K. Sinha and G.K. Mehta, Nucl. Phys. and Solid State Phys. (India) 25B (1982).
10. S.C.L. Sharma, G.K. Mehta, R.K. Chowdhury, D.M. Nadkarni and S.S. Kapoor, Nucl. Phys. A355 (1981) 13.
11. A.K. Sinha, M.M. Sharma, S.C.L. Sharma, G.K. Mehta and D.M. Nadkarni, J. Phys. G : Nucl. Phys. 8 (1982) L85.

12. D.E. Cumpstey and D.G. Vass, Proc. Symp. on Phys. and Chem. of Fission (Jülich, 1979), IAEA, Vienna (1980) Vol. 2, p. 223.

13. V.N. Andreev, V.G. Nedopekin, and V.I. Rogov, Yad. Fiz. 25 (1977) 732.

14. E. Piasecki, M. Sowinski, L. Nowicki, A. Kordyasz, E. Cieslak and W. Czarnacki, Nucl. Phys. A255 (1975) 387.

15. L. Nowicki, E. Piasecki, J. Sowolewski, A. Kordyasz, M. Kisielinski, W. Czarnacki, H. Karwowski and P. Koczon, Nucl. Phys. A375 (1982) 187.

16. S.L. Whetstone, Jr. and T.D. Thomas, Phys. Rev. 154 (1967) 1174.

CHAPTER V

ANGULAR DISTRIBUTION OF LONG-RANGE ALPHA PARTICLES IN FISSION

5.1 Introduction

Light charged particle (LCP) accompanied fission represents an interesting phenomenon in the study of the fission process. It is a potential source of information about the configuration of the fissioning nucleus at the instant of scission and the subsequent dynamics of the fission. The striking feature of the LCP emission as discussed in Chapter 2 is that their angular distribution is strongly peaked perpendicular to the fission fragment direction. It has been concluded on the basis of the energy and angular distributions of these particles that they are emitted from the space between the fission fragments at time close to that of the snapping of the neck (the scission point). Several hypotheses on the emission mechanism of LCP viz., the pre-scission evaporation model[1], the post-scission emission model[2], the sudden snap model[3] and the statistical model[4] are in vogue. However, none of them is able to account for all the

observed characteristics, and it is not yet established whether the LCPs are born before or after the scission.

The experiments[5-14] on the angular distribution of the light charged particles about the fission-axis and other multidimensional correlations have yielded some information on the configuration of the nucleus at the scission point. A large body of trajectory calculations[1] have been performed which study the motion of the three charged bodies in their mutual Coulomb field. However, there is always an uncertainty in locating the scission point in these calculations which reflects in the non-uniqueness of the information derived about the dynamical variables at scission. Moreover, this does not shed much light on the basic mechanism of the LCP emission. The angular distribution of LCPs about the space-fixed axis (incident projectile direction) could provide valuable information on the emission mechanism of these LCPs. This aspect of the LCPs is not studied well. The present work is an effort to understand the LCP emission mechanism in the light of anisotropy about the incident projectile direction as described in this chapter. Section 5.2 gives the review of the existing works on this aspect. The next section describes the experimental technique used in the experiment to discern the angular distribution. Section 5.4 presents the details of the data analysis

employing the Monte Carlo calculations and the method of determining the anisotropy of the angular distributions. In Section 5.5, we describe the results of the above measurements and the last section presents the discussion of these results in the perspective of emission mechanism.

5.2 Review of the Existing Situation

Considerable amount of efforts have been invested in the past to study various features of the ternary fission process in the thermal neutron-induced fission of ^{235}U and the spontaneous fission of ^{252}Cf. The experiments on the binary and ternary fissions have revealed that the ternary fission possesses all the characteristics of binary fission except for some minor differences due to the energetics. However, the physics of the ternary fission is not very clear, which is evidenced by the existence of various models as mentioned in the foregoing section. The pre-scission model of Ramanna et al.[1] contends that the LCP is evaporated from the excited fissioning nucleus between the saddle point and the scission point. In the sudden snap model advanced by Halpern[3], the LCP is left behind during the sudden collapse of the neck of the elongated nucleus, and the probabilities of the emission of different LCPs depend upon the different amount of energy required to emit the particles. According to the statistical model[4], at any instant during the

descent of the nucleus from the saddle to the scission point, there exists a statistical equilibrium. The probability distribution of various parameters of the fragments such as the fragment masses, excitation energies and the angular distributions are a direct consequence of equilibrium at scission. The probability of ternary fission relative to the binary fission is evaluated from the phase-space available to both types of fission. The measurements on the properties of ternary fission have not thrown much light on the basic mechanism of the ternary fission. Attempts have been made to study the angular distribution of LCPs about the fission axis at higher excitation energy[21]; but the LCP-fragment correlation has been observed to be insensitive to excitation energy except for some change in width of the angular distribution compared to that in thermal neutron-induced fission.

The angular distribution of binary fission fragments in neutron-induced fission near the fission threshold exhibits a forward peaking about the incident neutron beam. The behaviour of the ternary-fragment angular distribution is unclear and has not been studied well. The existing experiments have yielded conflicting results. The behaviour of the LCP angular distribution is expected to depend upon the fact whether the LCP-emission takes place before or after the scission. The angular distribution of the ternary fragments and the LRA's (long-range alpha-particles,

the major constituent of LCPs) in 14 MeV neutron-induced fission of ^{238}U was explored by Ramanna et al.[1] using the emulsion-technique. They observed that the LRA distribution was peaked fore and aft along the beam direction and the associated fragments were peaked at 90° to the beam direction. This behaviour of ternary fragments was opposite to the behaviour of fragments in binary fission. The result seemed to indicate that the ternary fission process was distinctly different from the binary fission. They argued that this is the characteristics of the particles evaporated from the compound nucleus having a large angular momentum. The anisotropy observed was much larger than predicted by the statistical theory of evaporation of particles and was ascribed to the neutron emissions from the compound nucleus before alpha emission. All other characteristics of the fission, such as kinetic energy distribution, mass distribution etc. are known to be very similar in the two cases of the binary and ternary fissions (LCP-accompanied fission). In another measurement, 17.5 MeV proton-induced fission of ^{238}U, Atneosen et al.[27] observed that the ternary fission fragments have nearly the same 0°-peaked angular distribution as the binary fission fragments. The results of Ramanna et al.[1] and Atneosen et al.[27] are contradictory to each other besides having a substantial contribution from second and third chance fissions. The observed angular distribution arises

from contribution due to a number of nuclides fissioning at different excitation energies. In yet another work, Nadkarni[28-29] performed the measurements on the angular distributions of ternary fission fragments and the LRA's about the neutron beam direction in 3 MeV neutron induced fission of ^{235}U. Again, the ternary fragment anisotropy was found to be opposite from that of binary fragments. It is worth noting that even at higher excitation energies, the alpha-fragment angular correlation does not undergo any major change and the perpendicularity of the LRAs to the fission axis is preserved. The results of Ramanna et al.[1] and Nadkarni[28-29] are similar and they have proposed that the LRA emission takes place as an outcome of evaporation before the scission point. There exists an inconsistent picture on the angular distribution of the ternary fission and the question remains whether the LRAs are emitted before or after the scission. There is, at present, no data available on the angular distributions of the LRAs or ternary fragments which could ascertain the behaviour of ternary fission in an unambiguous manner. It is, therefore, desirable to measure the angular distribution at lower energies to arrive at more definite conclusion. The angular distribution of LCPs about the space-fixed axis (incident neutron direction) is expected to bring about a change in anisotropy (isotropic distribution in thermal fission) in going from thermal to

energetic neutrons. The trend of the anisotropy could offer valuable information on the emission mechanism of these LCPs.

5.3 Angular Distribution of the Light Charged Particles Using a Particle Telescope

The low probability of occurrence of the ternary fission, particularly for fast neutrons, makes it difficult to investigate the angular distribution of LRAs using the conventional techniques. We have developed a technique[32] which employs a simple ΔE-E semiconductor telescope to extract the angular information of the particles incident on it, with respect to the telescope-axis.

(a) Technique

A semiconductor detector particle telescope consists of a thin ΔE-detector in conjunction with an E-detector. The particle incident upon the ΔE-detector loses a small fraction of its energy, ΔE, during its passage through it, the remainder being absorbed subsequently in the E-detector. The energy loss ΔE depends upon the attributes of the particle viz., charge, mass and the initial energy. It is also dependent upon the angle of incidence about the normal to the detector. The energy-losses in the ΔE and E-detectors serve to identify

uniquely the charged particle species by utilizing the particle identification function (PI) due to Goulding et al.[30].

The energy loss in the ΔE-detector is proportional to the thickness Δx of the detector for normal incidence. However, if the particle is incident on the telescope at an angle θ with the telescope axis, it suffers an energy-loss proportional to the slant thickness traversed in the ΔE-detector (Figure 5.1). Therefore, the ΔE-signal carries an information pertaining to the angle θ as given by the relation

$$\text{Cos } \theta = \frac{\Delta x}{\Delta x'} \qquad (5.3.1)$$

where θ, Δx and $\Delta x'$ are the parameters as illustrated in Figure 5.1. The problem of determining the angle θ reduces to finding $\Delta x'$ using the known parameters namely ΔE, E and the normal thickness Δx of the ΔE-detector. The range-energy tables[31] for light charged particles in the detector material being known quite accurately, one can use them to obtain $\Delta x'$ and thus the value of θ can be found from Equation 5.3.1.

The technique was tested by demonstrating the isotropicity of the angular distribution of the long-range alpha particles emitted in thermal neutron-induced fission of ^{235}U. The method enables the use of a broad-area source and allows a 2π-symmetry of detection. It

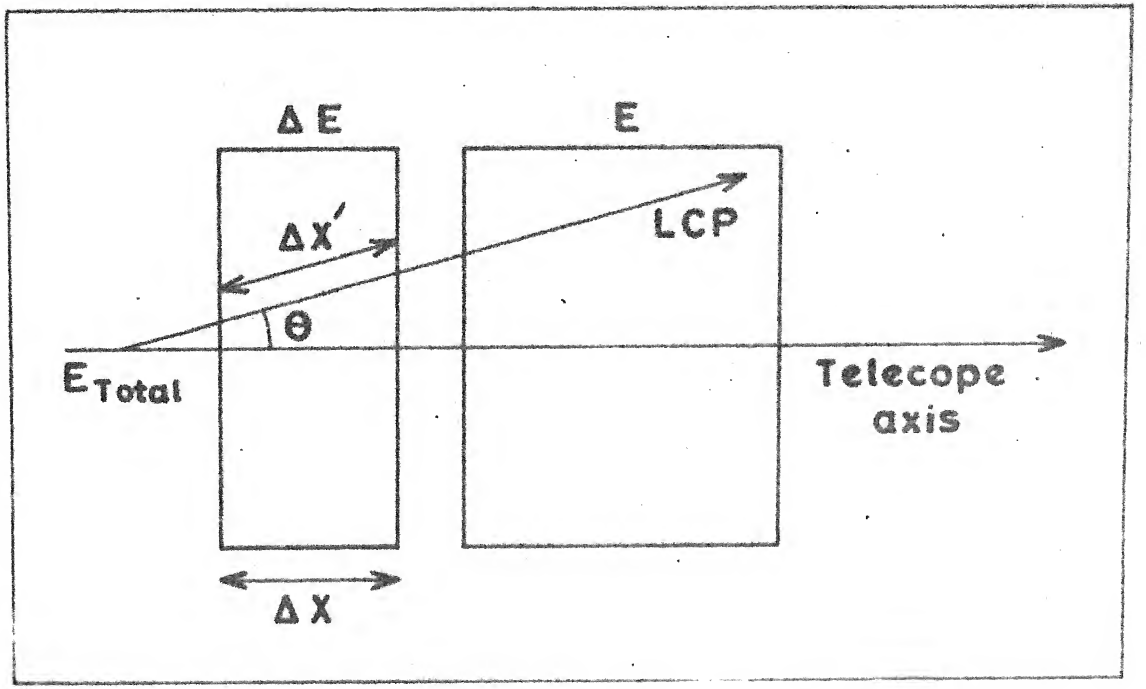

FIG. 5.1 Schematic diagram of the proposed technique employing particle telescope.

is, thus, especially suitable in the study of rare processes such as the LCP-emission in fast neutron fission. Further, it is capable of determining the angular distribution of various light particles simultaneously because it employs a particle telescope.

(b) Experimental details

The detection geometry of the experiment is shown in Figure 5.2. A fissile source of ^{235}U having an area of 400 mm^2 and thickness 5 mg/cm^2 was used. The telescope used consists of a 500 μm thick surface-barrier E-detector and a totally depleted ΔE-detector of thickness 50 μm. Both the detectors have an active area of 300 mm^2. The axis of the telescope was along the direction of the neutron beam. An aluminium foil was placed before the telescope to stop the fission fragments and the natural alpha particles from reaching the particle telescope. The neutrons were generated as discussed in Section 3.2. The distance of the ^{235}U source from the neutron producing target was such that the neutron divergence was $\leq 10^{o}$. The data were recorded at the following neutron energies : thermal, 140 ± 30 keV, 170 ± 25 keV, 200 ± 25 keV, 400 ± 200 keV, 600 ± 180 keV and 1000 ± 170 keV. The large spread at higher energies was due to the use of a 6 Ci tritium target. The data were recorded event-by-event on a magnetic tape using a 3-parameter data-acquisition

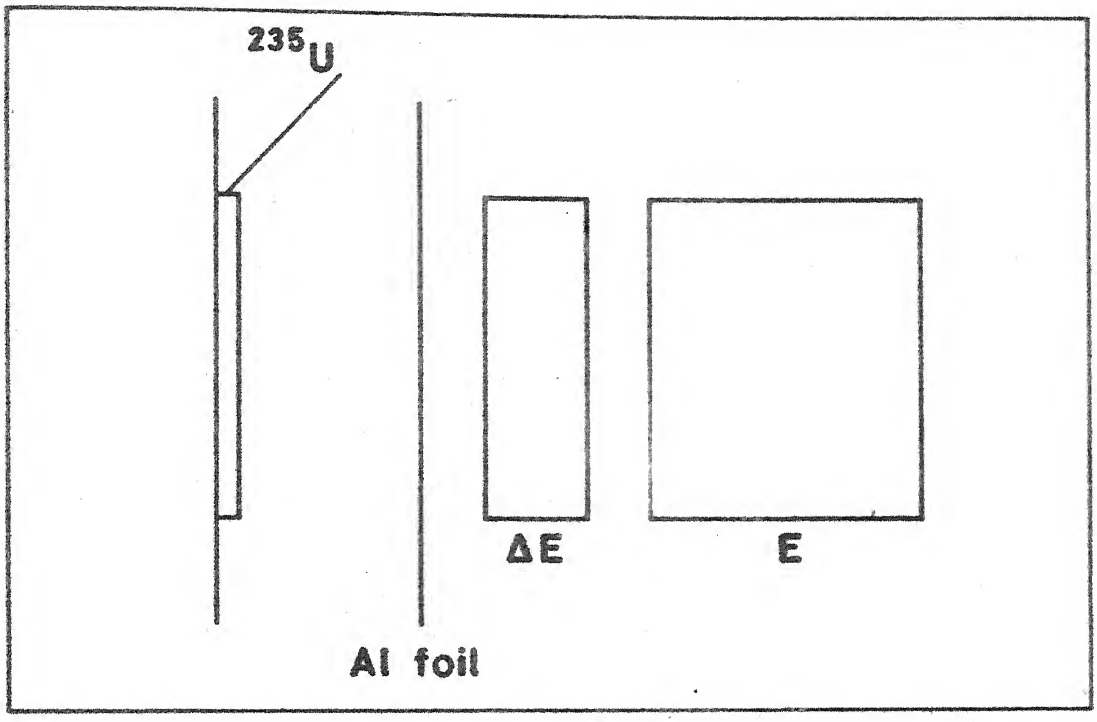

FIG. 5.2 The geometry of the detection system

system described in Section 3.4 and the analysis was done off-line on DEC-1090 computer.

5.4 Data Analysis

The expected angular distribution for a point source (isotropic emission) in thermal neutron-induced fission would be rectangular with a sharp cut-off angle as shown in Figure 5.3. However, due to the use of broad-area source to help in overcoming the count-rate problem, the contribution to the angular distribution arises from every point of the source. This causes a smearing in the measured angular distribution. The actual angular distribution can be disentangled from the experimental one by the Monte Carlo simulation of the experimental geometry.

(a) Monte Carlo calculation

The Monte Carlo calculations of the angular distribution for the broad-area source assuming the isotropic emission were performed. Figure 5.3 shows the calculated angular distribution of long-range alpha particles for the point source and the actual broad source used in our experiment. The expected and the experimental angular distribution using Equation 5.3.1 for thermal neutron induced fission are displayed in Figure 5.4. The experimental angular distribution exhibits excellent agreement with the calculated one except for

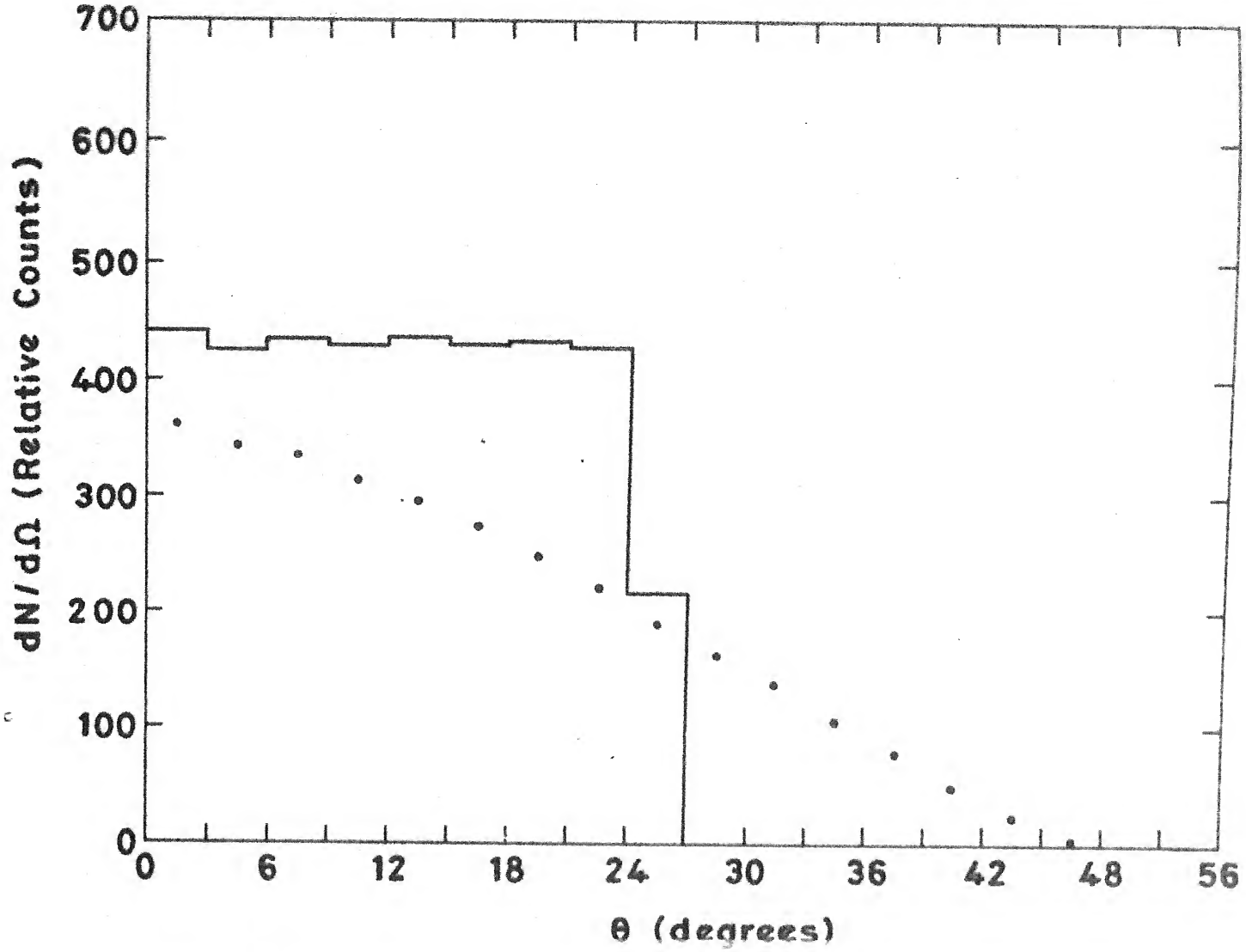

FIG. 5.3 The calculated (Monte Carlo) angular distribution for a point source and a broad source.

very small angles. The Cosθ term evaluated from Eqn. 5.3.1 contains the errors contributed by the uncertainty in the ΔE-detector thickness, detector resolutions and a small contribution due to the particles undergoing channeling in the detector crystal. The channeling effect, however, is small as there are only a few directions in the crystal lattice along which this is possible and therefore would be statistically insignificant. The uncertainty in the angle θ is maximum around $\theta \simeq 0^{\circ}$ because of 1/Sinθ term in solid angle evaluation. At larger values of θ, the error is small ($\simeq \pm 3^{\circ}$). Thus the technique offers reasonably good angular resolution except for small angles. This explains the disagreement between the calculated and the experimental curves in Figure 5.4 for small values of θ. The angular distribution curves (calculated and experimental) tend to be linear for larger angles. The latter part of the curves can be fitted to straight lines employing the method of least squares. On comparing the slopes of least squares fitted straight lines for the curves of Figure 5.4, we find that the agreement between the slopes is excellent. The identicality of the slopes (within the error limits) of the calculated and experimental curves for thermal fission provides a test of the present technique. The slope of the curves are expected to exhibit the variation with different anisotropies. The Monte Carlo calculations for various

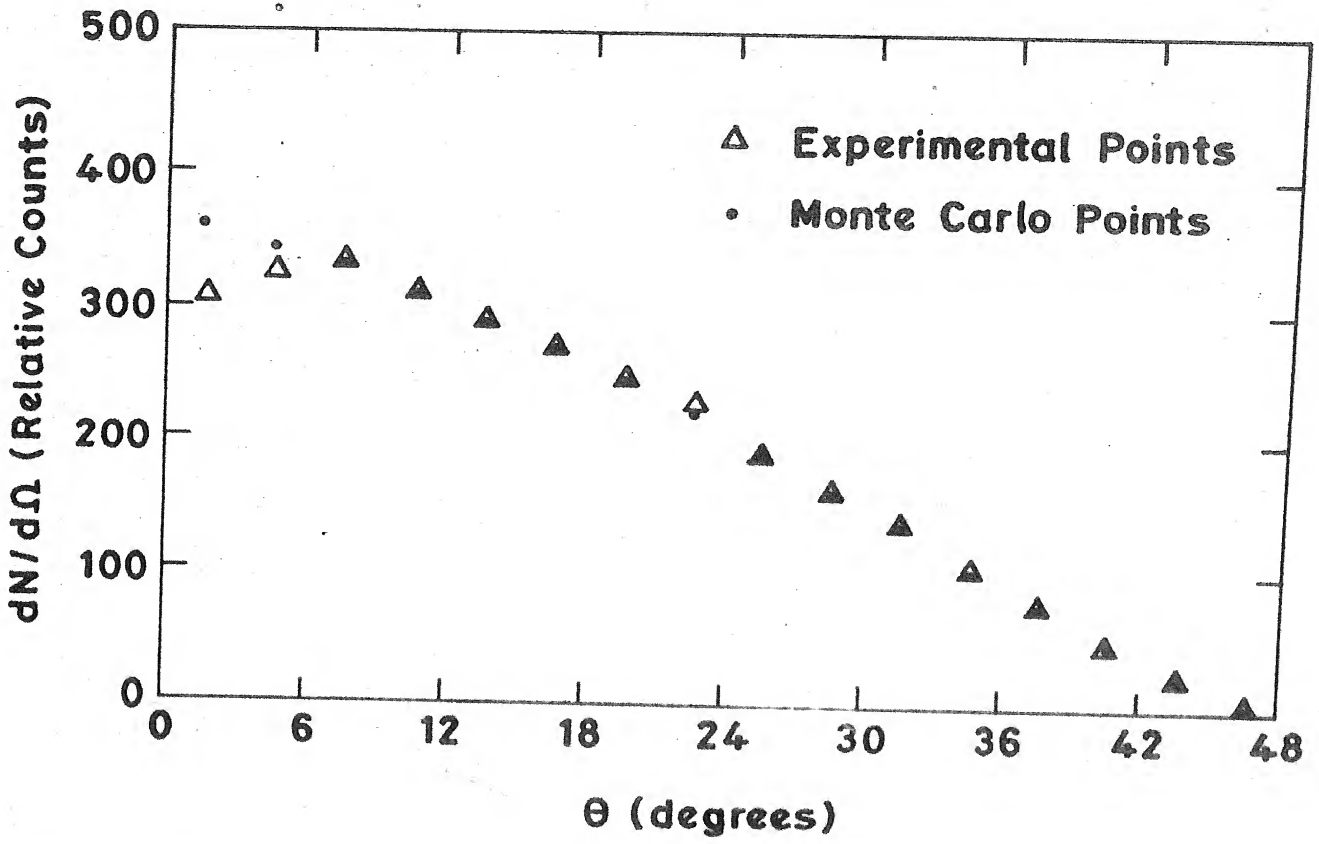

FIG. 5.4 The calculated (Monte Carlo) and experimental angular distributions of LRAs emitted in thermal neutron fission.

degrees of anisotropy in the angular distribution were carried out. The input distributions were assumed to go as

$$W(\theta) = 1 + \alpha \cos^2\theta \qquad (5.4.1)$$

where α represents the anisotropy in the angular distribution. The positive value of α indicates a fore and aft peaking and a negative one shows the perpendicular peaking.

(b) Calibration curve

The slopes of the experimental angular distributions at all energies of neutrons, show a decline compared to the thermal neutron run, indicating a preference for emission of LRAs in perpendicular direction to the beam. This corresponds to the negative value of α. Figure 5.5 illustrates the variation of slopes of the Monte Carlo curves calculated with negative values of α. The points for various anisotropies can be fitted to a straight line. Thus, the straight line in Figure 5.5 serves as a calibration curve for quantitative determination of the anisotropy of the experimental angular distribution obtained from above technique.

5.5 Results

The angular distribution measurements of the

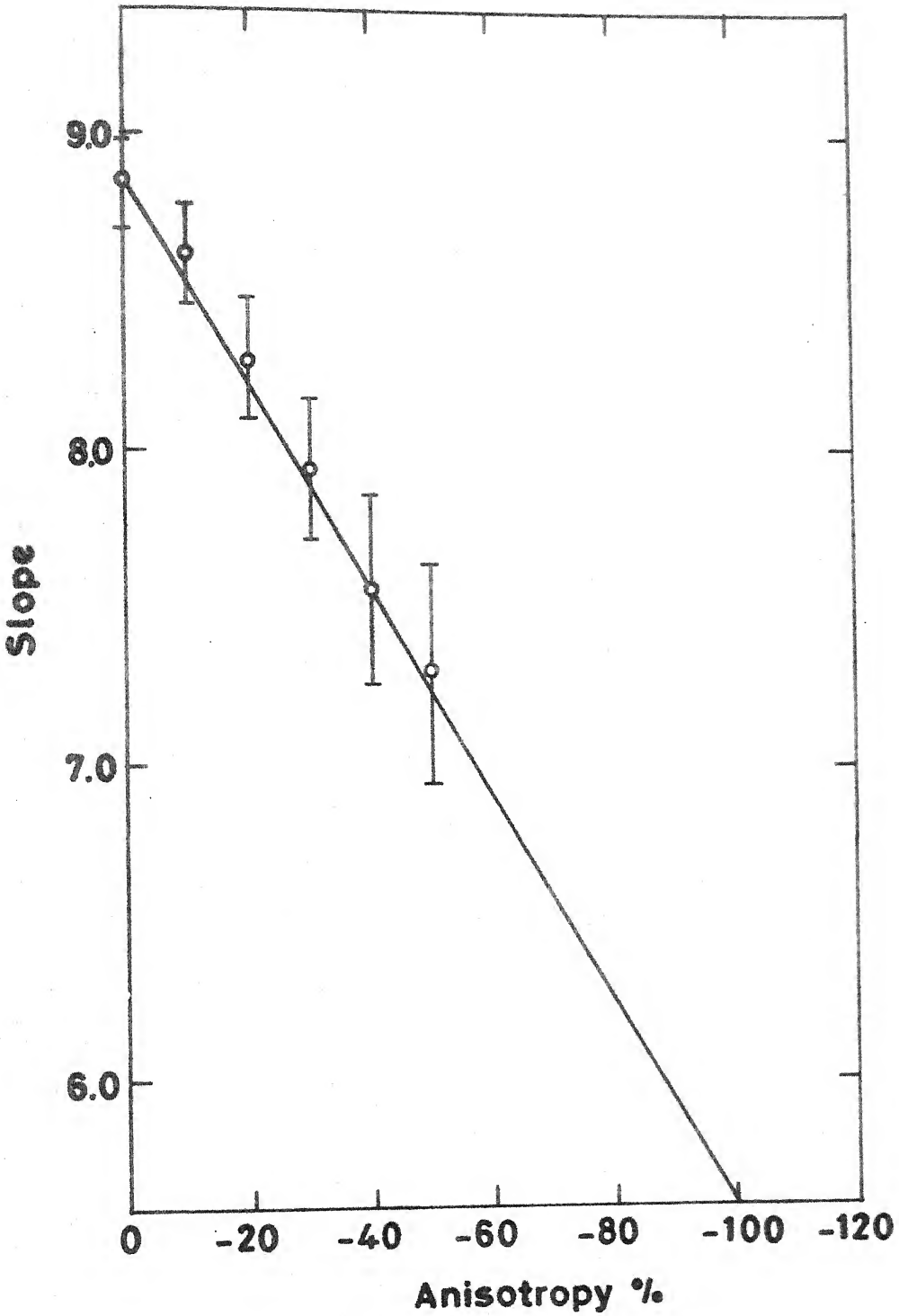

FIG. 5.5 The slope of the least-square fitted straight lines as a function of anisotropy.

long-range alpha particles emitted in the fission of ^{235}U were performed at various neutron energies between 100 keV and 1 MeV. The anisotropies (the value of α) of the angular distribution using the calibration curve are given in Table 5.1

Figure 5.6 shows schematically the results of angular distributions measured. It is notable that the LRA anisotropy is very high near 100-200 keV neutron energy. This is the energy region where the p-wave interaction is predominant and the p-wave contribution becomes about 50-60 % of the total fission cross- section[33].

Table 5.1

Anisotropy (α) of the angular distribution of LRAs at various neutron energies.

Energy of incident neutrons	Anisotropy (α)
140 ± 30 keV	-85 ± 28 %
170 ± 25 keV	-87 ± 32 %
200 ± 25 keV	-94 ± 31 %
400 ± 200 keV	-10 ± 28 %
600 ± 180 keV	-25 ± 19 %
1000± 170 keV	-50 ± 27 %

The interaction of the $\ell = 1$ neutrons with ^{235}U ($J^{\pi} = 7/2^{-}$) leads to the excited levels 2^{+}, 3^{+}, 4^{+} and 5^{+} which become accessible to the compound nucleus at the saddle point. By small variations in the neutron energy, any of

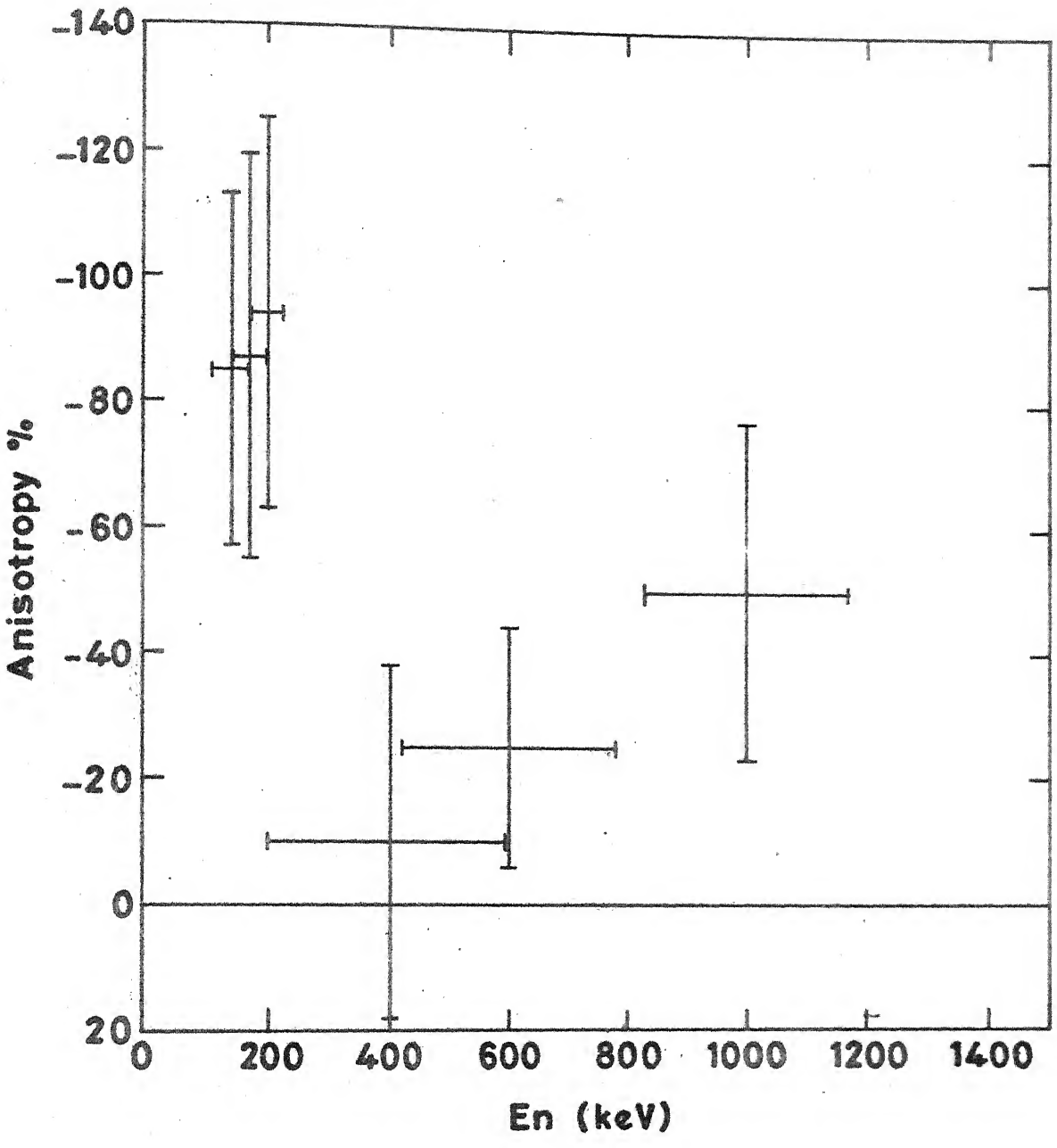

FIG. 5.6 The anisotropy of the LRAs at different neutron energies.

these states could be selectively excited. So, it is possible that some of these excited channels at the transition point may have some vital role in producing high anisotropy. The anisctropy near 400 keV is small and starts rising up beyond 400 keV upto 1 MeV. The signature of the anisotropy throughout the region 100-1000 keV is found to be negative.

5.6 Discussion

The LRA angular distribution is found to peak perpendicular to the neutron beam direction at all neutron energies from 100 keV to 1 MeV. Assuming that the alpha-fragment angular correlation does not undergo any drastic change from thermal to fast neutron fission, the ternary fragment angular distribution will inevitably be peaked forward and backward to the neutron direction. This behaviour is similar to that of the binary fission fragments. Our results are in clear contradiction to Ramanna et al.[1] and Nadkarni[28-29] who proposed that the LRA emission takes place due to evaporation before the scission point. The present results make the emission of α-particles before the scission point as unlikely. Besides the observation that the LRA-distribution is peaked perpendicular to the neutron direction points towards the following possibilities. First, the identical behaviour of the binary and ternary-fragment angular

distributions suggests a similarity in binary and ternary fission mechanisms. It seems that the K-distributions at saddle point are same for binary and ternary fission and that the LRA-emission favours small values of K. Second, the 90°-peaking of the LRAs cannot occur unless it is assumed that the fragmentation takes place prior to the LRA-emission, where the ternary fragments retain the same behaviour as binary i.e., forward peaking and the LRAs are forced to move perpendicularly to the fragments resulting in 90°-peaking. Our results, therefore, lend credence to the assertion that the LRA emission takes place bit later than the scission. This idea seems to be in agreement with Feather's post-scission evaporation model[2]. However, the evaporation of α-particles from the fragments is unlikely due to entirely different properties associated with the evaporation as discussed in Section 2.2b. The models which can predict the angular distributions as observed by us are the sudden snap model and the statistical model. Therefore, the models which explain the LCP-emission in the vicinity of scission or bit later in time, from the neck of the stretched configuration are supported by the present work.

REFERENCES

1. R. Ramanna, K.G. Nair, S.S. Kapoor, Phys. Rev. 129 (1963) 1350.
2. N. Feather, Proc. Royal Soc. of Edinburgh 66A (1964) 192; Proc. Royal Soc. of Edinburgh 68A (1969) 329.
3. I. Halpern, Proc. Symp. Phys. Chem. Fission, Salzburg, Vol. 2 (1965) 369.
4. P. Fong, Phys. Rev. C3 (1971) 2025.
5. Z. Fraenkel, Phys. Rev. 156 (1967) 1283.
6. M.J. Fluss, S.B. Kaufmann, E.P. Steinberg and B.D. Wilkins, Phys. Rev. C7 (1973) 353.
7. G.K. Mehta, J. Poitou, M. Ribrag and C. Signarbieux, Phys. Rev. C7 (1973) 373.
8. G.M. Raisback and T.D. Thomas, Phys. Rev. 172 (1968) 1272.
9. K. Tsuji, A. Katase, Y. Yoshida, T. Katayama, F. Toyofuku and H. Yamamoto, Proc. Symp. Phys. Chem. Fission, Rochester, Vol. 2 (1973) 405.
10. D.M. Nadkarni, S.K. Kataria, S.S. Kapoor and P.N. Rama Rao, Nucl. Phys. A196 (1972) 209.
11. H.W. Schmitt, J.H. Neiler, F.J. Walter and A. Chetan-Strode, Phys. Rev. Lett. 9 (1962) 427.
12. Y. Gazit, A. Katase, G. Ben-David and R. Moreh, Phys. Rev. C4 (1971) 223.

13. R.K. Choudhury, S.S. Kapoor, D.M. Nadkarni, P.N. Rama Rao and S.R.S. Murthy, Prämana 6 (1976) 64.

14. C. Carles, M. Ashgar, T.P. Doan, R. Chastel, M. Ribrag and C. Signarbieux, Proc. Symp. Phys. Chem. of Fission, Vienna Vol. 2 (1969) 119.

15. Y. Boneh, Z. Fraenkel and I. Nebenzahl, Phys. Rev. 156 (1967) 1305.

16. A. Katase, J. Phys. Soc. Japan 25 (1968) 933.

17. P. Fong, Phys. Rev. C2 (1970) 735.

18. T. Krogulski and J. Blocki, Nucl. Phys. A144 (1970) 617.

19. A.R. de L. Musgrove, Aust. J. Phys. 24 (1971) 129.

20. P.B. Vitta, Nucl. Phys. A170 (1971) 417.

21. M. Rajagopalan and T.D. Thomas, Phys. Rev. C5 (1971) 2064.

22. F. Fossatti and T. Pinelli, Nucl. Phys. A249 (1975) 185.

23. B. Krishnarajulu and G.K. Mehta, Prämana 4 (1975) 74.

24. A. Gavron, Phys. Rev. C11 (1975) 580.

25. M. Dakowski, E. Piasecki and L. Nowicki, Nucl. Phys. A315 (1979) 370.

26. A.K. Sinha and G.K. Mehta, Phys. Rev. C (To be published).

27. R.A. Atneosen, T.D. Thomas and G.T. Garvey, Phys. Rev. 139 (1965) B307.

28. D.M. Nadkarni, Nucl. Phys. A112 (1968) 241.

29. D.M. Nadkarni, BARC Report-318 (1968).

30. F.S. Goulding and B.G. Harvey, Ann. Rev. Nucl. Sci. 25 (1975) 167.

31. L.C. Northcliffe and R.F. Schilling, Nucl. Data Tables, A7 (1970) 233.

32. M.M. Sharma, S.C.L. Sharma, A.K. Sinha and G.K. Mehta, Nucl. Instr.Meth. (To be published).

33. J.G. Cunninghame, G.P. Kitt and E.R. Rae, Nucl. Phys. 27 (1961) 154.

34. S.C.L. Sharma, G.K. Mehta, R.K. Chowdhury, D.M. Nadkarni and S.S. Kapoor, Nucl. Phys. A355 (1981) 13.

CHAPTER VI

ANGULAR DISTRIBUTION OF POLAR LIGHT CHARGED PARTICLES IN THERMAL NEUTRON INDUCED FISSION OF ^{235}U

6.1 Introduction

Most of the light charged particles emitted during fission have angular distributions peaked around 90° with respect to fission fragment direction. However, about 2 % of the LCPs are found to be emitted along the fission direction as discussed previously and are referred to as polar particles. These LCPs have been studied by many authors[1-8] in thermal neutron induced fission of ^{235}U and spontaneous fission[9-11] of ^{252}Cf. Various experimental features viz., the intensity[5,11,12], the energy spectra[5,7,12] of polar particles and the associated fission fragments, the mass distributions[5,7,12] of fission fragments in coincidence with polar particles and the angular distributions of polar particles[2,3,10] have been investigated. The experimental observations indicate that the intensity and energy spectra of polar LCPs are weakly dependent on the fissioning nuclei[7].

The angular distributions of polar light charged particles are not known well. The mechanism of this phenomenon is still unclear and many hypotheses[6] have been advanced. Some of the models have been partly successful in explaining some of the experimental characteristics. But, in the absence of reliable data on the angular distribution of these LCPs, it is difficult to test the validity of the proposed hypotheses in terms of the actual nature of the polar emission. This emphasizes the importance of performing the precise measurements of these angular distributions. However, very low probability of emission of these particles makes the measurement of the angular distributions very difficult. The efforts in this direction in the past have been confined either to thermal neutron fission where the fission cross-section is fairly large or the spontaneous fission of ^{252}Cf.

6.2 Review of the Previous Work

Adamov et al.[10] measured the angular distributions of the polar light charged particles emitted in spontaneous fission of ^{252}Cf. The measurements were performed at mean angles 0°, 45°, 60° and 90° from the fission axis, where they did not distinguish between the light and heavy fragments. The yield ratio $Y(0^{\circ})/Y(90^{\circ})$ of protons, tritons and alpha particles were found to be (121 ± 14) %., (2.0 ± 0.30) % and (4.44 ± 0.08) %. The yield ratio for

protons is striking in that the proton yield at small angles is very large compared to that at 90° (Figure 6.1). This is the only published result on the angular distribution of protons. However, there are some reservations about this result due to the fact that the energy of the polar protons in this measurement was observed to be half the accepted value. Moreover, in the measurements by Adamov et al., there are only two experimental points in the polar region, i.e. 0° and 45°. Thus, it was difficult to say anything about the general shape of the angular distributions. Piasecki[3,5] et al. carried out the measurements on the angular distribution of polar alpha particles in thermal neutron fission of ^{235}U using semiconductor detector. Figure 6.2 shows the angular distribution of α-particles due to various authors. The solid line represents the measurements by Piasecki et al.[3], the dot-dash line indicates the angular distribution by Adamov et al.[10] for ^{252}Cf and the dashed line is the work due to Caitucoli et al.[13]. If an isotropic emission of α-particles in the centre of mass (c.m.) of the α-particle and fragment system is assumed, the angular distribution of α-particles would look like a forward-peaked distribution in the lab. system. The circles show the angular distribution if the particles were emitted isotropically from the fully accelerated fragments. It is clear from this figure that the angular distribution of polar α-particles is not yet known with a

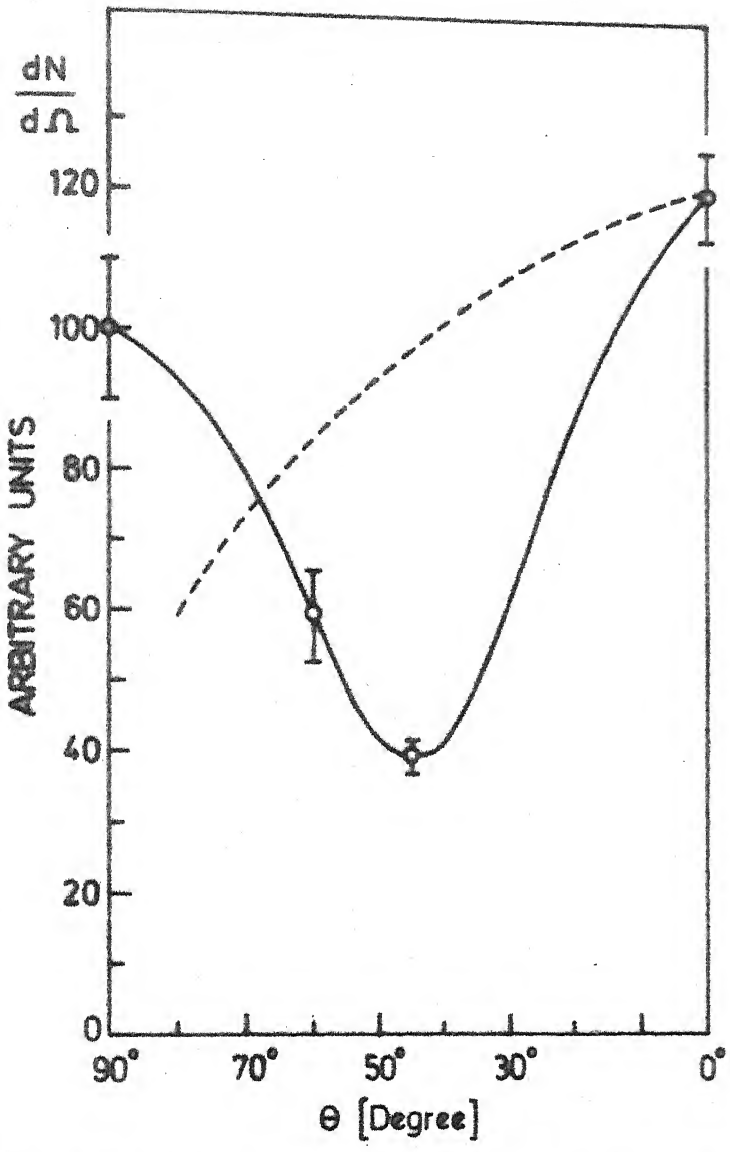

Fig. 6·1 The angular distribution of protons due to various authors [After Piasecki and Nowicki[6]]

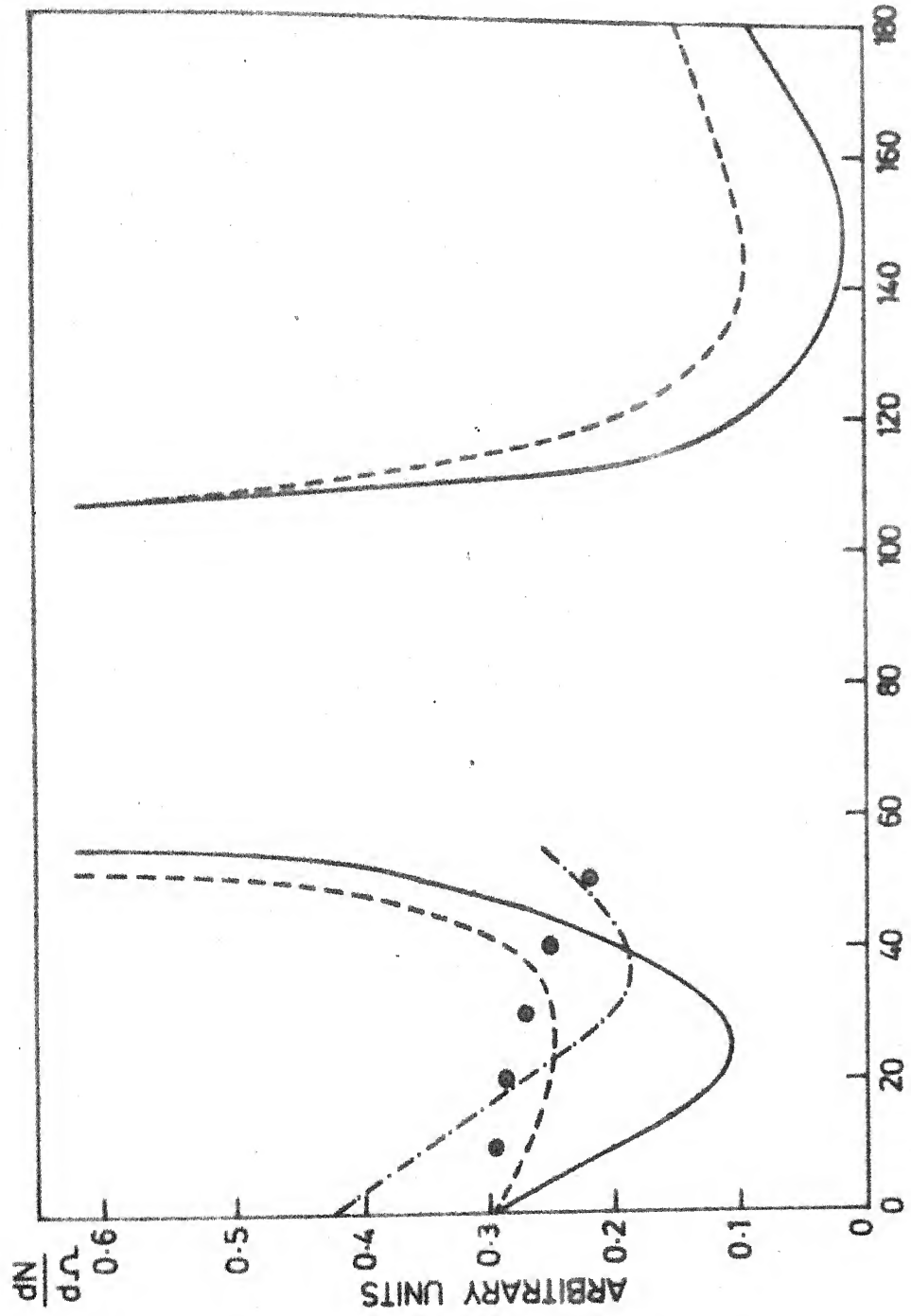

Fig.6·2 The angular distribution of α-particles [After Piasecki and Nowicki[6]]

fair degree of consistency and that this distribution is anisotropic not only in the lab system but also in the centre of mass system of the fragment and alpha particle[14].

Piasecki and Nowicki[6] have examined the validity of the evaporation hypothesis where the in-flight de-excitation of the fragments through α-particle evaporation is assumed to be responsible for the polar emission. The observed angular distribution, although not known accurately, is not compatible with the predictions of this model. The angular distribution of polar particles with respect to the fission axis is strongly peaked along the fission axis (especially for protons). This strong focussing is too large to be explained by in-flight evaporation, which appears as a result of the anisotropy of emission in the c.m. system, whereas the evaporation demands that the emission should be isotropic in the c.m. system. Another quantity of interest which should be in conformity with a model is the integrated polar to equatorial ratio. This also requires the knowledge of the polar angular distribution and the demarcation line between the polar and equatorial regions. This again points towards the importance of performing better and contiguous measurements of these angular distributions.

6.3 Angular Distribution Measurement

The low probability of emission of polar particles,

using the conventional techniques,does not allow the contiguous determination of the angular distribution as aforesaid. We have used the double-ionization chamber geometry, which has been discussed in Chapter 4, for the angular distribution measurements. In the following, we describe how this geometry, which was devised for simultaneous measurement of the yields of the equatorial and polar LCPs,was exploited to extract the information on the angular distributions.

(a) Outline of the method

The double ionization-chamber geometry allows the use of a broad area source and thus gives a reasonable count-rate of the equatorial and polar LCPs without sacrificing the angular resolution, as discussed in Chapter 4. The present geometry utilizes a multi-hole collimator which divides a single ionization-chamber into two, namely the LIC and the UIC. A fragment passing through the collimator gives a pulse from the LIC and the UIC and the associated light particle is detected by a particle telescope. Thus, a four-fold coincidence between E, ΔE, LIC and UIC ensures that both the fragment and the LIC have passed through the collimator hole, implying that a polar event has been detected. The size of the collimator holes is so chosen that for a four-fold coincidence event (polar events) the angle

which an LCP makes with the fragment lies within the polar region. The 3 mm collimator size represents the maximum size of the collimator holes with insignificant contamination of the polar events by equatorial ones, For this size of collimator holes, the Monte Carlo calculations show that the contamination of the polar LCPs by the equatorial LCPs are negligible for alpha particles whereas it is about 0.6 % for polar protons. This represents an upper limit on the possible contaminations in polar LCPs. Figure 6.3c shows the relative detection efficiency of polar events as a function of the angle between the fragment and the LCP. It is found that the efficiency is maximum around 14° and negligible after 34°, which is the upper limit on the angle of the polar angular distribution. Thus, the maximum likelihood of the events detected is within a narrow cone about the fission axis. However, the demarcation line between the polar and equatorial regions is not well-defined. Piasecki et al.[6] have taken the convention which says that the polar region is limited to the angles 0°-25° and 155°-180° with respect to the fission axis. According to the classical calculations[15], the maximum angle of the shadow cone about the fission axis for an LCP produced from the neck comes out to be 45°. This, in principle, means that the equatorial LCPs will not intrude this region and the tail of the equatorial angular distribution

will contribute only a little to this region, as has been found from the measurements by Piasecki et al.[1].

Assuming that the angular distribution of polar LCPs is represented by a Gaussian curve with peak about fission axis ($\theta \simeq 0^{o}$) having a certain FWHM (Full width at half maximum), we can expose different parts of this distribution to the detector assembly by choosing different sizes of the collimators. Figure 6.3 shows the relative detection efficiency for the polar LCPs as a function of the angle between the LCP and the fragment for three collimator sizes namely 1 mm, 2 mm and 3 mm. It turns out from figure that the peak position of the detection efficiency and the cut-off angles of detection are different for the three collimator sizes. The relative detection efficiency for each collimator can be integrated over the angle and the ratios of yields for 1 mm and 2 mm, 2 mm and 3 mm collimators can be determined. These ratios would be different for different initial angular distributions used in calculating the efficiencies. The value of σ (variance) of an initial angular distribution for which the calculated efficiency ratio matches with the experimental ratio, will give the width of the polar angular distribution. Thus, the value of σ can be found experimentally for polar protons, tritons and alpha particles.

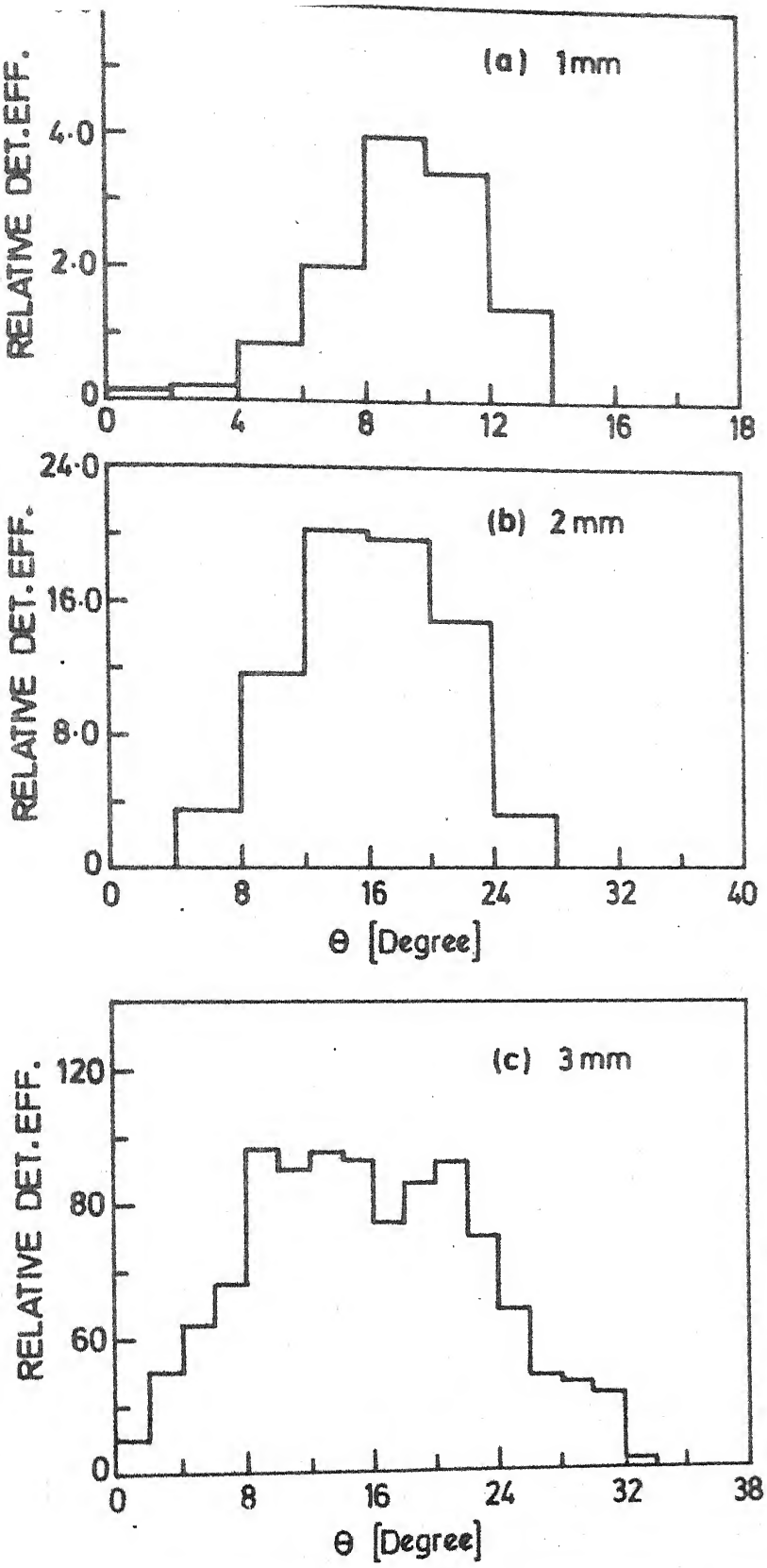

Fig. 6·3 The relative detection efficiency as a function of the angle between the fragment and the LCP

(b) Experimental details

The detection system and the experimental set-up are the same as described in Chapter 4. The double-ionization chamber geometry with a particle telescope (refer to Figure 4.1) has been used. The uranium-235 source was 5 mg/cm^2 thick with an active area of 4 cm^2. The particle telescope consists of a 75 μm thick ΔE-detector and a 500 μm thick E-detector, both of silicon. The experiment was conducted to study the angular distribution of polar LCPs in thermal neutron fission by the method as discussed above. The data were recorded for three collimator sizes, namely 1 mm, 2 mm and 3 mm. The total number of fissions for each run were monitored, which were used for normalizing various runs. The event-by-event data recording was done in the same way as in the study of the equatorial and polar LCPs, described in Chapter 4.

6.4 Data Analysis and Results

As mentioned in Chapter 4, the three parameters recorded were E, ΔE and a two-level logic pulse. The lower logic level of the third parameter indicated a 3-fold coincidence (equatorial event), the higher level denoted a four-fold coincidence (polar event). The equatorial and the polar events were sorted out and the particle identification was performed using Goulding's

power-law algorithm. Figure 6.4 shows the particle identification (PI) spectra for the equatorial and polar events obtained from an experimental run with 3 mm size collimator. The clear separation of the particles such as protons, tritons and alpha-particles is evident from the PI spectra. The region to the left of proton peak is attributed to the presence of γ-rays which appear in coincidence due to low cut-offs in the E and ΔE- detectors.

The energy spectra of the equatorial LCPs are shown in Figure 6.5 for 3 mm run. It should be mentioned that the energy spectra of protons do not give correct energy distribution because of insufficient thickness of the E-detector in our experiment. The use of a 75 μm thick ΔE-detector produces a 13 MeV cut-off in the α-particle spectrum as shown in Figure 6.5. The energy spectra of the polar LCPs are not given due to poor statistics. The distinction between the equatorial and polar LCPs has already been illustrated in Figure 4.9 using the present geometry. The identification of the polar LCPs has been quite unambiguous on the basis of the PI spectrum. Therefore, the distributions in the energy spectra due to low statistics and the insufficient thickness of the E-detector do not affect the yield measurement.

First, an experiment was performed using two (1 mm and 2 mm) collimators. The experiment with 1 mm collimator was intended to probe the polar LCP yields

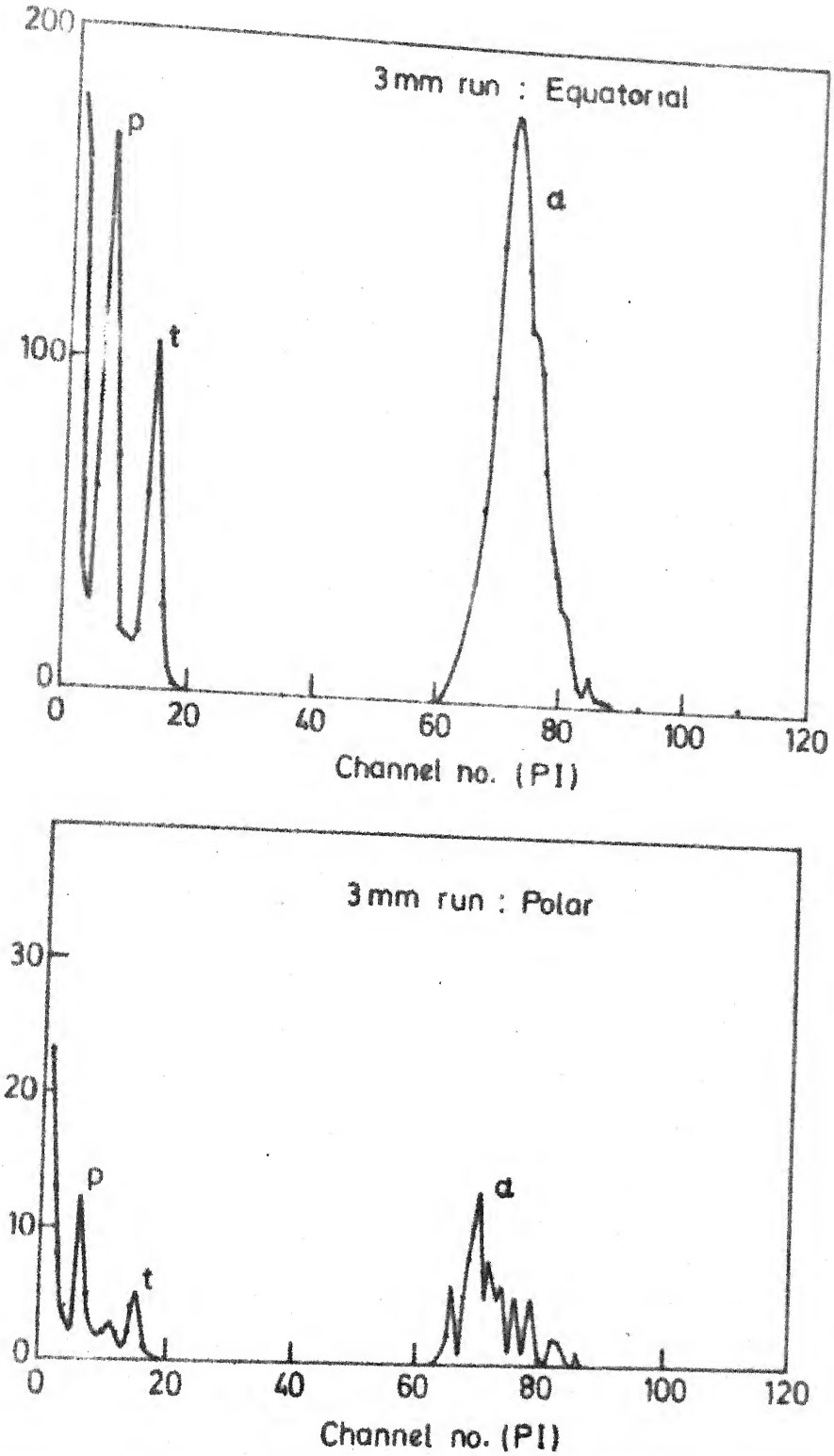

Fig. 6·4 The typical particle identification spectra for equatorial and polar LCPs (3mm run)

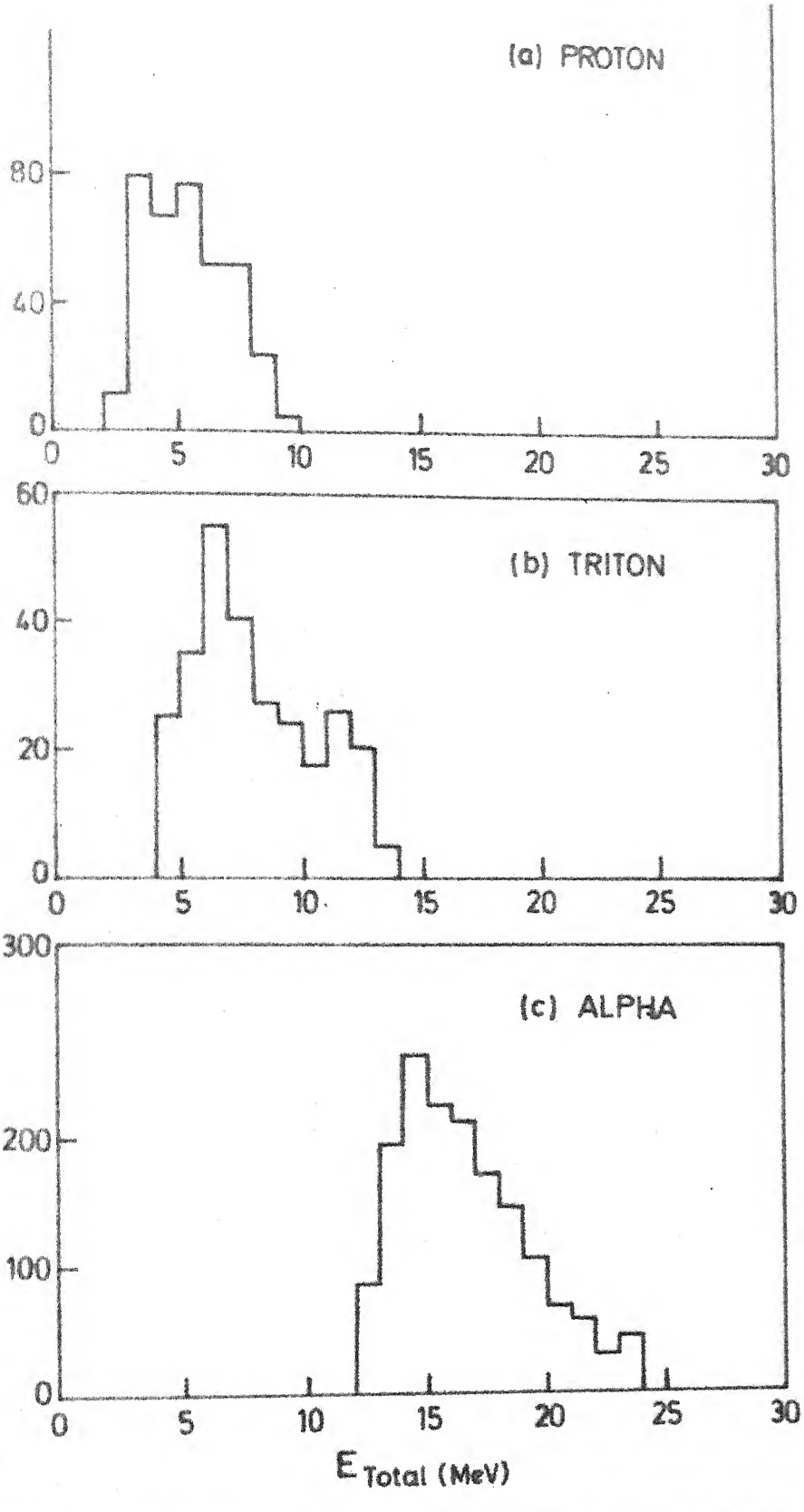

Fig. 6·5 The energy spectra of equatorial LCPs for 3 mm collimator run

in the directions very close to the fission axis. This fact is borne out from Figure 6.3a where the detection efficiency is maximum around 10^{o} about the fission axis. Since the use of 1 mm collimator scans a very narrow cone of the region, the detection efficiency is very small. The normalized yields of the polar LCPs (yield per fission) for both the collimators were found to be as shown in Table 6.1.

Table 6.1 : The yields of the polar LCPs per fission for 1 mm and 2 mm collimators.

LCP	1 mm Collimator	2 mm Collimator
α-particle	$(1.1 \pm 0.4)\times10^{-8}$	$(6.5 \pm 1.8)\times10^{-8}$
Proton	$(2.0 \pm 0.6)\times10^{-8}$	$(1.9 \pm 0.8)\times10^{-8}$

The yields of the polar protons are found to be same within the errors while for α-particles it increases by a large factor for 2 mm collimator. As can be visualized, the detection efficiency for a sharply peaked angular distribution will be rather insensitive to the collimator size. On the other hand, it will be strongly dependent on the collimator size for a broad angular distribution. As will be seen later, a narrow angular distribution reproduces the observed yields for protons. The sharp increase in the polar alpha particle yield for 2 mm collimator can be explained only by a very broad angular

distribution. However, due to poor statistics in 1 mm run, it was difficult to make a definite conclusion about the exact width of the angular distribution. In this experiment, the statistics of tritons were too poor to arrive at any conclusion on the polar triton angular distribution.

The experiment was then repeated with 2 mm and 3 mm collimators. The yields per fission of the polar LCPs obtained in this experiment are summarized in Table 6.2.

Table 6.2 : The yields of the polar LCPs per fission for 2 mm and 3 mm collimators.

LCP	2 mm Collimator	3 mm Collimator	Yield ratio (3 mm/2 mm)
α	$(2.40\pm0.41)\times10^{-8}$	$(8.15\pm0.91)\times10^{-8}$	3.39 ± 0.96
t	$(0.56\pm0.19)\times10^{-8}$	$(1.88\pm0.44)\times10^{-8}$	2.96 ± 1.67
p	$(2.18\pm0.39)\times10^{-8}$	$(3.45\pm0.60)\times10^{-8}$	1.58 ± 0.56

While comparing the yields of the α-particles in 2 mm collimator runs in Tables 6.1 and 6.2, it should be noted that the results of Table 6.2 used a 75 μm thick ΔE-detector giving a large cut-off ($\lesssim$ 13 MeV) compared to a 50 μm thick ΔE-detector used in the preliminary experiment (2 mm and 1 mm runs of Table 6.1). Therefore, the Tables 6.1 and 6.2 can not be compared directly. However, the ratio of the yield of the α-particles for the configurations having a 50 μm and 75 μm ΔE-detectors in 2 mm

run agrees with the ratio of the detection efficiencies within the errors for these configurations respectively. The data in Table 6.1, however, were not used for any quantitative deductions. The absolute yields of the equatorial LCPs obtained in different runs, which were determined after correction for efficiencies, were found to be consistent with the known results.

It is found that the yield of α-particles for 3 mm run increases by a factor of about three over 2 mm run. This shows that the polar α-particle angular distribution is so wide that it contributes significantly to the yield even at higher angles which become accessible for bigger size collimator. However, for protons the ratio is 1.58 ± 0.56 (0.95 ± 0.63 in 1 mm/2 mm run). This clearly indicates that polar proton angular distribution is quite narrow compared to the alphas. The situation in the case of triton angular distribution, for which statistics were poor, seems to be similar to that of alpha particles.

For quantitative determination of the widths of the angular distributions, we employed Monte Carlo simulation[17]. The relative detection efficiencies of the polar events for 2 mm and 3 mm collimators respectively were calculated by integrating over the allowed angular range of polar region by the collimators. The initial angular distribution was assumed to be Gaussian peaking along the fragment axis with a given variance(σ). The ratio

of efficiencies for 3 mm to 2 mm collimator for various values of σ are shown in Figure 6.6. The points given in the figure were fitted to a straight line using the method of least-squares. This serves as a calibration curve for the determination of the width of the angular distribution. The value of σ can be interpolated from the given curve for the experimental ratios provided in Table 6.2. The values of σ for various LCPs thus found from experiment are listed in Table 6.3.

Table 6.3 : The width of the angular distribution of the polar LCPs.

LCPs	σ
alpha	$(28.0 \pm 7.0)^{\circ}$
proton	$(13.0 \pm 6.0)^{\circ}$
triton	$(25.0 \pm 15.0)^{\circ}$

It is clear from the values of σ that alpha-particle angular distribution is very broad compared to protons. The tritons also seem to behave in the similar fashion as the alpha particles.

6.5 Discussion

The angular distribution of polar LCPs plays an important role in establishing the credibility of a model.

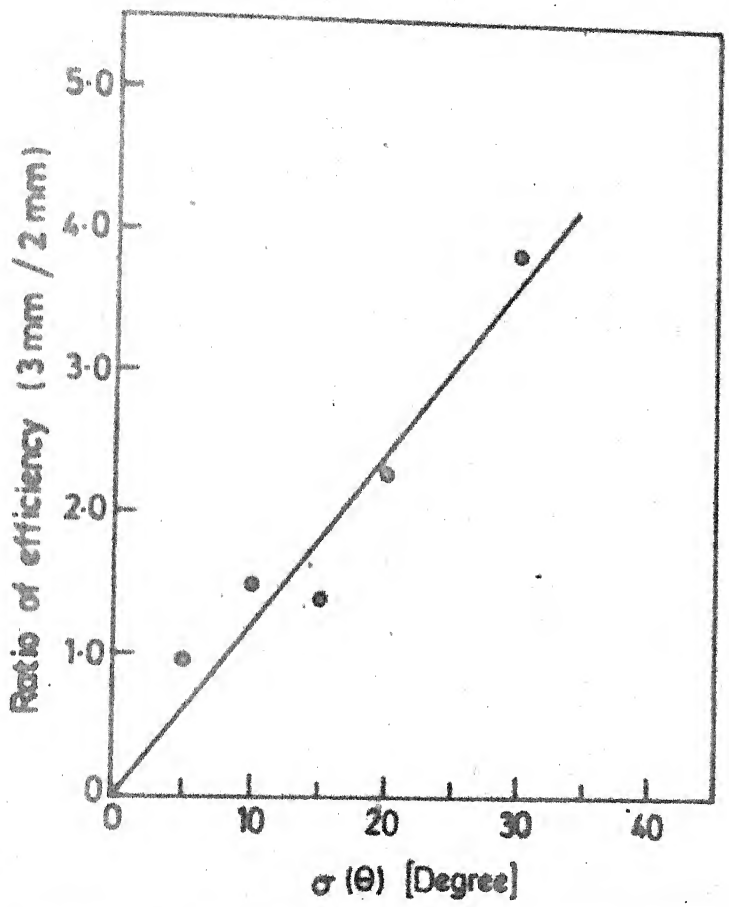

Fig. 6.6 The Monte Carlo efficiency ratio (3 mm to 2 mm) as a function of σ of the angular distribution

The evaporation model is the only model which has been studied in detail referring to all the available experimental data. It has been shown[12] that some theoretical predictions of the evaporation model agree well with the experimental observations. The angular distributions, which were known only very approximately, did not allow a proper verification of the validity of the model. The large anisotropy along the fission-axis for the protons (narrow angular distribution) seemed to be incompatible with the predictions of the evaporation model. Our results give the variance of proton angular distribution to be $(13.0 \pm 6.0)^{\circ}$. The narrow angular distribution observed in our experiment seems to be going against the evaporation of protons in the light of the fact that the emission of LCPs if it is a consequence of evaporation, results in the isotropic distribution in the centre-of-mass system. The later, when transformed to the laboratory system would result in the distributions as produced in Figure 6.2 by dotted curve, indicating a small anisotropy in the laboratory frame.

The angular distribution of polar alpha particles and tritons are found to be very broad, the variance of the distributions being $28.0^{\circ} \pm 7.0^{\circ}$ and $25.0^{\circ} \pm 15.0^{\circ}$ respectively. The error in the width of the triton angular distribution is large due to relatively low intensity of these particles. However, it seemsto

indicate the fact that the angular distributions of alpha particles and tritons are quite broad compared to protons, and the anisotropy about the fission axis in the laboratory system is quite small. These distributions, therefore, can be taken to be almost isotropic in the centre-of-mass system of the fragment plus the particle. This shows as if the polar emission of alpha particles and tritons is a manifestation of charged-particle evaporation from the fully accelerated fragments and brings out the fact that the polar protons behave quite differently compared with the composite particles ^{3}H and ^{4}He. The different behaviour of the polar protons and the polar composite particles (^{3}H and ^{4}He) may imply a different basic mechanism for the two kind of polar LCPs. It should be noted that the angular distributions of tritons and alphas for broadside emissions (equatorial) are also almost identical. Cumpstey and Vass[11] obtained the full width at half maximum of the angular distribution of α-particles to be $17.0^{\circ} \pm 1.00^{\circ}$ which is comparable to the value $18.7^{\circ} \pm 0.8^{\circ}$ obtained by Guet et al.[18] for α-particle distribution in the thermal neutron-induced fission of ^{235}U. For tritons[11] the FWHM is $17^{\circ} \pm 1^{\circ}$, which is consistent with the results of Raisbeck and Thomas[19]. Thus, it is found that the angular variations for tritons and α-particles are very similar for equatorial as well as polar emissions. This may suggest that the configurations

indicate the fact that the angular distributions of alpha particles and tritons are quite broad compared to protons, and the anisotropy about the fission axis in the laboratory system is quite small. These distributions, therefore, can be taken to be almost isotropic in the centre-of-mass system of the fragment plus the particle. This shows as if the polar emission of alpha particles and tritons is a manifestation of charged-particle evaporation from the fully accelerated fragments and brings out the fact that the polar protons behave quite differently compared with the composite particles ^{3}H and ^{4}He. The different behaviour of the polar protons and the polar composite particles (^{3}H and ^{4}He) may imply a different basic mechanism for the two kind of polar LCPs. It should be noted that the angular distributions of tritons and alphas for broadside emissions (equatorial) are also almost identical. Cumpstey and Vass[11] obtained the full width at half maximum of the angular distribution of α-particles to be $17.0^{\circ} \pm 1.00^{\circ}$ which is comparable to the value $18.7^{\circ} \pm 0.8^{\circ}$ obtained by Guet et al.[18] for α-particle distribution in the thermal neutron-induced fission of ^{235}U. For tritons[11] the FWHM is $17^{\circ} \pm 1^{\circ}$, which is consistent with the results of Raisbeck and Thomas[19]. Thus, it is found that the angular variations for tritons and α-particles are very similar for equatorial as well as polar emissions. This may suggest that the configurations

at the instant of release of ^{3}H and ^{4}He particles are same for the equatorial and polar emissions, suggesting a common mechanism for them. This idea is again fortified by our observations[20-21] on the similarity of the variation of the yields of various LCPs in the equatorial and polar emissions for keV neutron induced fission of ^{235}U. The nuclear orbiting hypothesis seems to be promising in view of the similarities in the attributes of the equatorial and the polar LCPs. Recently, the trajectory calculations[22] performed with the presence of attractive nuclear force at scission, which could explain the polar emission as bending of the alpha-particle trajectory originating from the neck, provide support to this model. Therefore, a single mechanism for the origin of equatorial and polar LCPs can not be ruled out. However, the fact remains that the protons behave differently than tritons and alpha particles, be it an equatorial or polar emission.

REFERENCES

1. E. Piasecki, M. Dakowski, T. Krogulski, J. Tys and J. Chwaszczewska, Phys. Lett. B33 (1970) 568.
2. E. Piasecki, J. Blocki, Nucl. Phys. A208 (1973) 381.
3. E. Piasecki and J. Blocki, Nucl. Phys. A212 (1973) 628.
4. E. Piasecki, M. Dakowski and A. Kordyasz, Proc. of Symp. on Phys. and Chem. of Fission (Rochester) Vol. 2, IAEA, Vienna (1974) 383.
5. E. Piasecki, M. Sowinski, L. Nowicki, A. Kordyasz, E. Cieslak and W. Czarnacki, Nucl. Phys. A255 (1975) 387.
6. E. Piasecki and L. Nowicki, Proc. of Symp. on Phys. and Chem. of Fission (Jülich) Vol. 2, IAEA, Vienna (1979) 193.
7. V.N. Andreev, V.G. Nedopekin and V.I. Rogov, Yad. Fiz. 25 (1977) 732.
8. D.M. Nadkarni, S.K. Kataria, S.S. Kapoor and P.N. Rama Rao, Nucl. Phys. A196 (1972) 209.
9. J.A. Adams and R.R. Roy, Nucl. Sci. Engg. 63 (1977) 41.
10. V.M. Adamov, L.V. Drapchinsky, S.S. Kovalenko, K.A. Petrzhak, L.A. Pleskachevsky and I.I. Tyutyugin, Phys. Lett. 48B (1973) 311.
11. D.E. Cumpstey and D.G. Vass, Proc. Symp. on Phys. and Chem. of Fission (Jülich), Vol.2, IAEA, Vienna (1980) 223.

12. L. Nowicki, E. Piasecki, J. Sobolewski, A. Kordyasz, M. Kisielinski, W. Czarnacki, H. Karwowski, P. Koczon and C. Signarbieux, Nucl. Phys. A375 (1982) 187.

13. F. Cäitucoli, B. Leroux, P. Perrin, G. Barreau, M. Ashgar and N. Carjan, Unpublished.

14. E. Piasecki and J. Blocki, Acta Phys. Pol. B5 (1974) 247.

15. E. Piasecki, M. Dakowski, J. Blocki, L. Nowicki, INR Report 1720/IA/PL/A (1977).

16. M.M. Sharma, A.K. Sinha and G.K. Mehta, Silver Jubilee Physics Symposium (India) 24B (1982) 97.

17. I.M. Sobol, ''The Monte Carlo Method'', Mir Publishers, Moscow (1975).

18. C. Guet, C. Signarbieux, P. Perrin, H. Nifenecker, B. Leroux and M. Ashgar, J. Phys. Lett. 39 (1978) L-213.

19. G.M. Raisbeck and T.D. Thomas, Phys. Rev. 172 (1968) 1272.

20. A.K. Sinha, M.M. Sharma, S.C.L. Sharma, G.K. Mehta and D.M. Nadkarni, J. Phys. G : Nucl. Phys. 8 (1982) L85.

21. M.M. Sharma, A.K. Sinha and G.K. Mehta, Nucl. Phys. and Solid State Physics (India) 25B (1982).

22. A.K. Sinha and G.K. Mehta, Phys. Rev. C (To be published).

CHAPTER VII

SUMMARY AND CONCLUSIONS

Light charged particle emission studies contribute to the understanding of the scission configuration and the dynamics of fission at the scission stage. The present work is purported to the study of the angular distributions and yields of these light charged particles emitted during fission induced by neutrons of energies between 100 keV to 1 MeV. The thesis can be divided mainly into two parts. The first is an effort to understand the effect of excitation energy on the yield of the equatorial and the polar LCPs. The effect of excitation energy has been further investigated for the long-range alpha particles by studying their angular distributions about the incident neutron direction. In the second part, angular distributions of the scantily emitted polar LCPs have been studied in order to throw some light on the prevalent emission mechanisms.

The angular distribution measurements of the long-range alpha particles emitted in the neutron

induced fission about neutron direction have been performed in the energy range 100 keV to 1 MeV. A technique for the angular distribution measurements using a particle telescope has been developed. The telescope not only identifies the type of the particle but also furnishes the information on the angle of the incident particle. Since the technique allows the use of a broad area source, the Monte Carlo simulations were carried out to distangle the information on the angular distributions from the experimental data. The alpha particle angular distribution about the neutron direction thus determined has been found to be perpendicularly peaked at all energies in the above region. The magnitude of the anisotropy around 200 keV neutron energy is striking which seems to have a bearing on the interaction of the p-wave neutrons (which predominates around this energy) with the target. The anisotropy recedes near 400 keV and then displays an increasing trend upto 1 MeV. The anisotropy of the LRAs perpendicular to the neutron direction with an increase of small excitation energy has been interpreted to assert that the LRA emission as a pre-scission phenomenon is unlikely and that it takes place in the neighbourhood of scission.

The behaviour of the yields of the equatorial and the polar LCPs (p,t and α) has been studied in 200 keV and 1 MeV neutron-induced fission of ^{235}U. The yields

of the α-particles and tritons do not show any significant variation at above energies compared to thermal neutron induced fission. The yield of the α-particles, which exhibits a near constancy at 200 keV in contrast to a 20 % increase observed earlier, is explicable on the basis of the high anisotropy of the LRAs perpendicular to the neutron beam. The high anisotropy of the LRAs at 200 keV as observed in our experiment implies that more ternary fragments are emitted along the neutron direction than perpendicular to it. However, due to the use of a collimator configuration in the present detection system, the fragments associated with an equatorial LCP are detected preferentially normal to the neutron direction. The increase in the LRA yield at 200 keV, as observed earlier, would not be reflected in the present experiment. Therefore, an appropriate correction would have to be made in the yields of the LRAs at higher energies by employing our data on the angular anisotropy.

The tritons also seem to behave in a similar fashion as the α-particles. However, the protons show an increase in the yield both at 200 keV and 1 MeV neutron energies. The variations in the yields of the equatorial and the polar LCPs at higher excitation energies compared to thermal neutron fission have been found to be similar. This similarity in the variations in the yields may contend that the origin of the equatorial and the polar

LCPs is same, but polar emission is observed due to a different configuration at scission than equatorial emission. The polar emission could possibly be the manifestation of the nuclear orbiting of the LCPs born from the neck at the instant of scission. The idea receives further impetus from the trajectory calculations performed in our laboratory with the inclusion of attractive nuclear force near the scission point. Thus, the equatorial and the polar emissions could be perceived as two phenomena originating from a single source.

The angular distribution of the polar LCPs about the fission axis is an important tool to test the validity of various hypotheses propounded on the polar emission. An attempt is made to provide some information on this vital aspect of the polar LCPs. The angular distributions of the polar LCPs were measured by varying the collimator size (1 mm, 2 mm and 3 mm) as described in Chapter 6 for exposing the different parts of the polar angular distributions. The width of the angular distributions which were assumed to be Gaussian was determined for polar protons, tritons and the alpha particles. The proton angular distribution was found to be quite narrow ($\sigma = 13^{\circ} \pm 6^{\circ}$) compared to that of tritons ($25^{\circ} \pm 15^{\circ}$) and the alpha particles ($28^{\circ} \pm 7^{\circ}$). The narrow angular distribution of protons is not expected in the framework of the evaporation hypothesis.

However, the broad angular distribution of the polar tritons and alpha particles still maintains that the emission of the alpha particles and tritons could be the result of evaporation during the acceleration of the fission fragments.

The angular distribution of polar tritons and alpha particles are very similar. This reflects the similarity in the behaviour of the polar tritons and alpha particles in contrast to that of protons. The different behaviour of protons has already been observed in our studies on the yields of the equatorial and the polar LCPs. It turns out that the protons have an altogether different trend whether it be the yield study at higher excitation energy or the angular distributions of the LCPs, both in the equatorial and polar emissions. Therefore, there could be no reservations as to why the protons can not have a different emission mechanism than the composite particles (^{3}H and ^{4}He).

APPENDIX

THEORY OF ANGULAR DISTRIBUTION IN FISSION

The angular distribution in low energy fission has been adequately understood in terms of a few levels (saddle-point states) in the transitions nucleus. The theory is based upon two assumptions. First, the two fission fragments are assumed to separate along the direction of nuclear symmetry-axis. Second, it is assumed that the transition from the saddle point to scission point is so fast that the Coriolis forces do not change the values of K established at the saddle point. In other words, the K-distribution is frozen in at the second barrier for low energy fission. The couplings that provide for the angular momentum exchange between the individual nucleons and the collective rotation of the nucleus as a whole are relatively weak, and there is consequently not enough time in rapid descent from the saddle point to permit an appreciable amount of reorientations or changes in K. An evidence for the frozen-state of the K-distribution beyond the saddle point is given by the sharpness of the fragment angular distributions observed in fission occuring near the threshold. The preservation of this relationship between the saddle and scission points implies that the angular distribution of fission products will bear the same relationship to the original specified direction.

The direction of the nuclear symmetry axis is described by asymmetric-top wave functions D^{I}_{MK} in terms of the total spin I, projection M on the beam axis and the projection K on the nuclear symmetry axis(Figure A.1). For a fission process proceeding through a channel with quantum number I, M and K, the fragment angular distribution is given by[1]

$$W^{I}_{MK}(\theta) = \frac{2I+1}{2} \left| D^{I}_{MK}(\theta) \right|^2 \qquad (A.1)$$

The fission-fragment angular distribution associated with the rotational band of a particular K and parity is written as

$$W_K(\theta) = \sum_{I,M} \sigma_f(I,K,\pi)\, W^{I}_{MK}(\theta) \qquad (A.2)$$

where σ_f represents the differential fragment cross-section. The overall angular distribution is calculated by summing over the various contributing K-states.

In the case of fission initiated by the impact of faster particles, there may be a correlation between the direction of the incidence beam and of the fragment emission. This correlation depends on the distribution of I and M values with which the compound nucleus is formed, as well as on the K-values of the states available to the fissioning nucleus at the saddle point. For relatively small energies (close to the fission threshold) at which a single angular momentum state of the incident particle may play an important role, specific effects may occur associated with

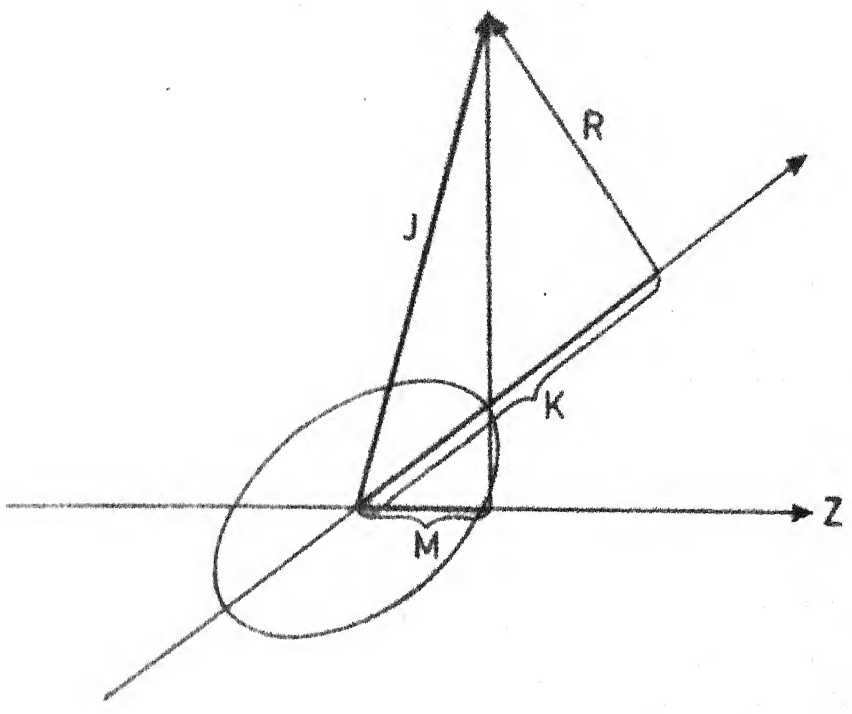

Fig. A.1 Angular momentum coupling scheme for a deformed nucleus. The vector J defines the total angular momentum. The quantity M is the component of J on the space-fixed Z axis (the beam direction). The quantity K is the component of J along the nuclear symmetry axis. The collective rotational angular momentum R is perpendicular to the nuclear symmetry axis [After Vandenbosch and Huizenga[1]

the dominance of a single or a few fission channels. For larger energies of the incident particle, the fissioning nuclei may pass through a great number of different states at the saddle point, with different angular momentum quantum numbers. However, a systematic tendency for anisotropy in the fragment emission results from the fact that M- and K-values are not distributed uniformly from -I to +I, but are concentrated towards numerically small values. The channel spectrum is expected to exhibit a marked preference for small K-values, especially so for even-even nuclei. The tendency towards small values of M implies that for large I, the nuclear angular momentum vector points preferentially in a direction perpendicular to the incident direction. Moreover, for small K-values the nuclear axis is oriented predominantly perpendicular to the angular momentum vector. Consequently, the distribution of the fission fragments is peaked in the forward direction.

The capture of a neutron in an odd-N target produces an even-even fissioning nucleus. Even the capture of a thermal neutron leads to an excitation energy in the compound nucleus which is considerably in excess of the lowest fission barrier for the even-even transition nucleus. Hence, for fission induced by neutron-capture of odd-N targets the saddle state can be characterized by a Gaussian K-distribution. Halpern and Strutinsky[2] assume the following form

$$F(K) \;\alpha\; \exp\left(-\frac{K^2}{2K_o^2}\right); \qquad K \leq I$$
$$= 0 \qquad\qquad K > I \tag{A.3}$$

where
$$K_o^2 = \frac{T}{\hbar^2}\,\mathcal{J}_{eff} \tag{A.4}$$
$$\mathcal{J}_{eff}^{-1} = \mathcal{J}_{11}^{-1} - \mathcal{J}_{\perp}^{-1} \tag{A.5}$$

and K_o^2 is directly related to the deformation of the transition nucleus. T is the nuclear temperature at the fission saddle, and $\mathcal{J}_{11}$ and $\mathcal{J}_{\perp}$ are moments of inertia for rotation parallel and perpendicular to the nuclear symmetry axis, respectively.

For a Gaussian K-distribution an exact expression[1] for the fission fragment angular distribution can be written by proper weightings of J, M and K. If the target and projectile spins are included the exact equation for the angular distribution is

$$W(\theta) \;\alpha\; \sum_{J=0} \sum_{M=-(I_o+s)}^{I_o+S} \left\{ \sum_{\ell=0}^{\infty} \sum_{s=I_o-s}^{I_o+s} \sum_{\mu=-I_o}^{I_o} \frac{(2\ell+1)\left|C^{S,\ell,J}_{M,0,M}\right|^2 \left|C^{I_o,s,S}_{\mu,M-\mu,M}\right|^2}{\sum_{\ell=0} (2\ell+1)\,T_\ell} \right.$$
$$\left. \times \sum_{K=-I}^{I} \frac{(2I+1)\left|d^I_{M,K}(\theta)\right|^2 \exp\left(-\frac{K^2}{2K_o^2}\right)}{\sum_{K=-I}^{I} \exp\left(-\frac{K^2}{2K_o^2}\right)} \right\} \tag{A.6}$$

The quantities I_o, s and S are the target spin, projectile spin, and channel spin respectively, where $S = I_o+s$. The total angular momentum I is given by the sum of the channel spin and orbital angular momentum; $I = S+\ell$. The projection of I_o on space-fixed axis is μ, where the projection of I on the space-fixed axis is M. The quantities $C^{S,\ell,J}_{M,O,M}$ and $C^{I_o,s,S}_{\mu,M-\mu,M}$ are Clebsch-Gordon coefficients.

The Gaussian weighting of K-values in above equation is an assumption which is not expected to be valid for low energy neutron fission of odd-N targets. However, this assumption allows to parameterize the theoretical angular distributions in a simple and straightforward way, so that one can look for discontinuities or rapid changes in the K-distribution.

Owing to the difficulty in evaluation of $D^{I}_{M,K}(\theta)$ functions, it can be approximated with the following relation[3]

$$D^{I}_{M,K}(\theta)^{2} = \pi^{-1}[(I+\tfrac{1}{2})^2 \sin^2\theta - M^2-K^2+2MK\cos\theta]^{-1/2} \quad \ldots\ldots \quad (A.7)$$

In the limit of target and projectile spins to be zero and assuming that no particle emission from the compound nucleus occurs before fission (i.e., M = 0)

$$W^{I}_{M=0,K}(\theta) = \frac{2I+1}{2\pi}[(I+\tfrac{1}{2})^2 \sin^2\theta - K^2]^{-1/2} \quad (A.8)$$

With a Gaussian distribution, the angular distribution for a particular I (for M = 0) is

$$W^{1}_{M=0}(\theta) = \frac{(2I+1)\int_{0}^{(I+\frac{1}{2})\sin\theta} [(I+\frac{1}{2})^2\sin^2\theta - K^2]^{-\frac{1}{2}} \exp(\frac{-K^2}{2K_o^2})dK}{2\pi \int_{0}^{(I+\frac{1}{2})} \exp(\frac{-K^2}{2K_o^2})\,dK} \quad \ldots\ldots \quad (A.9)$$

which can be evaluated explicitly[4] as

$$W^{I}_{M=0}(\theta) = \frac{\frac{\pi}{2}(2I+1)\exp[-(I+\frac{1}{2})^2\sin^2\theta/4K_o^2]J_o[\frac{i(I+\frac{1}{2})^2\sin^2\theta}{4K_o^2}]}{2\pi(\pi^{1/2}/2)(2K_o^2)^{1/2}\,\mathrm{erf}[(I+\frac{1}{2})/(2K_o^2)^{1/2}]} \quad \ldots. \quad (A.10)$$

where J_o is the zero-order Bessel function with an imaginary argument, and $\mathrm{erf}[(I+\frac{1}{2})/\sqrt{2K_o^2}]$ is the error-function defined by

$$\mathrm{erf}(x) = \frac{2}{\pi}\int_{0}^{x} \exp(-t^2)dt \quad (A.11)$$

Above form can be obtained most directly from simple geometrical considerations. The fragments emitted from the nucleus with spin I come off on a cone of half angle $\mathrm{Cos}^{-1}(K/I)$. The fragments come off at all azimuths with equal probability. If now the vector I is rotated around the beam axis, the distributions of the fragments becomes

$$W_{I,K} = \frac{2I}{4\pi^2}(I^2\sin^2\theta - K^2)^{-1/2} \quad (A.12)$$

where θ is the angle between the fragment direction and the

incident beam. The normalization is such that on a sphere,

$$\int W_{I,K}(\theta)\, d\Omega = 1$$

Now $W_{I,K}$ is averaged over Gaussian K-distribution. The distribution for a fixed I and a given K_o^2 is then

$$W_{I,K_o} = \frac{2I}{4\pi^2} \frac{\int_0^{I_o \sin\theta} dK \exp\left(\frac{-K^2}{2K_o^2}\right) (I^2\sin^2\theta - K^2)^{-1/2}}{\int_0^1 dK \exp\left(-\frac{K^2}{2K_o^2}\right)}$$

$$= \sqrt{\frac{2}{\pi}} \frac{N}{2\pi} \frac{1}{2K_o} \exp\left(\frac{-I^2\sin^2\theta}{4K_o^2}\right) J_o\left(\frac{I^2\sin^2\theta}{4K_o^2}\right) \qquad (A.13)$$

where N is a normalization constant.

This expression of the distribution has been obtained by approximating the $D^I_{M,K}(\theta)$ function. This is the semi-classical expression for the angular distribution of fission fragments proposed by Bohr[5].

For values of $I^2/4K_o^2$ not much larger than unity, the anisotropy may be approximated by

$$\frac{W(0^\circ)}{W(90^\circ)} = 1 + \frac{1}{2}\left(\frac{I}{2K_o}\right)^2 \qquad (A.14)$$

The distribution W_{I,K_o} may be integrated numerically over I^2 from zero upto a maximum value I^2_{max}. The resultant angular distribution is peaked forward and backward along the beam, as one would expect from simple geometrical considerations.

The result of nonzero target or projectile spin is to introduce a component of the total compound nuclear angular momentum which need not lie in the plane perpendicular to the beam. This results in smearing of the fore-aft peaking and a decrease in the anisotropy.

The fission observed at bombarding energies of several tens of MeV generally come from a number of nuclides. Some fission occurs in the compound nucleus originally formed by the incoming projectile. Other fission occurs in the species that result from the evaporation of one or more neutrons. If it is assumed that only fission and neutron emission can occur, an observed angular distribution is a superposition of distributions from the set of nuclides generated by the neutron evaporation. The mean excitation energy at which fission occurs in a given nuclide is the excitation energy of the original compound nucleus minus the binding energy and kinetic energy carried off by evaporating neutrons.

The degree of fission-fragment anisotropy for particle-induced reactions depends on both the I and K distribution. Increasing the weighting of high I states serves to increase the anisotropy. This may be accomplished by increasing the projectile energy or mass. On the other hand, the K-distribution is a nuclear property characterized by K_o^2, which depends upon $\mathcal{J}_{eff}\, T/h^2$. As the excitation energy increases, the value of T increases, leading to

larger values of K_o^2. The anisotropy decreases with increasing K_o^2. In the case of second-chance fission where (n,n'f) becomes energetically possible, the fragment anisotropy will be unusually large due to a small value of K_o^2 associated with the low excitation energy and nuclear temperature near the fission barrier.

Since the magnitude of anisotropy is largely dependent upon the value of K_o^2, it becomes important to know the variation of this quantity with excitation energy. The interpretation of the energy dependence is straightforward if only first-chance is occuring. The calculation of K_o^2 from the anisotropy by a relation (A.6) given above requires projectile transmission coefficients $T_\ell(E)$ which are computed with optical model theory with spin-orbit interaction.

REFERENCES

1. R. Vandenbosch and J.R. Huizenga, ''Nuclear Fission'', Academic Press, New York (1973).

2. I. Halpern and V.M. Strutinsky, Proc. of 2nd United Nations International Conference on the Peaceful Uses of Atomic Energy (Geneva), Vol. 15 (1958) p. 408, United Nations, New York.

3. J.A. Wheeler, In ''Fast Neutron Physics'' (Eds. J.B. Marion and J.E. Fowler) Pt. II (1963) p. 2051, Wiley (Interscience), New York.

4. J.R. Huizenga, A.N. Behkami and L.G. Moretto, Phys. Rev. 177 (1969) 1826.

5. A. Bohr, Proc. of United Nations International Conference on Peaceful Uses of Atomic Energy (Geneva), Vol. 2 (1956) p. 151, United Nations, New York.

87523

PHY-1983-D-SHA-ANG